

University of Montana

ScholarWorks at University of Montana

Graduate Student Theses, Dissertations, &
Professional Papers

Graduate School

2017

CATIONIC LATEX NANOPARTICLES IN ELECTROKINETIC CHROMATOGRAPHY: SYNTHESIS, CHARACTERIZATION, AND APPLICATION TO THE SEPARATION OF EXPLOSIVES

Julie Rebecca McGettrick
University of Montana, Missoula

Follow this and additional works at: <https://scholarworks.umt.edu/etd>

Let us know how access to this document benefits you.

Recommended Citation

McGettrick, Julie Rebecca, "CATIONIC LATEX NANOPARTICLES IN ELECTROKINETIC CHROMATOGRAPHY: SYNTHESIS, CHARACTERIZATION, AND APPLICATION TO THE SEPARATION OF EXPLOSIVES" (2017). *Graduate Student Theses, Dissertations, & Professional Papers*. 11072.
<https://scholarworks.umt.edu/etd/11072>

This Dissertation is brought to you for free and open access by the Graduate School at ScholarWorks at University of Montana. It has been accepted for inclusion in Graduate Student Theses, Dissertations, & Professional Papers by an authorized administrator of ScholarWorks at University of Montana. For more information, please contact scholarworks@mso.umt.edu.

CATIONIC LATEX NANOPARTICLES IN ELECTROKINETIC CHROMATOGRAPHY:
SYNTHESIS, CHARACTERIZATION, AND APPLICATION TO THE SEPARATION OF EXPLOSIVES

By

JULIE REBECCA MCGETTRICK

Bachelor of Arts with Honors in Chemistry, Smith College, Northampton, Massachusetts, 2008

Dissertation

presented in partial fulfillment of the requirements
for the degree of

Doctor of Philosophy
in Analytical Chemistry

The University of Montana
Missoula, MT

August 2017

Approved by:

Scott Whittenburg, Dean of The Graduate School
Graduate School

Christopher Palmer, PhD.
Department of Chemistry and Biochemistry

Earle Adams, PhD.
Department of Chemistry and Biochemistry

Orion Berryman, PhD.
Department of Chemistry and Biochemistry

Michael DeGrandpre, PhD.
Department of Chemistry and Biochemistry

Tony Ward, PhD.
School of Public and Community Health Sciences

© COPYRIGHT

by

Julie Rebecca McGettrick

2017

All Rights Reserved

CATIONIC LATEX NANOPARTICLES IN ELECTROKINETIC CHROMATOGRAPHY:
SYNTHESIS, CHARACTERIZATION, AND APPLICATION TO THE SEPARATION OF EXPLOSIVES

Advisor: Christopher Palmer

Chairperson: Earle Adams

Electrokinetic chromatography (EKC) is a powerful analytical technique that uses the instrumentation of capillary electrophoresis (CE) and the principles of chromatography to separate ionic and neutral analytes. A capillary is filled with background electrolyte (BGE), and when a voltage is applied ionic species migrate to the electrodes. Neutral compounds have no mobility, so a pseudo-stationary phase (PSP) is added to the BGE that consists of an ionic group to provide mobility and a hydrophobic group to interact with analytes. Analytes interact with the PSP which changes their apparent mobilities, leading to a separation. It is possible to coat the negatively charged silica surface of a capillary with a cationic polymer, reverse the polarity of the electrodes, and use a cationic PSP to perform separations. This is the subject of this dissertation.

RAFT polymerization was used to create diblock copolymers that self-assemble into latex nanoparticles and used as PSPs for EKC. Two cationic monomers, [2-(Acryloyloxy)ethyl]trimethylammonium chloride (AETMAC) and (3-Acrylamidopropyl)trimethylammonium chloride (APTAC), and three hydrophobic monomers, butyl acrylate (BA), ethyl acrylate (EA), and methyl acrylate (MA) were investigated. RAFT polymerization was an effective way to create the desired materials, and several techniques were used for characterization. Unexpected band broadening was observed when the nanoparticles were used as PSPs, so an additional cationic homopolymer, PAETMAC, was needed to coat the capillaries to prevent hydrophobic interactions at the capillary surface. The linear solvation energy relationships (LSER) model was used to compare different cationic latex nanoparticles. The choice of cationic block did not affect selectivity, but nanoparticles with MA cores showed a significant difference from nanoparticles with EA or BA cores. Finally, PAETMAC coated capillaries and cationic latex nanoparticles were used to separate anions and nitro compounds found in explosives residues. Separations can be performed in less than 10 minutes. The hydrophobic anions perchlorate and thiocyanate are retained by the nanoparticles, and acetonitrile was added to the BGE to reduce band broadening of these analytes. Future directions for this work include further characterization of the diblock copolymers, further optimization of the explosives separation, and the development of a portable fluorescence quenching detection system.

Acknowledgments

First and foremost, I would like to thank my advisor, Chris Palmer, for getting me started on this project and for all the support and guidance over the course of this research. I am so grateful to have found a project that combines my interests in both organic and analytical chemistry. In the past five years I have learned so much, not just about chemistry but about teaching, presenting, and life. Thanks also to the members of my committee and the faculty of the chemistry department. My research would not be where it is today without Jesse Hyslop, who taught me about RAFT polymerization, CE, EKC, and so much more! The anionic nanoparticles synthesized by Jesse, Leah Hall, and Hungngai (Jane) Chuk were the foundation I built my work upon, and that data set was a useful comparison for my own data. My time in the lab was much more enjoyable thanks to great conversations with Will Penny. Thanks for getting me to take up running! Thanks also to Virginia Porden, Derek Shultz, and Hannah Wright for being awesome labmates. Kim Brown assisted with the synthesis of several macroCTAs and diblock copolymers, two of which turned out to be the best performers.

I had the amazing opportunity to participate in the National Science Foundation's East Asia and Pacific Summer Institute (EAPSI) program in 2016. I am very grateful to Professor Emily Hilder for hosting me at the University of South Australia, to Dario Arrua for supporting me during my time at UniSA, and most of all to Adam Sutton. Adam helped brainstorm ideas for the EAPSI proposal, helped me learn about Australia and navigate UniSA paperwork before I arrived, welcomed me into the research group, and taught me about polymer analysis by NMR and non-aqueous CE. This fellowship would not have happened without Adam! I was fortunate to meet another Montanan in Australia, Nathan Williamson. Adam, Nathan, and I had some great conversations, and the paper we published together was much better because of them.

Finally, I could not have completed graduate school without the support of my family and friends. I had the pleasure of participating in the Missoula City Band, Missoula Community Concert Band, First Presbyterian Church Handbell Choir, and Grace United Methodist Church choir and handbell choir. Music is my counterweight to science, and I met many wonderful people through these organizations. Jon and Cindy Ekstrand and Meghan and Jack Rhodes have become my Montana family over the past several years. I would not be where I am today without the physical, emotional, and financial support of my parents Jim and Mavis Pyle. Thanks most of all to my husband Tristan McGettrick for being my partner in this Montana adventure.

Table of Contents

Abstract	ii
Acknowledgements	iii
List of Figures	vi
List of Tables	ix
List of Equations	xi
List of Abbreviations	xii
Prologue	1
Chapter 1 – Separation Science Background and Theory	12
1.1 Development of Chromatography	12
1.1.1 Gas Chromatography	13
1.1.2 Liquid Chromatography	15
1.1.3 Capillary Electrophoresis	16
1.1.4 Electrokinetic Chromatography	16
1.2 Theory	17
1.2.1 Chromatography Theory	18
1.2.2 Linear Solvation Energy Relationships	21
1.2.3 Electrophoresis Theory	23
1.2.4 Electrokinetic Chromatography Theory	25
1.3 Research Aims	26
Chapter 2 – Synthesis and Characterization of Cationic Latex Nanoparticles	28
2.1 Introduction	28
2.1.1 RAFT Polymerization	28
2.2 Experimental	32
2.2.1 Synthesis	32
2.2.1.1 Chain Transfer Agent Synthesis.....	32
2.2.1.2 MacroCTA Synthesis	33
2.2.1.3 Diblock Copolymer Synthesis	33
2.2.2 Characterization	35
2.3 Results and Discussion	36
2.3.1 Synthesis	37
2.3.2 Characterization	41
2.3.2.1 MacroCTA	42

2.3.2.2 Diblock Copolymers	47
2.4 Conclusions	53
Chapter 3 – Development of a Cationic Capillary Coating	55
3.1 Introduction	55
3.2 Experimental	58
3.2.1 Synthesis	58
3.2.2 Characterization	59
3.2.3 Capillary Coating for CE and EKC	59
3.3 Results and Discussion	60
3.3.1 Polymer Synthesis and Characterization	60
3.3.2 PAETMAC Treated Capillaries.....	62
3.3.3 Commercial Cationic Polymer Treated Capillaries	66
3.3.4 Effect on EKC Peak Shapes	68
3.4 Conclusions	70
Chapter 4 – Evaluation of Cationic Latex Nanoparticles as Pseudo-Stationary Phases	71
4.1 Introduction	71
4.2 Experimental	72
4.3 Results and Discussion	75
4.3.1 Homologous Series	75
4.3.2 Selectivity	79
4.3.3 Linear Solvation Energy Relationships	83
4.4 Conclusions	87
Chapter 5 – A Method for the Separation of Explosives Residues	89
5.1 Introduction	89
5.2 Experimental	93
5.3 Results and Discussion	95
5.3.1 Nitroaromatic and Nitramine Compounds	95
5.3.2 Anions	107
5.3.3 Optimizing Conditions for Simultaneous Separations	111
5.4 Conclusions	117
Chapter 6 – Conclusions and Future Directions	119
6.1 Conclusions.....	118
6.2 Future Work	121
References	124

List of Figures

Figure P-1: Chemical Structures of Selected Explosives	10
Figure 1-1: Intermolecular Forces	21
Figure 1-2: Explosives and Anions Separated by EKC and CE	27
Figure 2-1: Generic structure of a CTA	28
Figure 2-2: Schematic of the RAFT Mechanism	30
Figure 2-3: CTA Used by the Palmer Research Group	30
Figure 2-4: Monomers Used in this Research	31
Figure 2-5: ^1H NMR of AETMAC Monomer	37
Figure 2-6: ^1H NMR of AETMAC MacroCTA	38
Figure 2-7: Reaction Progress of JM51 AETMAC MacroCTA	39
Figure 2-8: ^1H NMR of APTAC Monomer	40
Figure 2-9: ^1H NMR of APTAC MacroCTA	40
Figure 2-10: Titrations of JM21 AETMAC and JM61 APTAC MacroCTA	43
Figure 2-11: MALDI-TOF Mass Spectrum of 2-Polyvinylpyridine	45
Figure 2-12: MALDI TOF Mass Spectrum of JM158 AETMAC and JM90 APTAC	46
Figure 2-13: ^1H NMR of JM142 EAAETMAC in D_2O	48
Figure 2-14: ^1H NMR of JM142 EAAETMAC in CDCl_3	48
Figure 2-15: Non-Aqueous CE of BAAETMAC, EAAETMAC, and MAAETMAC Nanoparticles	49
Figure 2-16: NMR of BAETMAC, EAAETMAC, and MAAETMAC used for diffusion NMR	50
Figure 2-17: Biexponential Fits for the Attenuation of Nanoparticle Signals	51
Figure 2-18: Diffusion Coefficients and Hydrodynamic Radii	52
Figure 2-19: TEM Image of EAAETMAC Nanoparticle JM136	53
Figure 3-1: Unexpected Band Broadening in Alkyl Phenyl Ketones	56

Figure 3-2: Unexpected Retention of Alkyl Phenyl Ketones at the Capillary Surface	57
Figure 3-3: MALDI-TOF MS Spectra of Four Batches of PAETMAC	61
Figure 3-4: Alkyl Phenyl Ketones are Not Retained by a PAETMAC Coating	62
Figure 3-5: Ohm's Law Plots of Tris-Acetate Buffer at pH 4, 5, 6, 7, and 8	63
Figure 3-6: Average EOF for 100 Injections at pH 4, 5, 6, 7, and 8.....	64
Figure 3-7: The EOF for Each of 100 Injections at pH 4, 5, 6, 7, and 8	65
Figure 3-8: Alkyl Phenyl Ketones with Excellent Peak Shapes	66
Figure 3-9: EOF for Each Injection with Five Different Cationic Capillary Coatings	67
Figure 3-9: Separations with EAAETMAC Nanoparticles and Polymer Coated Capillaries	69
Figure 4-1: Selectivity Changes with PSP Concentration	77
Figure 4-2: Retention Factor and Efficiency of Alkyl Phenyl Ketones Over 100 Injections	79
Figure 4-3: Nanoparticle Size vs Methylene Selectivity	80
Figure 4-4: Composite LSER Hydrophobic Core Comparison	85
Figure 4-5: Composite LSER Hydrophilic Shell Comparison	85
Figure 5-1: Nanoparticle and PAETMAC Coated Capillary Comparison	95
Figure 5-2: JM137, JM136, JM132 Core Comparison for Explosives	99
Figure 5-3: Benzene Sulfonic Acid is Used as an Internal Standard	101
Figure 5-4: Separations with 0.1%, 0.3%,. And 0.5% KB3A BAAPTMAC	102
Figure 5-5: Separations with a 68.5 cm and 35 cm Capillary.....	103
Figure 5-6: KB3 and KB4 Nanoparticle Explosive Comparison	106
Figure 5-7: Ion Resolution Improves with Capillary Length	108
Figure 5-8: Anion Peak Shape Changes with Concentration	109
Figure 5-9: Thiocyanate and Perchlorate Interact with PSP	110
Figure 5-10: Acetonitrile Improves Thiocyanate and Perchlorate Peak Shapes	112

Figure 5-11: 20% Acetonitrile with Increasing Concentrations of PSP	113
Figure 5-12: 10% and 20% Acetonitrile with a 48.5 cm Capillary	114
Figure 5-13: Calibration Curve Comparison for Five Explosive Compounds	116
Figure 6-1: The Fluorescence Quenching Detector Developed by Vincent Schnee	122
Figure 6-2: Separation of Explosives by JRM27 BAAPTAC-Fluorescein Nanoparticles	123

List of Tables

Table P-1: Timeline of the History of Explosives	7
Table P-2: Properties of Selected Explosives	10
Table 2-1: Synthetic Conditions for MacroCTAs	33
Table 2-2: Synthetic Conditions for Diblock Copolymers	34
Table 2-3: ¹ H NMR Characterization Data for MacroCTA	42
Table 2-4: Titration Characterization Data for MacroCTA	44
Table 2-5: MacroCTAs Characterized by MALDI-TOF MS	47
Table 2-6: Nanoparticle Size Characterization by DLS and Diffusion NMR	52
Table 3-1: Synthetic Conditions of Four Batches of PAETMAC	59
Table 3-2: Properties of Four Batches of PAETMAC	61
Table 3-3: EOF Generated by the Four Capillary Coatings	67
Table 3-4: EOF Generated by the Four Commercial Cationic Polymers	68
Table 3-5: Theoretical Plate Counts Using Different Cationic Capillary Coatings	70
Table 4-1: LSER Solutes and Descriptors	74
Table 4-2: Systematic Variable Changes on EKC Performance	75
Table 4-3: Comparison of μ_{eo} , μ_{PSP} , and α_{CH_3} of Different Nanoparticles	78
Table 4-4: Repeatability Study for Alkyl Phenyl Ketones	79
Table 4-5: Methylene Selectivities of Cationic and Anionic Latex Nanoparticles	81
Table 4-6: Polar Group Selectivity for Cationic Latex Nanoparticles	81
Table 4-7: Polar Group Selectivity Comparison Between PSPs	83
Table 4-8: LSER Results for 10 Cationic Latex Nanoparticles	84
Table 4-9: Composite LSER Results	85
Table 4-10: Comparison to Other LSERs Studies of PSPs	86

Table 5-1: Retention Factors for Nitroaromatics with Anionic and Cationic PSPs	96
Table 5-2: Retention Factors for Nitroaromatics with Cationic Coated Capillaries	98
Table 5-3: Absorbance of Explosives at Three Different Wavelengths	100
Table 5-4: Normalized Mobilities with the KB Cationic Nanoparticles	104
Table 5-5: Retention Factors with the KB Cationic Nanoparticles	105
Table 5-6: Anion Interactions with Polymers in Solution	111
Table 5-7: R ² Values from Calibration Curves	116
Table 5-8: LOD, LOQ, and R2 Values from Calibration Curves	117

List of Equations

Equation 1-1: Chemical potential	17
Equation 1-2: Partition Coefficient	18
Equation 1-3: Entropy and Enthalpy in Chemical Potential	18
Equation 1-4: Chromatography Equilibrium Ratio	19
Equation 1-5: Retention Factor in Chromatography	19
Equation 1-6: Selectivity	20
Equation 1-7: Van Deempter Equation	20
Equation 1-8: Master Resolution Equation	21
Equation 1-9: Polarity Index	21
Equation 1-10: Solvent Scales	22
Equation 1-11: Kamlet-Taft LSER Model	22
Equation 1-12: Abraham LSER Model	22
Equation 1-13: Electrophoretic velocity of an ion in solution in an electric field	23
Equation 1-14: Zeta Potential and Electrophoretic Mobility	24
Equation 1-15: Apparent Mobility	24
Equation 1-16: Calculating Mobility from Retention Data	25
Equation 1-17: Retention in EKC	25
Equation 1-18: Resolution in EKC	26
Equation 2-1: Number Average Molecular Weight	44
Equation 2-2: Weight Average Molecular Weight	44
Equation 2-3: Dispersity	44
Equation 5-1: Normalized Mobility	100

List of Abbreviations

2,4-DNT – 2,4-Dinitrotoluene

2,6-DNT – 2,6-Dinitrotoluene

2-AM – 2-Amino-4,6-Dinitrotoluene

2-NT – 2-Nitrotoluene

3-NT – 3-Nitrotoluene

4-AM – 4-Amino-2,6-Dinitrotoluene

4-NT – 4-Nitrotoluene

AETMAC – [2-(Acryloyloxy)ethyl]trimethylammonium Chloride

AMPS – 2-acrylamido-2-methyl-1-propane Sulfonic Acid

APTAC – (3-Acrylamidopropyl)trimethylammonium Chloride

BA – Butyl Acrylate

CE – Capillary Electrophoresis

CMC – Critical Micelle Concentration

CTAB – Cetyl Trimethylammonium Bromide

DNA – 3,5-Dinitroaniline

DNB – 1,3-Dinitrobenzene

EA – Ethyl Acrylate

EKC – Electrokinetic Chromatography

GC – Gas Chromatography

HMX – High Melting Explosive

HPLC – High Pressure Liquid Chromatography

MA – Methyl Acrylate

MALDI-TOF MS – Matrix Assisted Laser Desorption/Ionization Time of Flight Mass Spectrometry

NB – Nitrobenzene

NMR – Nuclear Magnetic Resonance

NYG – Nitroglycerin

PETN – Pentaerythritol Tetranitrate

PSP – Pseudo-stationary Phase

RDX – Rapid Detonating Explosive

SDS – Sodium Dodecyl Sulfate

SEC – Size Exclusion Chromatography

TET – Tetryl

TNB – 1,3,5-Trinitrobenzene

TNT – 2,4,6-Trinitrotoluene

Prologue

Few chemicals have had as profound of an effect on the world as explosives, which have played an important role in human civilizations for centuries in both war and peace. The development and exploration of energetic materials shaped the world we know today by changing the dynamics of warfare and allowing Europeans to conquer much of the globe. They also led to advances in science, and made impressive feats of engineering possible. The number of energetic materials today is much greater than centuries ago and many are used for destructive purposes, so the ability to detect and analyze different types of explosives is critical. The goal of this dissertation research was to develop a single method to separate two important classes of compounds found in explosives, anions and nitro compounds, which typically require two analytical techniques. This prologue introduces the history and background of explosives.

The earliest explosive is a mixture of saltpeter (potassium nitrate), brimstone (sulfur), and charcoal in a 6:1:1 ratio known as black powder. Early alchemists experimented with these ingredients to learn more about their nature and discovered that certain formulations could cause “a noise exceeding the roar of strong thunder and a flash brighter than the most brilliant lightning”¹. The earliest records of black powder come from ancient China. A Chinese text from 850 A.D. warned that “some have heated together sulfur, realgar, and saltpeter with honey; smoke and flames result, so that their hands and faces have been burnt, and even the whole house where they were working burned down”². The Chinese called this mixture “fire drug” and used it in pyrotechnics, rockets, and incendiary weapons². The knowledge of this seemingly magical mixture worked its way west and reached Europe in the 13th century. The English Friar Roger Bacon described a recipe for black powder in his book “*de secretis operibus artis et naturae et nullitate magia*” in 1242.³

It was not long before Europeans began using black powder in weaponry. Berthold Schwartz, known as the “powder monk” is often credited with inventing the first firearms, but very little is known about his life and he may in fact be a legend. The first black powder weapons were bombards, early cannons that were little more than a tube closed on one end. The bombards were loaded with powder and either bolts or iron balls, and a red-hot rod would be inserted through a touch hole to set off the powder and launch the projectile. King Edward III was the first to employ bombards in battle against the French in 1346². Weapons fueled by black powder changed the nature of warfare from a physical contest of strength and muscle to a contest of resources. Cannons could knock down the stone walls of castles, changing the dynamics of sieges. The city of Constantinople was thought to be impregnable until the Turkish Sultan Mehmed II toppled it with 18 foot-long bombards². Cannons on sailing ships fundamentally changed the nature of warfare at sea as well. Instead of small, maneuverable vessels that would ram enemy ships or get close enough for soldiers to board; large ships with cannons would simply blast holes in enemy ships and sink them. However, both black powder and guns were expensive to build and required skilled gunners, blacksmiths, and engineers. Europe transformed from a land of feudal lords and city states to centralized nations that could afford these new weapons. Although other cultures knew and used black powder, they did not develop it with the zeal of the Europeans.

Black powder was used by European countries to control the rest of the world. The Portuguese captain Vasco da Gama sailed around Africa to the Indian Ocean in 1498, then returned with warships four years later and violently established a forced trading monopoly in India². Hernán Cortés intimidated the Aztecs with his cannons when he reached the New World in 1519, and gunpowder helped establish the European’s dominance there². English and Dutch slave traders would trade guns and powder for African slaves. China may have developed black powder first, but Chinese guns were no match for European guns in the Opium War in 1841².

Black powder was also used for sinister purposes on the home front. In 1604 a group of English revolutionaries led by Robert Catesby were tired of being persecuted for their Catholic faith and plotted to blow up the Parliament Building with the King and other important government officials inside. The group rented a cellar room under Parliament Hall with convenient access to the River Thames and began stocking it with barrels of powder. Guy Fawkes was chosen to ignite the powder the day Parliament convened. However, one of the Lords received an anonymous letter warning him not to attend on that day because Parliament “shall receive a terrible blow”². He took it to King James I, who suspected the letter was referring to an explosion. He ordered the castle searched, and the storeroom of powder and Guy Fawkes were discovered. The conspirators were hunted down, and those who were not shot during capture were executed.

Black powder began to be used for peaceful purposes several centuries after it was adopted for war. In 1673 the Dutch man Christiaan Huygens developed a *moteur à explosion* which used a small charge of powder to force air through a one-way valve to create a power stroke². This precursor to the internal combustion engine unfortunately ran into problems because Hyugens could not figure out how to deliver a successive series of charges. In 1627 Kasper Weindl demonstrated that black powder could be used to split rocks; he went on to blast in mines that had been abandoned because the rock was too hard to crack manually². Black powder became the dominant explosive in mining until the invention of dynamite in the 1800s.

The study of black powder led to advancements in chemistry as well. Early chemists Robert Boyle and Robert Hooke were fascinated with how this powder could create fire even in an evacuated bell jar. Hooke’s experiments with black powder convinced him that fire was not an element and helped him develop an early theory about combustion. The French chemist Antoine-Laurent Lavoisier also studied combustion. Lavoisier was appointed to the French Gunpowder Administration in 1775, where

he researched more efficient ways to prepare saltpeter. Thanks to Lavoisier's reforms, which included quantitative instructions, improved record keeping, productivity bonuses, and price structures, French black powder became some of the highest quality in the world². When the American Revolutionaries needed a supply of gunpowder to fight the British, France was happy to oblige.

One of most important chemical companies today got its start in the explosives industry during this time. Eleuthère Irénée DuPont was born in Paris in 1771 and studied gunpowder making with Lavoisier in France³. The family moved to America in 1800 and he decided to start a powder mill after finding the available gunpowder high in price and poor in quality. He raised funds and bought machinery in France, where they were enthusiastic about supporting American industry because it could only hurt the British³. E. I. Dupont de Nemours & Company built a mill in Wilmington, Delaware on the Brandywine River which became operational in 1804. The company survived some early financial hardships and explosions, and was taken over by Irénée's sons after his sudden death in 1834. The firm existed as a partnership until 1902, when it was taken over by three DuPont cousins and incorporated in Delaware. Lamot DuPont was a talented chemist, and Henry Du Pont was a ruthless businessman who acquired many small powder mills and consolidated the black powder manufacturing industry. The company eventually began to manufacture dynamite when it became apparent that new explosives technology was superseding black powder. DuPont dominated the explosives industry and was ordered to divest under the Sherman Antitrust Act in 1912³. DuPont has since expanded into the materials science, automotive, and oil and gas industries and is a much more diverse company today.

Black powder was the only explosive and propellant available for nearly 900 years. Today it has been replaced by smokeless powders and high explosives, which are more reliable and do not produce the acrid smoke that black powder does. There are still a few manufacturers that produce black powder

for reenactments and history buffs, but the explosive that changed the world is now essentially obsolete.

Explosives based on nitro compounds did not begin to be developed until the 19th century. In the 1830's French chemists Henri Braconnot and Theophile Jules Pelouze found that starches like paper and cotton could be nitrated by dissolving them in nitric acid, and found that these preparations were easily combustible⁴. The German scientists Christian F. Schoenbein and R. Boetter independently developed guncotton, or nitrated cellulose, in 1845. In 1846 Ascanio Sobrero discovered nitroglycerin, but abandoned working with it after discovering its explosive properties⁵. Several energetic compounds were developed and used for other purposes, but their explosive natures were not exploited until later. Picric acid was developed in 1771 by the French chemist Pierre Woulfe, and trinitrotoluene was prepared by the German scientist J. Willibrand in 1863; both were used in the dye industry⁴. RDX was first synthesized in 1899 for medicinal purposes.

Alfred Nobel's invention of dynamite revolutionized the explosives industry. Immanuel Nobel and his son Alfred developed a manufacturing process for nitroglycerin in 1863, and Alfred Nobel invented the metal blasting cap detonator in 1864, but turned his attention to safety after several explosions destroyed the family's factory and killed his brother Emil. In 1866 he mixed nitroglycerin with kieselguhr, an inert diatomaceous earth that stabilized the explosive, and sold it as dynamite. In 1867 J.H. Norribin and C.J. Ohlsson developed a form of dynamite that used ammonium nitrate and sawdust to absorb the nitroglycerin. Nobel bought their patent in 1870, and went on to patent gelatinous dynamite in 1875. Dynamite was used for mining and demolition, such as the blasting of Flood Rock in New York Harbor in 1885 to make it safer for navigation⁴.

Smokeless powders are an alternative to black powder that use high explosives such as nitrocellulose and nitroglycerin. These formulations produce far less smoke, which made it easier to see

after firing guns. The French scientist Paul Vieille invented the first smokeless powder in 1884 from nitrocellulose, which he called Poudre B⁴. Alfred Nobel developed a double-base smokeless powder he called Ballistite in 1888. The British developed a similar product called Cordite, which was used extensively in the Boer War in what is now South Africa⁴.

Today's common military explosives began being developed in the early 20th century. C. Haussermann developed a trinitrotoluene manufacturing process in Germany that was much cheaper than the direct nitration of toluene. The Germans began using TNT as the filler in explosive shells in 1902; the Americans followed suit in 1912. When World War I broke out the Germans converted their dye factories to explosives production facilities and used high explosives with devastating effect. When the allies blocked their access to Chilean saltpeter they utilized the recently developed Haber-Bosch process to produce ammonia from nitrogen and became independent of outside sources. After the war the United States dedicated scientific resources to ammunition developments which led to RDX, PETN, EDGN, and lead azide becoming military explosives⁴. RDX had great power but was sensitive to detonation. The British tried several approaches to stabilizing RDX: Composition A contained 9% beeswax, Composition B was a mixture of TNT and RDX, and Composition C contained 11.7% plasticizing oil. Composition C was refined over the years and the current standard is C4. During WWII scientists discovered ternary mixtures were effective for armor-piercing projectiles, and a PETN-RDX-TNT mixture called PTX-2 was used extensively.

In recent times a growing threat is the use of improvised explosive devices by terrorist organizations or individuals. Increased airport security measures were spurred by the bombing of PanAm Flight 103 over Lockerbie in 1988. Notable explosions caused by terrorists include the Oklahoma City bombing in 1995, train bombing in Madrid in 2004, London subway bombing in 2005, the Boston Marathon bombing in 2013, the attacks in Paris in 2015, the airport bombing in Brussels in 2016, and the

attack at an Ariana Grande concert in Manchester, England in 2017. These attacks are often carried out with explosive mixtures containing inorganic salts such as nitrates, chlorates, or perchlorates and a fuel like oil or sugar⁶, and often include metal pieces to cause shrapnel damage. Unlike military grade explosives, these ingredients are easily available and cheap to obtain.

A brief timeline of explosives development is shown in Table P-1.

Table P-1: Timeline of Explosives Development

850	Chinese text describes an alchemy experiment with charcoal, brimstone, and saltpeter
1242	Roger Bacon records his secret formula for black powder
1654	Glauber first prepares ammonium nitrate
1830	Welter discovers picric acid can be used as an explosive
1846	Sobrero discovers nitroglycerin
1846	Schonbein and Bottger independantly each prepare nitrocellulose
1863	Wertens first prepares TNT
1867	Nobel mixes nitroglycerin and Kieselguhr clay, patents it as ghur dynamite
1877	Mertens first prepares Tetryl
1877	Jousselin first prepares nitroguanidine
1885	Turpin uses picric acid instead of black powder in munition shells
1889	Nobel patents Ballistite, the first smokeless powder
1894	PETN first prepared
1899	RDX first prepared for medicinal use by Henning
1914	TNT becomes the standard explosive used by all armies in World War I
1920	Herz discovers RDX can be used as an explosive
1940	Bachmann's RDX contains 8-12% of an impurity that turns out to be HMX
1950	ANFO (Ammonium Nitrite Fuel Oil) developed
1952	First Polymer Bonded Explosives (PBX) developed at Los Alamos National Lab

The Science of Explosives

Explosions happen when a large amount of energy is generated and suddenly released. There are three types of explosions: atomic, physical, and chemical. Atomic explosions are caused by energy released by the fission of the nuclei of radioactive material. Physical explosions happen when matter suddenly changes state, such as when hot lava reaches the ocean and the water rapidly evaporates⁵. Chemical explosions are caused by a chemical reaction, and these will be the focus of this discussion.

When a fuel and an oxidant react there are three possibilities: combustion, deflagration, or detonation. Combustion is an exothermic chemical reaction between a substance and oxygen that usually results in a flame. If the heat is reduced, the flame will extinguish. Unlike ordinary flammable materials, energetic materials contain both an oxidant and a fuel so additional oxygen is not necessary. These materials are capable of either deflagration or detonation, which are both self-sustaining processes that can be initiated by a flame, high temperature, shock, or friction. In deflagration energy is transferred thermally at less than the speed of sound, and the deflagrating formulation often makes a crackling or hissing noise. Detonation occurs when energy is transferred by a shockwave rather than thermally. The shockwave can travel between 1500 – 9000 m/s, and is ignited either by heat or shock. Detonation is more likely when the energetic material is confined and the gaseous products have nowhere to escape, dramatically increasing the pressure.

Energetic materials can be broadly characterized by use as propellants, explosives, or pyrolants. Both propellants and explosives quickly produce large volumes of gaseous products. Propellants are used to generate propulsion forces by forcing the gas through a nozzle and typically deflagrate, while explosives are used to produce destructive forces and typically detonate. Pyrolants contain metals such as lithium, magnesium, aluminum, or titanium and are used to generate very high temperatures rather than gaseous products. They are used in a variety of pyrotechnic devices like igniters for rockets. The

physicochemical properties are not very different; propellants can detonate and explosives can deflagrate under the right conditions. Explosives can be classified as either high explosives or low explosives depending on their detonation velocity. High explosives are further classified as primary, secondary, or tertiary explosives by their stability. Primary explosives are very sensitive to detonation by heat, friction, or shock. They are often used as blasting caps to detonate the more stable secondary explosives. Tertiary explosives are very stable and require a booster of secondary explosives; they are used for mining and construction. Explosives can be classified as commercial or military, and organic explosives can also be classified by their functional groups, such as nitroaromatic, nitramine, or nitrate ester.

The most well-known explosive is 2,4,6-trinitrotoluene, or TNT. It is one of the most widely used military explosives because it is very stable and relatively insensitive to impact and friction. 1,3,5-Trinitro-1,3,5-triazacyclohexane, also known as RDX for Rapid Detonating eXplosive, is another military explosive often found in plastic explosive formulations. 1,3,5,7-Tetranitro-1,3,5,7-tetrazacyclooctane, or HMX (High Melting eXplosive, which is known as Her Majesty's eXplosive in Great Britain) is similar to RDX and is used in rocket propellants and charges for artillery shells. 2,4,6-*N*-tetranitro-*N*-methylaniline, 2,4,6-trinitrophenylmethylnitramine, or Tetryl, is used as a base charge in blasting caps and detonators and as a booster explosive because it is much less stable than TNT. Pentaerythritol tetranitrate (PETN) is used in detonating cord and plastic explosives. Nitroglycerin (NG) is used in dynamite. Some properties are listed in Table P-2, and the molecular structures are shown in Figure P-1.

Table P-2: Properties of Selective Explosives

Explosive	Molecular Weight ⁷ (g/mol)	Density ⁷ (g/mL)	Melting Point ⁷ °C	Ignition Point ⁷ °C	Vapor Pressure ⁷ (torr)	Heat of Explosion ⁸ MJ/kg	Oxygen Balance ⁸ %	Detonation Velocity ⁸ m/s
TNT	227.13	1.65	80.65	295	5.8 E -6 at 25 C	5.07	-73.9	6900
RDX	222.26	1.83	204	295	4.6 E-9 at 25 C	5.40	-21.6	8750
HMX	296.16	1.96	280	335	3 E -9 at 100 C	5.36	-21.6	9100
Tetryl	287.15	1.73	129.5		5.7 E -9 at 25 C	5.53	-47.4	7570
PETN	316.2	1.78	141.3		1.4 E-8 at 25 C	5.90	-10.1	8400
NG	227.09	1.59	13.2	250	3.1 E -4 at 26 C	6.32	+3.5	7600

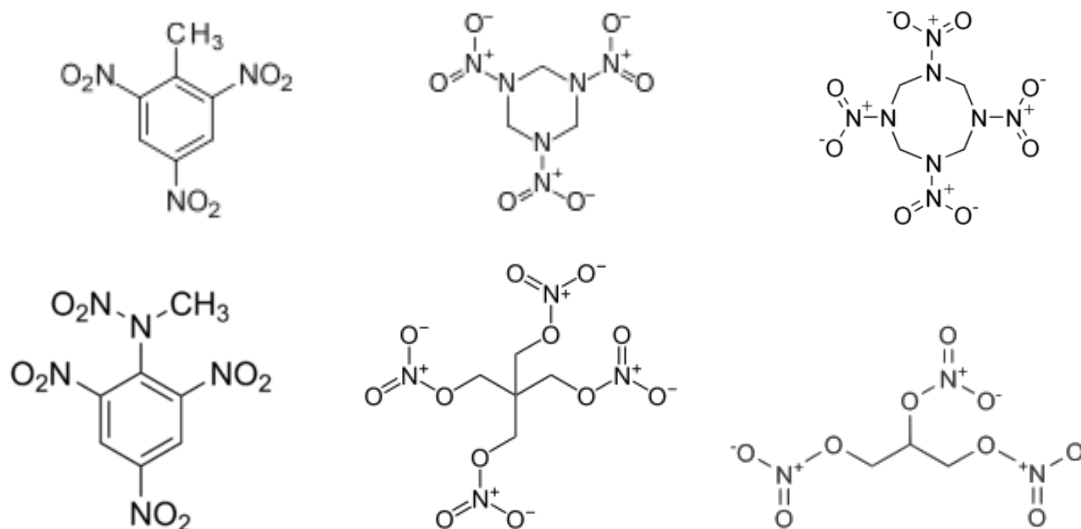


Figure P-1: Molecular Structures of Selected Explosives. From top left to bottom right: TNT, RDX, HMX, Tetryl, PETN, and NG.

Due to their sensitivity, explosive compounds are not the only ingredient in an explosive formulation. Metals such as aluminum may also be added to help generate heat. Slurry explosives are used in mining and consist of aqueous solutions of ammonium nitrate with sensitizers added. Polymer binders are frequently used to give the formulation the desired mechanical properties. The polymers can be inert, such as polyurethane, or energetic materials themselves like the azide polymers BAMO and GAP⁸. Plastic bonded explosives (PBX) are made by mixing RDX, HMX, or TNT with liquid copolymers, which can then be cast as warheads. Multiple explosive compounds can be used in a given formulation. TNT mixed with ammonium nitrate is known as Amatol, TNT combined with aluminum is Tritonal, and TNT with HMX is Octol.

An increasingly common type of explosive is the improvised explosive device, or IED. The military grade explosives are tightly regulated, but IEDs are made from oxidizers and fuels that can be legally obtained at low cost. Common fuels include fuel oil and sugar, and ammonium nitrate fertilizers are often used as oxidants. According to Bryce Tappan at Los Alamos National Laboratory, potassium chlorate mixed with nitrobenzene is a formulation seen often in Pakistan.

Explosives are essential for militaries around the world, but are increasingly being used by terrorist organizations and individuals with a harmful agenda. The need for continuing research into explosives detection is critical to protect public safety by preventing detonations and for forensics personnel after a blast has occurred. This is the goal of this research project.

Chapter 1: Separation Science Background and Theory

Separation science is critical to a number of applications, fields, and industries, including the analysis of explosives. The ability to break down a mixture and quantify each component makes it possible to analyze many complex samples. Two important separation methods used in this research are chromatography and electrophoresis. The history and theory of these techniques will be described in this chapter, and the specific aims of this research project will be presented.

1.1 Development of Chromatography

Chromatography was first developed by Mikhail S. Tswett, a Russian botanist who was interested in plant pigments. He earned a doctorate in Geneva, but when he moved back to Russia his foreign degree was not accepted so he needed to go back and earn Russian degrees. In his Russian master's thesis Tswett described how some solvents could extract the pigments from leaves while others could not, and showed that this was because the pigments were adsorbed to the plant tissue more strongly than petroleum ether, but less strongly than to ethanol⁹. These interactions could also take place on cellulose based filter paper; which gave him the idea to try separating compounds with powdered substances. Tswett moved to Warsaw in 1901 and began experimenting with hundreds of different adsorbents to see their effects on chlorophyll pigments. He developed a method where a filtered plant solution was shaken together with an adsorbent powder, then precipitated. Different pigments could then be extracted off the powder with different solvents⁹. He mentioned an early description of chromatography in a lecture in 1903, but did not yet use the terminology. In 1906 Tswett published the seminal papers in the German journal *Berichte der Deutschen Botanischen Gesellschaft* describing how to separate pigments with a calcium carbonate column with the chromatographic method¹⁰. Chromatography means "color writing" in Greek, but it is also a clever wordplay as his family name Tswett also means color¹⁰. He published his book *Chromophylls in the Plant and Animal World* in

1910 for his Russian doctoral thesis, which contained a section on chromatography that included a diagram of the set-up, lists of solvents and adsorbents, and warnings about which adsorbents would chemically react with the pigments being separated¹⁰.

Many chemists at the time were not impressed with Tswett's work and the new technique of chromatography lay dormant for several decades. In 1930 Edgar Lederer used chromatography to separate xanthophylls in egg yolk, and this work was cited by several research groups in Europe to investigate natural substances¹⁰. In 1937 two Hungarian scientists published a textbook, *Die Chromatographische Adsorptionsmethode*, which greatly helped chromatography gain acceptance.

A major breakthrough came in 1941 when A. J. P. Martin and R. L. M. Synge published a paper on partition chromatography¹¹. They introduced the idea of separations based on differences in the partition between two liquid phases; one which was immobilized in a silica gel and an immiscible one that could flow past it. They developed the theory of chromatography and introduced the idea of "theoretical plates" based on ideas from distillation. Martin and Synge ultimately won the Nobel Prize in Chemistry for developing partition chromatography in 1952. Martin went on to develop paper chromatography with A. H. Gordon in 1943. Paper chromatography was much simpler and faster than traditional chemistry techniques and was quickly adopted by biochemists studying amino acids and saccharides. Several groups around this time tried planar variations of chromatography, from Izmailov and Shraiber's "spot chromatography" to Meinhard and Hall's "surface chromatography" to Justus Kirchner's "chromatostrips"¹². Egon Stahl coined the term "thin layer chromatography" in a 1956 paper and was instrumental in standardizing the technique.

1.1.1 Gas Chromatography

Martin and Synge hinted at the concept of gas chromatography in their 1941 paper by saying "The mobile phase need not be a liquid but may be a vapor."¹¹ Vapor phase chromatography was

introduced by Martin and A. T. James in 1951¹³. In the early days columns were packed with stationary phases made by impregnating crushed fire bricks with non-polar chemicals such as squalene or stopcock grease¹⁴. The original detector was a gas density balance made of a Wheatstone network of capillary tubes drilled out of a solid block of copper¹⁵. During the 1950s the flame ionization detector, katharometer, and the β -ray detector were introduced.

Marcel Golay at Perkin-Elmer was interested in the theory behind separations, and to simplify his experiments he used an open tubular capillary to simulate a channel through a packed column. Performance in open tubular capillaries was dramatically improved compared to packed columns, and when he presented his findings at the GC Symposium in Amsterdam in 1958 his chromatograms produced a "gasp of astonishment from the audience"¹⁶. Early capillary columns were made from stainless steel, which was cheap but had several problems¹⁷. The tubing often had residual oils inside from the manufacturing process and needed to be carefully cleaned prior to coating with stationary phase. The metal had active sites that would cause tailing on polar compounds unless a surfactant was added to mask them, and a thick coating of stationary phase was needed to cover the uneven metal surface. In 1960 Dennis Desty and coworkers at British Petroleum developed an instrument that could draw long glass coils, making it possible to use glass capillaries in GC¹⁸. Initial glass capillaries had very short lifetimes because the stationary phase would only adsorb if the surface was in an oxide form. The capillaries were brittle and impurities such as boron in borosilicate glass could interfere with analytes. In 1979 a breakthrough occurred when researchers at Hewlett-Packard described the manufacture and use of fused silica capillaries¹⁹. These flexible capillaries were coated with either silicone rubber or polyimide to prevent breakage and contained far fewer impurities. Stationary phases improved with the development of polysiloxane polymers and the ability to covalently bond them to the capillary surface. Today capillary GC is a mature technique that is standard in many laboratories.

1.1.2 Liquid Chromatography

Compared to gas chromatography, classical liquid chromatography was an inherently slow technique because the diffusion of analytes is much slower in a liquid than a gas. Csaba Horváth, an experienced gas chromatographer at Yale Medical School, was unimpressed with the state of liquid chromatography and set out to build an instrument. In 1965 he developed a modern liquid chromatograph that incorporated high pressures and a UV-Vis detector, which he called high pressure liquid chromatography, or HPLC¹⁷. He used pellicular particles coated with a thin adsorbant layer of carbon black as a packing²⁰. Picker Nuclear Company built a commercial instrument based on this work, which they called the Nucleic Acid Analyzer, and during the 1960s several other instruments became commercially available.

Theory suggested that smaller particles would lead to improved performance, but preparing columns with particles smaller than 30 μm was a challenge. In 1972 slurry packing was introduced that could handle 5 – 10 μm silica particles²¹. Silica is used because it is strong enough to withstand the pressure gradients and the surface can be modified with a variety of functional groups. Most early experiments used a polar stationary phase and non-polar mobile phases, but the development of siloxane bonded functional groups made reverse phase HPLC possible. Today C18 columns are the most popular and 92% of HPLC users are using reverse phase²². Smaller particle size increases efficiency but also leads to increasing backpressure. In 1997 Jorgenson devised a specialized instrument that could pack capillaries with 1.5 μm silica particles at 60,000 psi, then run separations at 19,000 psi²³. Plate numbers over 200,000 were obtained, even for highly retained compounds. Waters Corporation introduced the Acquity UltraPerformance Liquid Chromatography system in 2004²⁴, and today ultra-high pressure liquid chromatography (UPLC) is a popular technique for fast and efficient LC separations.

1.1.3 Capillary Electrophoresis

Another approach to separations is to use charge instead of pressure as the driving force. Electrophoresis was introduced as an analytical technique in 1930 by Tiselius when he separated alpha, beta, and gamma-globulin²⁵. Gels are often used as supports for electrophoresis, especially polyacrylamide gels for proteins denatured with sodium dodecylsulfate (SDS-PAGE). In 1967 Hjerten performed electrophoresis in a glass tube²⁵, and in 1981 Jorgenson and Lukacs introduced capillary zone electrophoresis (CZE)²⁶. Both CZE and gel electrophoresis have been incredibly useful for the separation of biomolecules including amino acids, peptides, proteins, and nucleic acids. CZE was instrumental in the completion of the Human Genome Project by automating the process and using high throughput capillary arrays²⁷.

1.1.4 Electrokinetic Chromatography

Capillary electrophoresis works well for separating charged species, but neutral compounds have no electrophoretic mobility of their own. In 1984 Terabe added a surfactant, sodium dodecyl sulfate (SDS), to a borate-phosphate buffer in an open tubular capillary and could separate a mixture of 14 phenols²⁸. This technique came to be known as micellar electrokinetic chromatography (MEKC) and the surfactant was called a pseudo-stationary phase (PSP). SDS is very effective as a PSP; it has a high mobility, produces efficient separations with sharp peaks, is commercially available in high purity, and is affordable. However, there are a few disadvantages. SDS cannot be used with a high percentage of organic modifier because it disrupts the micellar structure. Surfactants are incompatible with mass spectrometric detection, and high concentrations of surfactants in solution lead to high conductivity and Joule heating. Researchers have developed a range of alternative PSPs including microemulsions²⁹, cyclodextrins³⁰, carbon nanotubes³¹, molecular micelles and polymers.

Palmer and McNair introduced oligomerized sodium-10-undecylenate as a PSP in 1992^{32,33}. These molecular micelles, also known as polymeric surfactants, are surfactants that have been crosslinked in the core. These structures have no CMC, eliminating the problem of free surfactant in solution contributing to high conductivities, and can withstand high percentages of organic modifiers. However, there is limited control of the selectivity through functional groups. Wallingford and Ewing introduced polymer particles as PSPs³⁴, and Nilsson et al used polymer nanoparticles that were compatible with mass spectrometers in 2006^{35,36}. In 2010 Palmer and Hilder synthesized acrylic acid/butyl acrylate diblock copolymers that formed latex nanoparticles using RAFT polymerization^{37,38}, which provided greater control over the synthesis. Hyslop et al expanded these types of polymers to include 2-acrylamido-2-methyl-1-propane sulfonic acid (AMPS) anionic blocks and ethyl acrylate and methyl acrylate hydrophobic blocks to explore the effects of different core and shell chemistries on selectivity³⁹. The development of new PSPs is an ongoing project for many researchers interested in optimizing selectivity for a variety of applications.

1.2 Theory

Analytical techniques like chromatography are fundamentally the physical separation of compounds between two phases. Matter in a system has a certain amount of chemical potential, μ_i , which represents the free energy per mole of solute at constant temperature and pressure. Affinity for the solvent and dilution are taken into account by the equation

$$\mu_i = \mu_i^0 + RT \ln(C_i) \quad (1-1)$$

where μ_i^0 is the standard state chemical potential, R is the gas constant, T is the temperature, and c_i is the concentration. The standard state chemical potential depends on molecular interactions between the solute and solvent, and is lowest when interactions are favorable. Every compound has a different

chemical potential, and some will be solubilized more favorably in certain phases than others. For a solute in equilibrium between two phases the partition coefficient (K) is

$$K = \frac{a_1}{a_0} = e^{\frac{-\Delta\mu_i^0}{RT}} \quad (1-2)$$

where a_0 and a_1 are the activities in phase 0 and phase 1, and μ_i^0 is the difference in chemical potential for the solute in the two different phases. This difference can also be expressed by

$$\Delta\mu_i^0 = \Delta H_i^0 + T\Delta S_i^0 \quad (1-3)$$

showing that both entropy and enthalpy contribute. Separations are possible because of these differences. The most basic separation is liquid-liquid extraction, where two immiscible liquids are shaken together and the solute will partition into the phase where its chemical potential is lowest.

Most separations techniques use transport to facilitate the separation process. Transport can either be the solutes themselves moving towards equilibrium, or flow of a bulk carrier fluid. The net velocity can be expressed as $W = U + v$, where W is the sum of the velocities, U is the velocity caused by chemical potential gradients, v is the velocity caused by bulk displacement. The forces accelerating the bulk fluid are balanced out by resistance forces and an average steady state velocity is reached. The driving force could be gravity, a pump, or an electric field.

1.2.1 Chromatography Theory

The IUPAC defines chromatography as “a physical method of separation in which the components to be separated are distributed between two phases, one of which is stationary (stationary phase) while the other (the mobile phase) moves in a definite direction”⁴⁰. The stationary phase can be a packed column or an open tubular capillary. There are three types of separation: displacement, where a solute adsorbs to a solid stationary phase and is physically displaced by another solute; frontal

analysis, where a sample is fed continuously and components break through at different times depending on their affinity for the adsorbent; and elution, which is a series of adsorption/extraction processes as a sample moves down the column⁴¹. Elution is the most common form of chromatography for both analytical and preparatory work.

An analyte in chromatography partitions between the stationary phase and the mobile phase according to its partition coefficient K , which was defined in Equation 1-2. K can be inferred from the retention factor (k) with the equation

$$k = K \frac{V_s}{V_m} \quad (1-4)$$

where V_s is the volume of analyte in the stationary phase and V_m is the volume in the mobile phase. K is a ratio of concentrations, while k is a ratio of amounts. A compound that has a higher affinity for and spends more time in the stationary phase will take more time to reach the detector than a compound that spends less time in the stationary phase. The retention factor can be calculated from experimental data by looking at a chromatogram of the analyte and an unretained compound:

$$k = \frac{t_r - t_0}{t_0} \quad (1-5)$$

where t_0 is the time it takes the unretained compound to reach the detector, and t_r is the time it takes the retained analyte to reach the detector. The difference between t_r and t_0 is the time the analyte spent in the stationary phase.

Whether two compounds can be separated by chromatography is determined by the selectivity (α) of the system. Selectivity is driven by the chemical potentials of the analytes; it is easier to separate compounds with different molecular properties than it is to separate very similar compounds. Selectivity can be quantified as a ratio of retention factors, with the more retained compound as the numerator to give a value greater than one.

$$\alpha = \frac{k_B}{k_A} \quad (1-6)$$

Selectivity can be optimized by carefully controlling the stationary phase and mobile phase to maximize intermolecular interactions.

Another important factor is the efficiency of a chromatographic system. As a zone of analyte travels through a column or capillary it broadens due to diffusion and dispersion. The language used to describe this broadening is borrowed from distillation: imagine a column consists of a series of theoretical plates. A column of given length with more theoretical plates is more efficient than one with fewer, and the more theoretical plates there are in a given length of column, the smaller the height equivalent to a theoretical plate (HETP, or H). The plate model does not do a good job describing what takes place in a chromatographic system, but the terms are still used.

There are three important components in band broadening, which are expressed by the Van Deemter Equation

$$H = A + \frac{B}{v} + Cv \quad (1-7)$$

where A represents eddy diffusion in a packed column, B represents longitudinal diffusion, and C represents mass transfer kinetics. A is a significant term in liquid chromatography where an analyte must navigate through the small particles of stationary phase, while B is significant in gas chromatography because diffusion happens much more quickly in the gas phase. C can be significant in both techniques due to diffusion in the mobile phase (LC) or the stationary phase (GC). The B and C terms are proportional to velocity, and every chromatographic system has an optimal velocity where H is lowest and the separation is most efficient.

Resolution, or the ability to distinguish one peak from another, depends on the efficiency, selectivity, and retention. This is seen quantitatively in the master resolution equation

$$R_s = \frac{\sqrt{N}}{16} * \frac{\alpha-1}{\alpha} * \frac{k-1}{k} \quad (1-8)$$

To increase resolution between two peaks a chromatographer can increase efficiency through a longer or more efficient column, change the retention by altering the temperature in GC or changing the mobile phase in LC, or manipulate the selectivity by changing the stationary phase or mobile phase.

1.2.2 Linear Solvation Energy Relationships (LSER)

To optimize selectivity, it is crucial to understand the different intermolecular interactions taking place in a separations system. These include dispersion forces, dipole interactions, dipole-induced dipoles, and hydrogen bonding, which are shown in a diagram in Figure 1-1.

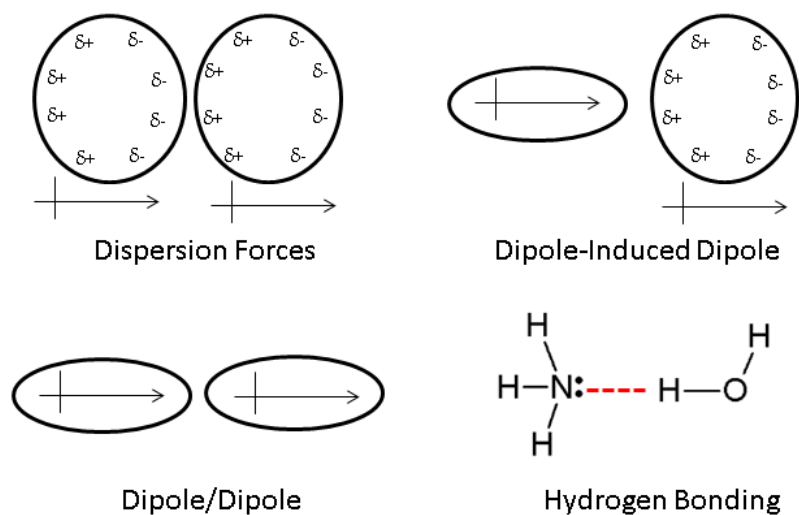


Figure 1-1: Four different intermolecular forces.

Several models have been developed to understand these interactions, starting by focusing on solvents. In 1974 Snyder⁴² took a set of solubility data for 82 volatile liquids published by Rohrschneider⁴³ and transformed the data into a polarity index (P'):

$$P' = \log(K_g)_{\text{ethanol}} + \log(K_g)_{\text{dioxane}} + \log(K_g)_{\text{nitromethane}} \quad (1-9)$$

where K_g'' is a measure of the excess retention of the solute relative to an n-alkane of equivalent molar volume, which corrects for the effect of dispersion interactions. Three selectivity parameters can be calculated that represent the fraction of P' contributed by interactions with ethanol by good proton acceptors; interactions with dioxane by good proton donors; or interactions with nitromethane through a large dipole moment. The parameters were then defined as:

$$X_e = \frac{\log(K_g'')_{ethanol}}{P'} \quad X_d = \frac{\log(K_g'')_{dioxane}}{P'} \quad X_n = \frac{\log(K_g'')_{nitromethane}}{P'} \quad (1-10)$$

These three parameters can be used to construct a triangular diagram that classifies solvent selectivity. Snyder classified the 82 solvents into 8 different groups.

One of the earliest forms of the LSER equation was developed to study solvents

$$SP = c + S(\pi^* + d\delta) + a\alpha + b\beta \quad (1-11)$$

where SP is a solvent parameter that can be measured, π^* is the solvent polarity, δ is the polarizability, α is the hydrogen bond donating ability, and β is the hydrogen bond accepting ability of a solvent⁴⁴.

Kamlet and Taft developed solvent scales for π^* , α , and β using spectroscopy to measure the frequency change of specific molecular probes that were carefully chosen to only reflect one type of interaction.

Abraham adapted the model for studying solutes instead of solvents and simplified the nomenclature. The current Abraham model has been used by many researchers and is expressed by the following equation⁴⁵

$$SP = c + vV + eE + sS + aA + bB \quad (1-12)$$

The SP used in chromatography is the log of the retention factor ($\log(k)$), which is related to the partition coefficient and chemical potential of the solute as described above. Each solute has a tabulated value for its McGowan characteristic volume (V), excess molar refraction (E), dipolarity/polarizability (S),

hydrogen-bond acidity (A), and hydrogen-bond basicity (B). The coefficients (v, e, s, a, and b) represent the difference between the two phases the solute is transferring between. The model views the transfer of a solute to a solvent as a three-step process: a cavity forms in the solvent, which breaks up the intermolecular forces between solvent molecules and is energetically unfavorable; a solute is inserted into the cavity; then intermolecular interactions take place between the solute and solvent molecules. The vV term in the equation represents the unfavorable cavity formation, and eE, sS, aA, and bB represent favorable interactions between the solute and solvent. The c term is a system constant that captures the phase ratio and anything not reflected in the other parameters. The coefficients are calculated using multiple linear regression analysis, with the solute descriptors as independent variables and the measured log(k) values as dependent variables. LSER can be run on different chromatographic systems and used to compare stationary phases⁴⁶.

1.2.3 Electrophoresis Theory

When an electric field is applied to an ion in solution, it will migrate at a velocity that is dependent on the field strength, the temperature, the electrolyte solution, and the ion's size and charge. The electrostatic forces accelerating the ion are opposed by the viscous force of the solution for a net electrophoretic velocity (v_{ep}) of

$$v_{ep} = \frac{qE}{6\pi\eta r_s} \quad (1-13)$$

where q is the charge of the ion, E is the electric field strength, η is the solution viscosity, and r_s is the hydrodynamic or Stoke's radius of the ion. The electric field strength is the voltage difference across a distance, V/L, where V is the voltage in volts and L is the distance over which the voltage is applied in cm. In CE, V is the applied voltage and L is the length of the capillary. The electrophoretic mobility (μ_{ep}) can also be calculated by dividing the velocity by the field strength. Electrophoretic mobility is related to the zeta potential (ζ) by the equation

$$\mu_{ep} = \frac{\epsilon_r \epsilon_0}{\eta} \zeta \quad (1-14)$$

where ϵ_r and ϵ_0 , are the relative permittivity and permittivity in a vacuum, and η is the viscosity of the surrounding fluid. The velocity is affected by temperature, which decreases the viscosity of the electrolyte solution. Ionic strength affects the sphere of counter ions surrounding the ion and also plays a role.

The electric field affects the electrolyte solution as well. CE capillaries are typically made of fused silica, which has a net negative charge from silanol groups at the surface. Cations in the electrolyte solution, which is usually called the background electrolyte (BGE), are attracted to the negative surface and form an electric double layer with a layer of fixed ions and layer of mobile ions. When an electric field is applied to the capillary the mobile ions migrate to the cathode, pulling the bulk liquid along with them. This electrically generated flow is known as the electroosmotic flow (EOF). Unlike systems with pressure driven flow like HPLC, which have a parabolic flow profile, the EOF has a flat flow profile. This reduces dispersion and band broadening and increases the efficiency of CE separations.

An analyte measured by CE will have an apparent electrophoretic mobility (μ_{app}) that is the sum of its electrophoretic mobility and the electroosmotic mobility of the BGE.

$$\mu_{app} = \mu_{ep} + \mu_{eo} \quad (1-15)$$

If the mobilities are in the same direction then μ_{app} is large and the analyte reaches the detector quickly, but if they are opposite μ_{app} is small, zero, or even negative if $|\mu_{ep}| \geq \mu_{eo}$. In this case the analyte will never reach the detector. In a typical CE system the EOF is in the direction of the cathode and cations have the greatest μ_{app} . To analyze anions, a cationic modifier can be added to the BGE that adsorbs to the silica surface of the capillary and creates a positive zeta potential. Anions in the BGE form the

electric double layer, and if the polarity of the electrodes is reversed the EOF will now be in the anodic direction and anions will have the greatest μ_{app} . By adding a neutral marker compound such as acetone, the μ_{ep} for a given analyte can be calculated by measuring the migration time of acetone (t_0) and the analyte (t_r) and using the equation

$$\mu_{ep} = \frac{L * L_t}{V} \left(\frac{1}{t_0} - \frac{1}{t_r} \right) \quad (1-16)$$

1.2.4 Electrokinetic Chromatography Theory

In EKC a PSP is added to the BGE to interact with neutral compounds. A PSP must have a charged region to provide electrophoretic mobility, and a region that can interact with the analytes of interest. This is often hydrophobic, but could target other intermolecular interactions as well. Ionic surfactants can be used as a PSP if they are added to the BGE in amounts above their critical micelle concentration (CMC) so that they form micelles with an ionic shell and hydrophobic core. The charged shell gives the micelles an electrophoretic mobility in the opposite direction of the EOF, and an apparent mobility that is slower than the EOF. Analytes are then able to partition between the BGE and the core of the micelles. Analytes travel at the velocity of the EOF in the BGE but at the velocity of the micelles when in the micelle core, which gives the analyte an apparent electrophoretic mobility and migration time somewhere between the t_0 and t_{PSP} . Analytes with different affinities for the micelles will have different apparent electrophoretic mobilities, which results in a separation.

The retention behavior of an analyte during EKC can be described by equation ²⁸:

$$k = \frac{t_r - t_0}{t_0 \left(1 - \frac{t_r}{t_{PSP}} \right)} \quad (1-17)$$

where t_r is the migration time of the analyte, t_0 is the migration time of an unretained compound, and t_{PSP} is the migration time of the PSP. At infinite PSP retention the equation becomes equation 1-5 for retention on a traditional stationary phase.

Resolution in MEKC is based on differences in electrophoretic mobility and separation selectivity, as described by the master resolution equation for EKC⁴⁷:

$$R_s = \frac{\sqrt{N}}{4} * \left(\frac{\alpha - 1}{\alpha}\right) * \left(\frac{k_2}{1 + k_2}\right) * \left(\frac{1 - \frac{t_0}{t_{PSP}}}{1 + \left(\frac{t_0}{t_{PSP}}\right)k_1}\right) \quad (1-18)$$

Resolution can be altered by changing the PSP, adding modifiers to the BGE, and modifying the capillary to change the EOF⁴⁸. Different surfactants will have different selectivities based on the hydrophobicity of the micelle core or the chemistry of the ionic head group. Using polymer PSPs instead of surfactants opens up more opportunities for differences in selectivity by increasing the chemistries available.

Additives include organic solvents and chiral species to enhance selectivity. Organic modifiers in the BGE lower the viscosity and typically reduce analyte retention, which will shorten analysis times. This can improve the separation, but care must be taken not to disrupt the PSP structure.

1.3 Research Aims

The goal of this dissertation research is to develop an EKC method to separate anions and nitro compounds commonly found in explosives and explosives residues. Although EKC has been used to separate the nitroaromatic explosives described in EPA Method 8330⁴⁹⁻⁵⁴, and CE has been used to separate anions found in explosives and post-blast residues⁵⁵⁻⁶¹, to the best of my knowledge a technique that combines these separations has not been described in the literature. Example electropherograms of an EKC separation of nitro compounds and a CE separation of anions found in explosives are shown in Figure 1-2. Although CE is a well-developed technique for the analysis of ions, there is room for improvement in the EKC separation, which takes over 40 minutes. A further literature review can be found in the introduction to Chapter 5.

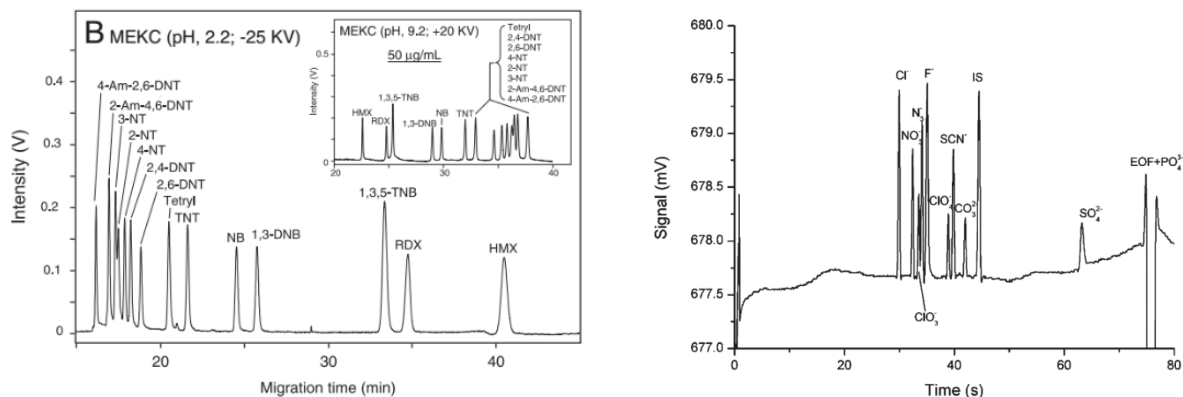


Figure 1-2: Explosives and Anions separated by EKC and CE^{52,57}

The project was divided into three specific aims:

1. Synthesize and characterize a variety of cationic latex nanoparticles.
2. Evaluate the performance of different nanoparticles as pseudo-stationary phases for EKC.
3. Develop a method to separate anions and nitroaromatics in a single analytical run.

Two cationic monomers and three hydrophobic monomers were used to synthesize six different types of diblock copolymers to use as PSPs. Their synthesis and characterization are described in Chapter 2. It was found that a separate cationic polymer coating was necessary to use with the cationic nanoparticles to prevent nanoparticle/analyte interactions at the capillary wall; this work is discussed in Chapter 3. The nanoparticles' performance as a PSP was characterized through LSER analysis; this work is found in Chapter 4. A mixture of anions, nitroaromatic, and nitramine compounds were separated using these cationic PSPs, which is presented in Chapter 5. Finally, conclusions and suggestions for future work are laid out in Chapter 6.

Chapter 2: Synthesis and Characterization of Cationic Latex Nanoparticles

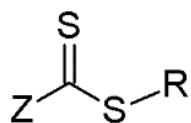
2.1 Introduction

This chapter will describe the synthesis and characterization of cationic latex nanoparticles by RAFT polymerization and self-assembly of amphiphilic diblock copolymers.

2.1.1 RAFT Polymerization

Free radical polymerization is a useful technique for creating materials with specific physical properties. A monomer is chosen that contains a vinyl group and the desired functional group. An initiator that decomposes into radicals either thermally or photochemically is used to begin the reaction. Unfortunately, the uncontrolled reaction often leads to a broad range of polymer chain lengths, which is described as the dispersity (\mathcal{D}). Controlled polymerizations use an agent to control the radical polymerization process and reduce the dispersity of the finished sample. Living polymerizations include functionality that is retained in the final polymer, allowing the polymerization to continue in a subsequent step. Examples of these types of controlled/living polymerizations include atom-transfer radical polymerization (ATRP), nitroxide mediated polymerization (NMP), and reversible addition-fragmentation chain transfer polymerization (RAFT). RAFT was developed by researchers at CSIRO in Australia and was introduced in a *Macromolecules* paper in 1998⁶². It uses a chain transfer agent (CTA) to reversibly add and fragment growing radical chains, and works well with a wide range of monomers.

The CTA is at the heart of RAFT polymerization. A CTA must have a S=C-S moiety which a propagating radical can add to and generate a tertiary radical intermediate, which can then fragment



and regenerate the double bond. CTAs also have an R-group and a Z-group, which act

as a good leaving group and to modify the reactivity, respectively. A generic

structure is shown in Figure 2-1. The choice of R-group and Z-group play an

Figure 2-1: Generic structure of a CTA

important role in the polymerization. The R-group must be stable enough to fragment off the CTA as $R \cdot$, but it should be more favorable to add to a monomer than a polymeric CTA⁶³. The Z-group moderates the reactivity of the CTA with transfer coefficients decreasing as follows: dithiobenzoates > trithiocarbonates > dithiocarbonates > dithiocarbamates⁶⁴. More reactive monomers must be used with a more reactive CTA, and less reactive monomers with a less reactive CTA for the best results. Trithiocarbonates, where the Z-group is connected to an S, have the added advantage that chain extension can take place on both sides⁶⁵.

A schematic of the RAFT mechanism is shown in Figure 2-2. In the first step an initiator (I) is used to start the propagation of radicals ($P_n \cdot$). In the second step, a radical can add to the center carbon in the CTA to form a tertiary radical intermediate. The R-group will then fragment to form $R \cdot$ and the CTA will reform a C=S bond. The $R \cdot$ can reinitiate other monomers to form more propagating chains ($P_m \cdot$). During chain equilibration propagating radical chains add and fragment with the CTA until the monomer in solution is gone. Termination reactions between chains can also occur, but this is less likely than in uncontrolled free radical polymerization. If the ratio of CTA to initiator is high, then most polymer chains will have a RAFT end-group at the end of polymerization and retain their living character. This means that the polymer can be reinitiated with a second monomer and easily create a diblock copolymer. By controlling the chemistry and the lengths of different blocks, a variety of polymer architectures can be created.

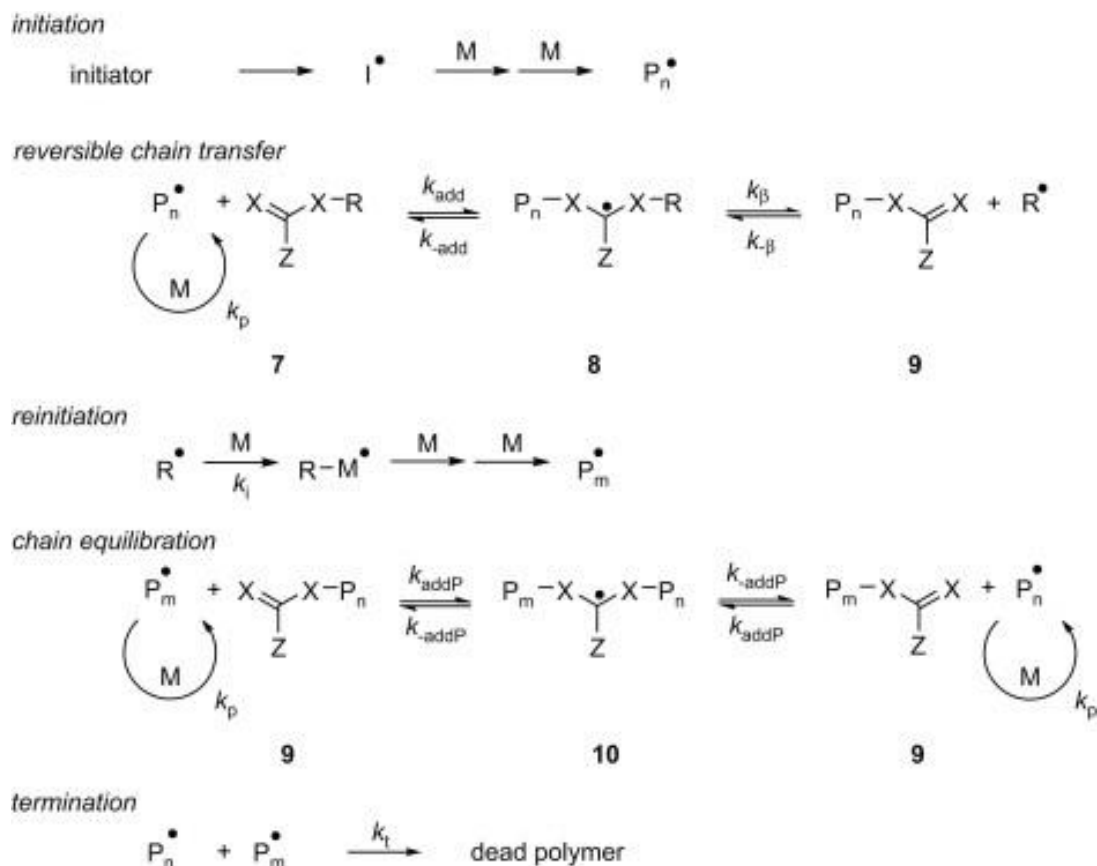


Figure 2-2: The RAFT Mechanism⁶⁶

A diblock copolymer containing an ionic, hydrophilic block and a hydrophobic block could be used as a PSP for EKC. The Palmer research group used RAFT polymerization to create diblock copolymers using acrylic acid and butyl acrylate using 2-[[[(butylsulfanyl)carbonothioyl]sulfanyl]propanoic acid as a CTA³⁷, which is shown in Figure 2-3. The procedure described by Ferguson et al⁶⁷ uses RAFT to first polymerize a hydrophilic monomer to form a macroCTA, a hydrophilic polymer with relatively short chains that contains the trithiocarbonate functionality.

When the Z-group is hydrophobic, these macroCTA chains are similar to surfactants. The macroCTA is then reinitiated and used to polymerize a hydrophobic monomer. The synthesis is performed in water, and the growing diblock copolymers form micelles. The hydrophobic monomer

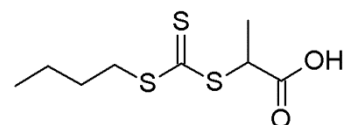


Figure 2-3: CTA used by the Palmer research group

will partition to the interior of the micelles which contain the reactive CTA groups, and polymerization continues inside the micelles. As polymerization progresses the micelles evolve into latex nanoparticles. Jesse Hyslop has expanded the scope of monomers to include 2-acrylamido-2-methyl-1-propane sulfonic acid (AMPS), methyl acrylate (EA), and ethyl acrylate (EA) using the CTA described by Ferguson³⁹ to create nanoparticles for use as PSPs. These are all anionic nanoparticles.

The first aim of this research was to expand the range to include cationic monomers. Two cationic monomers, [2-(Acryloyloxy)ethyl]trimethylammonium chloride (AETMAC) and (3-Acrylamido-propyl)trimethylammonium chloride (APTAC) were used to create cationic macroCTAs and three hydrophobic monomers, butyl acrylate (BA), ethyl acrylate (EA), and methyl acrylate (MA) were used for the hydrophobic cores. The structures of these monomers are shown in Figure 2-4.

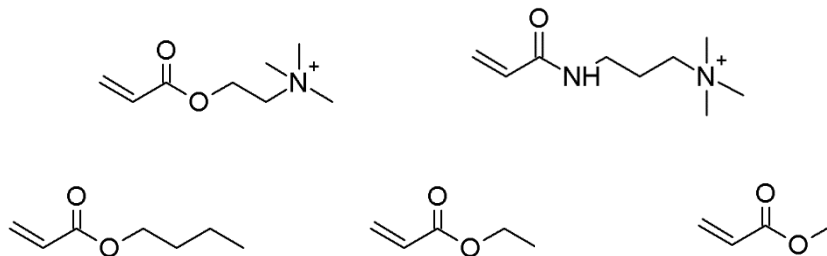


Figure 2-4: The structures of the monomers used in this research.
From top left: AETMAC, APTAC, BA, EA, and MA.

2.2 Experimental

2.2.1 Synthesis

All CTAs, macroCTAs, and diblock copolymers are named after the laboratory notebook page in which they are described. JM was the first notebook, JRM was the second notebook used to record

synthetic work, and KB was the notebook of undergraduate student Kim Brown. The polymers are referred to by a combined acronym where the hydrophobic monomer is listed before the hydrophilic monomer. For example, a butyl acrylate and [2-(Acryloyloxy)ethyl]trimethylammonium chloride diblock copolymer is referred to as BAAETMAC.

2.2.1.1 Chain Transfer Agent Synthesis

The chain transfer agent 2-[[butylsulfanyl]carbonothioyl]sulfanyl]propanoic acid was synthesized by the Ferguson procedure⁶⁷ with minor alterations. Water (6 mL), acetone (2 mL), 10 M sodium hydroxide (4.0 mL, 40 mmol), 1-butanethiol (6.2 mL, 58 mmol), and carbon disulfide (3.8 mL, 85 mmol) were combined in a roundbottom flask and stirred with a magnetic stir bar under nitrogen for 30 minutes. In an ice bath, 2-bromopropionic acid (3.7 mL, 41 mmol) was added dropwise, followed by 26.5 mL of 1.5 M sodium hydroxide. The solution was stirred under nitrogen for 18 hours. CTA was precipitated from solution with 10 mL of 10 M hydrochloric acid and extracted into dichloromethane. The organic fraction was evaporated in vacuo and the resulting oil was recrystallized from pentane. Three batches were used to polymerize cationic monomers and form macroCTA: JM5, LH117, and JRM8. JM5 was synthesized on 1/16/13, JRM8 was synthesized on 1/28/15, and LH117 was synthesized by Leah Hall before I began my work.

2.2.1.2 MacroCTA Synthesis

MacroCTA was synthesized by using the CTA to polymerize either AETMAC or APTAC cationic monomer. Over the course of this research 33 batches of macroCTA were synthesized. Some were used to make diblock copolymers, others were synthesized to study the reaction kinetics or develop characterization methods. The synthesis of JM51 AETMAC macroCTA is described as an example. AETMAC (1.736 g, 7.2 mmol) was washed with dichloromethane to remove inhibitor, then combined with CTA (0.1671 g, 0.7 mmol), and 4,4'-azobis(4-cyanovaleric acid) initiator (0.0220 g, 0.08 mmol) in 20

mL of deionized water. The solution was sparged with nitrogen for 20 minutes in an ice bath to remove oxygen, then was transferred to a sand bath and heated at 70° C for six hours. During some syntheses 1 mL aliquots were removed from solution and lyophilized for ¹H NMR analysis. Conditions for important batches are listed in Table 2-1.

Table 2-1: Synthetic Conditions for Selected MacroCTAs

Name	Monomer Type	Monomer	CTA	Initiator	Reaction Volume	Reaction Time	Reaction Temperature	Aliquots Taken?
JM51	AETMAC	1.736 g	0.1671 g	0.0220 g	20 mL	6 Hours	70° C	Yes
JM90	APTAC	3.186 g	0.2473 g	0.0295 g	20 mL	6 Hours	70° C	Yes
JM130	AETMAC	7.310 g	1.4081 g	0.1643 g	30 mL	6 Hours	70° C	No
JM157	AETMAC	1.798 g	0.1645 g	0.0242 g	20 mL	6 Hours	70° C	Yes
JM158	AETMAC	3.570 g	0.2403 g	0.0265 g	20 mL	6 Hours	70° C	Yes
KB1	APTAC	3.012 g	0.2567 g	0.0267 g	20 mL	6 Hours	70° C	No
KB2	AETMAC	3.172 g	0.2361 g	0.0243 g	20 mL	6 Hours	70° C	No
JRM1	AETMAC	18.414 g	3.5050 g	0.2103 g	100 mL	6 Hours	70° C	Yes

2.2.1.3 Diblock Copolymer Synthesis

Diblock copolymers were synthesized by chain extending a macroCTA with a hydrophobic monomer. An overhead stirrer was used to prevent phase separation, and monomer was added at 1 mL/hour via a syringe pump. Several hydrophobic monomers were tried to explore the effect of different chemistries on selectivity, including methyl acrylate, ethyl acrylate, butyl acrylate, hexyl acrylate, cyclohexyl acrylate, 2-ethyl phenyl acrylate, and styrene. Altogether 42 different nanoparticles were synthesized, but not all of them proved suitable for EKC. The ones that were studied in depth are described in Table 2-2 and include AETMAC and APTAC hydrophilic blocks and BA, EA, and MA hydrophobic blocks. The synthesis of nanoparticle JM132 BAAETMAC is presented below. JM130 AETMAC macroCTA (1.24 g, ~1 mmol) and initiator (0.0342 g, 0.1 mmol) were dissolved in 50 mL of deionized water. Butyl acrylate (6.7 mL, 47 mmol) was washed with 1 M sodium hydroxide and delivered by syringe pump at 1 mL/hour. The reaction was heated to 70° C under nitrogen and allowed

to continue overnight. The solution was dialyzed against deionized water in 2500 MWCO dialysis tubing. The dialyzed solution was concentrated down by rotary evaporation to 26% wt/wt, and 1 mL was lyophilized for wt/wt % determination and ¹H NMR analysis.

Two sets of nanoparticles were synthesized simultaneously in batches of six to try and reduce the variability in synthetic conditions. These were carried out by Kim Brown by placing all the required starting materials in a 30 mL vial with a magnetic stir bar. Six reactions took place in six vials that were connected by a series of nitrogen inlets and outlets in a 70° C oil bath. One set was made using KB1 APTAC macroCTA and one was made using KB2 AETMAC macroCTA.

Table 2-2: Synthetic Conditions for Selected Diblock Copolymers

Name	MacroCTA	Initiator	Hydrophobic Monomer	Monomer Volume	Reaction Volume	Method	Appearance	Wt %
JM132	1.23 g JM130	0.0342 g	BA	6.7 mL	50 mL	Overhead	Milky White	25.97%
JM136	1.23 g JM130	0.0375 g	EA	6 mL	50 mL	Overhead	Milky White	13.98%
JM137	1.23 g JM130	0.0360 g	MA	8 mL	50 mL	Overhead	Chunky Yellow	15.09%
JM142	0.41 g JM130	0.0324 g	EA	6 mL	50 mL	Overhead	Opaque Yellow	11.48%
KB3A	0.3 g KB1	0.0072 g	BA	1.8 mL	20 mL	Stir bar	Pale Yellow	9.96%
KB3C	0.3 g KB1	0.0072 g	MA	2.3 mL	20 mL	Stir bar	Opaque Yellow	7.78%
KB3D	0.3 g KB1	0.0072 g	BA	3.7 mL	20 mL	Stir bar	Yellow	7.35%
KB3F	0.3 g KB1	0.0072 g	MA	1.2 mL	20 mL	Stir bar	Clear Yellow	8.39%
KB4D	0.2 g KB2	0.0056 g	EA	2.2 mL	20 mL	Stir bar	Milky White	7.39%
KB4F	0.2 g KB2	0.0056 g	BA	2.9 mL	20 mL	Stir bar	Pale Yellow	6.11%

2.2.2 Characterization

Two types of NMR experiments were used: ^1H NMR and diffusion NMR. Aliquots taken from a macroCTA reaction mixture were lyophilized and reconstituted in approximately 0.7 mL of D_2O . A small amount of finished solid macroCTA was dissolved in approximately 0.7 mL of D_2O . NMR spectra were obtained either with a 400 MHz Bruker or a 500 MHz Varian instrument. Diblock copolymers were lyophilized and reconstituted in approximately 0.7 mL of D_2O or CDCl_3 .

Diffusion NMR experiments were performed on certain nanoparticles at the University of South Australia with the assistance of Nathan Williamson. Pulsed gradient stimulated echo (PGSTE) experiments were performed on a Bruker 600 MHz Avance III HD NMR Spectrometer equipped with a Diff30 gradient set, micro5 probe, and 5 mm RF coil. Sinusoidal shaped gradient pulses with a duration of 1.58 ms were used, and the observation time was set to 50 ms. Each experiment used 32 linearly spaced gradient steps and each step contained 16 scans. Two component diffusion coefficients were estimated by fitting the signal attenuation with a biexponential model using the Stejskal-Tanner equation in MATLAB. This provided random residuals and stable fits, and incorporated Monte-Carlo error analysis to estimate 95% confidence intervals of the fit parameter values. The diffusion coefficients were converted to hydrodynamic diameters with the Stokes-Einstein-Sutherland equation.

MALDI-TOF MS analysis was performed on a Bruker microFlex instrument equipped with a 337 nm nitrogen laser. Bruker Peptide Calibration Mix was used for calibration of the instrument, and 2,5-dihydroxybenzoic acid (DHB) was used as a matrix. Solutions of matrix and macroCTA were made at 10 mg/mL in a 70:30 mixture of 0.1% TFA in water and acetonitrile. A MSP BigAnchor 96 AnchorChip target plate was used. Spots were prepared by adding 1 μL of macroCTA solution to the target plate, then 3 μL of DHB solution was deposited on top and the solutions dried together. Spectra were taken in linear mode with a 20 kV acceleration voltage. 200 shots were taken with 90% laser power and 60 Hz

frequency per spectrum and summed. Bruker Compass for Flex Series software was used for instrument control and analysis. Spectra were baseline corrected and smoothed in FlexAnalysis, and then the mass lists were exported to Microsoft Excel for statistical analysis.

A Malvern Zetasizer Nano ZS was used for dynamic light scattering (DLS) measurements. Samples were diluted with water to 0.01% wt/wt and filtered through 0.45 μm nylon filters prior to analysis to remove dust or aggregates. The zeta potentials of 0.1% wt/wt aqueous solutions of nanoparticles in glass cuvettes were acquired with a Nicomp 380 ZLS Zeta Potential/Particle Sizer at the University of South Australia.

TEM images were taken with a JEOL JEM-2100F transmission electron microscope at the University of South Australia. Stock nanoparticle solutions were diluted to 0.002% wt/wt, and 5 μL were applied to carbon coated copper grids and allowed to air dry.

Non-aqueous CE was investigated at the University of South Australia with the assistance of Adam Sutton and research continued at the University of Montana. Aliquots of nanoparticle solution were lyophilized and reconstituted in organic solvent BGE. 10 mM ammonium acetate was used as the electrolyte and methanol, ethanol, and acetonitrile were used as solvents. Capillaries were coated with JM159 PAETMAC cationic capillary coating prior to analysis.

2.3 Results and Discussion

2.3.1 Synthesis

The CTA described by Ferguson⁶⁷ was used to facilitate RAFT polymerization in all experiments. This CTA was designed for work with acrylic acid monomers so the R-group contains a carboxylic acid.

Despite the functional group on the R-group not matching the quaternary amines of the cationic monomers, this CTA appears to work well for the polymerization of quaternary ammonium monomers.

MacroCTAs were synthesized using both AETMAC and APTAC monomers with a target degree of polymerization (DP) between 5 and 10 repeating units. In early syntheses the monomer solution was measured by volume, but this was not very accurate due to the high viscosity of the concentrated aqueous monomer solutions. In syntheses performed after 6/26/13 the solution was measured by mass and washed with dichloromethane to remove inhibitor. MacroCTA can be studied by ^1H NMR using D_2O as a solvent. During synthesis of several macroCTAs aliquots were removed from solution, frozen, lyophilized, and reconstituted in D_2O to monitor reaction kinetics. A ^1H spectrum of AETMAC monomer is shown in Figure 2-5:

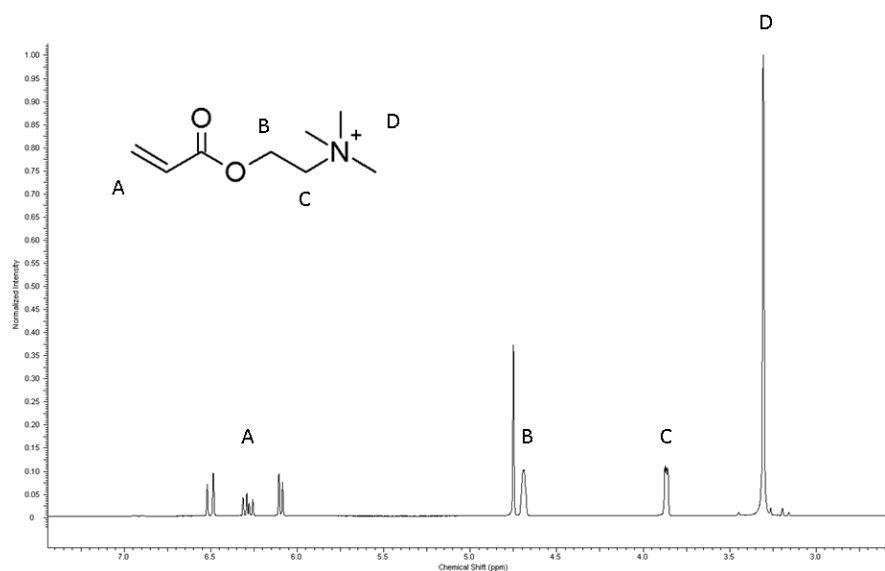


Figure 2-5: ^1H NMR Spectrum of AETMAC monomer

As the reaction progresses the vinyl peaks at 6.0 – 6.5 ppm disappear and are replaced by broad peaks at 1.5 – 2.5 ppm as the polymer backbone develops. Peaks B, C, and D on the cationic pendant chain broaden as monomer turns to polymer, and signals from the chain transfer agent appear from 1 – 2 ppm. A ^1H NMR spectrum of an AETMAC macroCTA is shown in Figure 2-6.

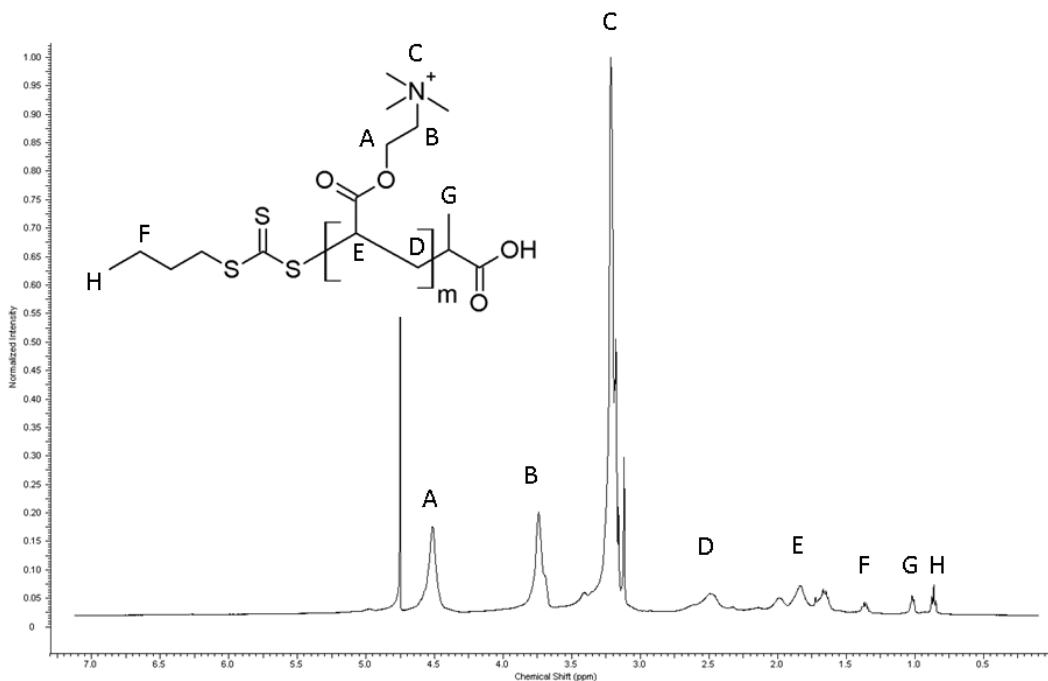


Figure 2-6: ¹H NMR Spectrum of AETMAC macroCCTA

The % conversion can be calculated by integrating the vinyl peaks (A in Figure 2-5) and the backbone peaks (D and E in Figure 2-6), and finding the ratio of polymer to total signal. There is some overlap with peaks from the end-groups, which introduces some error into the calculation. A graph of the polymerization progress can be made calculating the % conversion for each aliquot. There appears to be an initial retardation period, then conversion plateaus by hour four, as seen in the polymerization of JM51 AETMAC in Figure 2-7.

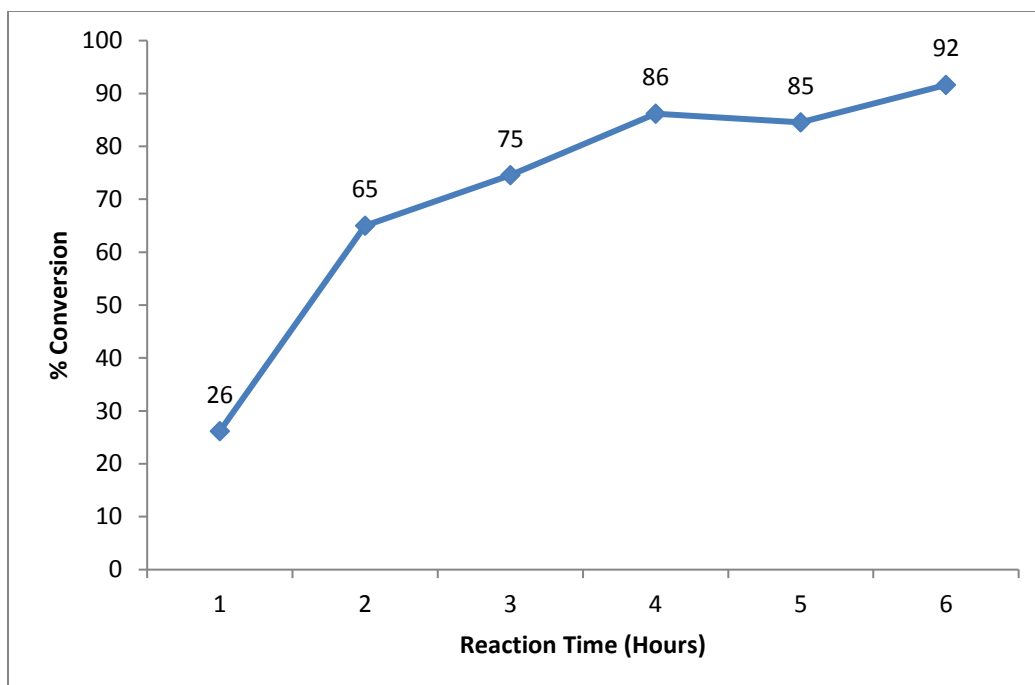


Figure 2-7: Polymerization of JM51 AETMAC macroCTA.

This process was undertaken for several batches of APTAC macroCTA as well. The ^1H NMR spectrum of APTAC monomer is shown in Figure 2-8. Unfortunately, one of the peaks on the APTAC pendant chain overlaps with a signal in the emerging polymer backbone, so it is more difficult to accurately calculate the % conversion. A ^1H NMR spectrum of APTAC macroCTA is shown in Figure 2-9. The vinyl peaks do decrease in size over the course of the reaction, and the signals from the pendant chains broaden. The two carbons next to the nitrogen atoms cannot easily be distinguished in the monomer, but can be seen separately in the polymer as the environment around them changes.

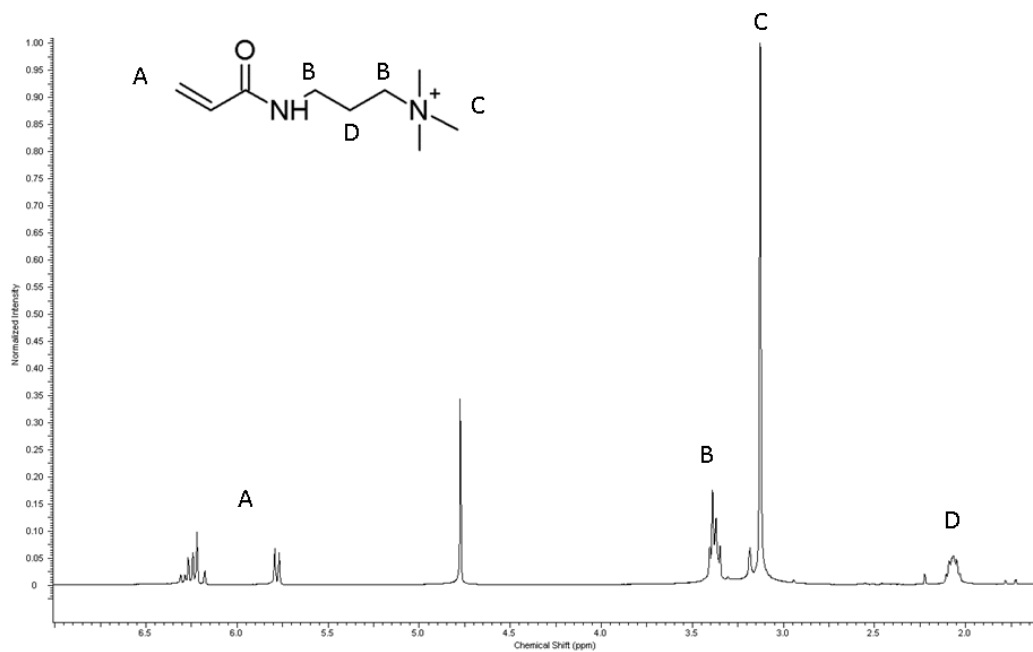


Figure 2-8: ^1H spectrum of APTAC monomer

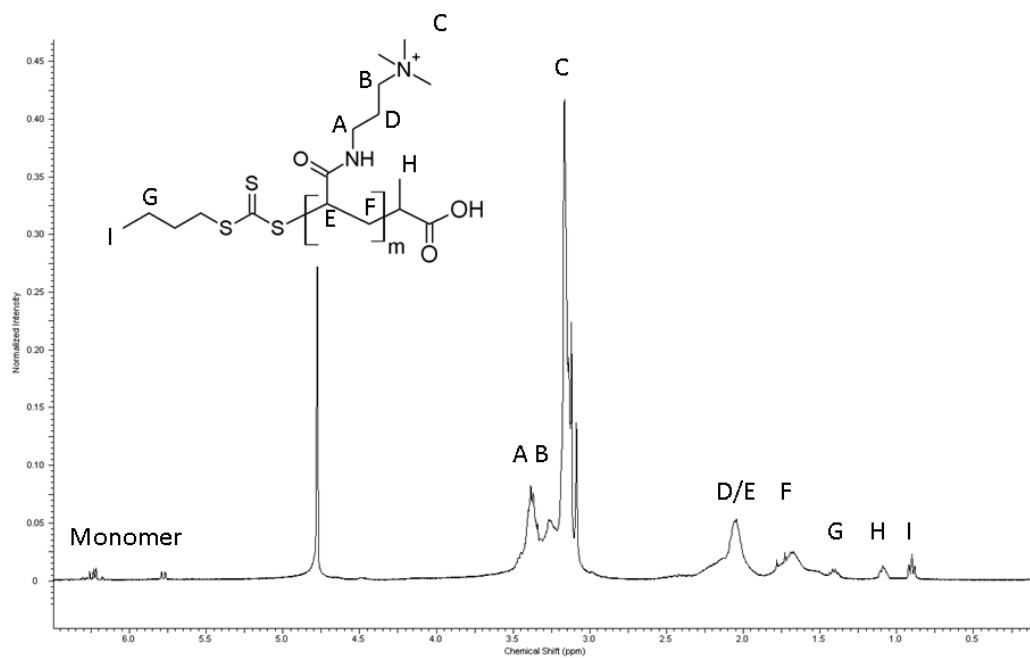


Figure 2-9: ^1H spectrum of APTAC macroCTA

Diblock copolymers are more challenging to synthesize. Due to their hydrophobic nature an overhead stirrer is used to prevent phase separation between the liquid monomers and the water used as a solvent. Despite this, most of the time solids were observed on the reaction flask and glass stir rod at the end of the reaction, suggesting that some of the hydrophobic monomer is polymerizing with itself to form insoluble hydrophobic homopolymer. This means that the stoichiometry of the initial reaction mixture will not directly translate into the degree of polymerization of the products. Of the hydrophobic monomers used, only methyl acrylate, ethyl acrylate, and butyl acrylate resulted in nanoparticles suitable for EKC. Even with the overhead stirrer it was very difficult to get the more hydrophobic hexyl acrylate, styrene, and 2-ethyl phenyl acrylate into solution enough to react with the macroCTA.

2.3.2 Characterization

The most common way to characterize synthetic polymers is size exclusion chromatography (SEC), which separates species by their hydrodynamic volume. A calibration curve must be made from low dispersity molecular weight standards. A universal calibration curve can be used by including the Mark-Houwink coefficients relating to intrinsic viscosity for different polymers. The polymer must be dissolved in a good solvent so the chain is in a random coil, not stretched or compressed. Unfortunately, SEC can result in significant errors if the polymer being analyzed is different than the polymers used to make the calibration curve, and there are not many cationic polymer standards commercially available. Researchers have shown that SEC is not an accurate technique for the analysis of cationic polymers because it is difficult to avoid non size-exclusion interactions⁶⁸. Therefore, SEC is not a reliable method for the characterization of the polymers synthesized in this research, so other methods were investigated.

2.3.2.1 MacroCTA

^1H NMR can also be used to calculate the degree of polymerization (DP). A big benefit to the Ferguson CTA is that the signal from the CH_3 on the end of butyl chain is distinct from all the polymer signals. Since there is only one of these per polymer molecule, the integration of this methyl peak can be set to 3 and then the ratio of polymer signal to end-group signal can be calculated. This is known as end-group analysis, and will reveal the degree of polymerization of the polymer chain⁶⁹. The number average molecular weight (M_n) can then be calculated. A drawback to this approach is that traces of monomer left in the sample will make the polymer signals bigger than they really are and over-inflate the calculated number. The NMR spectrum is an average of the all the different polymer chains in the sample, so nothing is learned about the polymer dispersity. The DP and M_n for several batches of macroCTA are shown in Table 2-3. These were calculated by integrating the two CH_2 signals on the ethyl group and the quaternary amine signals, dividing by the number of protons, then averaging the three results. The DP is then multiplied by the molecular weight of the repeating unit and the end-group mass is added to calculate M_n .

Table 2-3: ^1H NMR Characterization Data for AETMAC MacroCTA

MacroCTA	DP	M_n
JM7	18.0	3723
JM21	9.0	1974
JM27	6.7	1541
JM30	6.8	1564
JM31	6.6	1519
JM32	8.4	1858
JM40	4.3	1077
JM48	8.5	1878
JM50	6.9	1577
JM51	5.3	1256
JM63	13.7	2884
JM130	16.1	3360
JM157	8.3	1836
JM158	11.2	2430
JRM1	16.7	3478
KB2	11.2	2414

Since the R end-group contains a carboxylic acid, it should be possible to do end-group analysis of these polymers through an acid-base titration. The weight in grams of a sample of macroCTA is carefully measured, then the sample is titrated with standardized sodium hydroxide. There is one acid group per polymer chain, so assuming all the carboxylic acid protons are accessible, finding the end point will reveal how many moles are in solution. Dividing the mass of the sample by the number of moles should give the number average molecular weight of the polymer sample.

Titration attempts were made on several batches of AETMAC macroCTA solutions in water using 0.01 M NaOH that was standardized against KHP. Some drift was observed in early experiments, so pH readings were taken at 1 minute and 5 minutes after adding 0.1 mL of NaOH. For the first four base additions the reading is consistent at 1 and 5 minutes, but once the pH increased above 6 the pH would decrease by about 0.5 pH units over the course of five minutes, which can be seen in Figure 2-10. This made it difficult to determine where the endpoint in the titration was. This trend was not so apparent for APTAC macroCTA, although the end-point is still not very sharp. Titration attempts were made for seven batches of AETMAC macroCTA and four batches of APTAC macroCTA, the results are listed in Table 2-4. In some cases the degree of polymerization found through end-group analysis is higher than the theoretical degree of polymerization based on reaction stoichiometry.

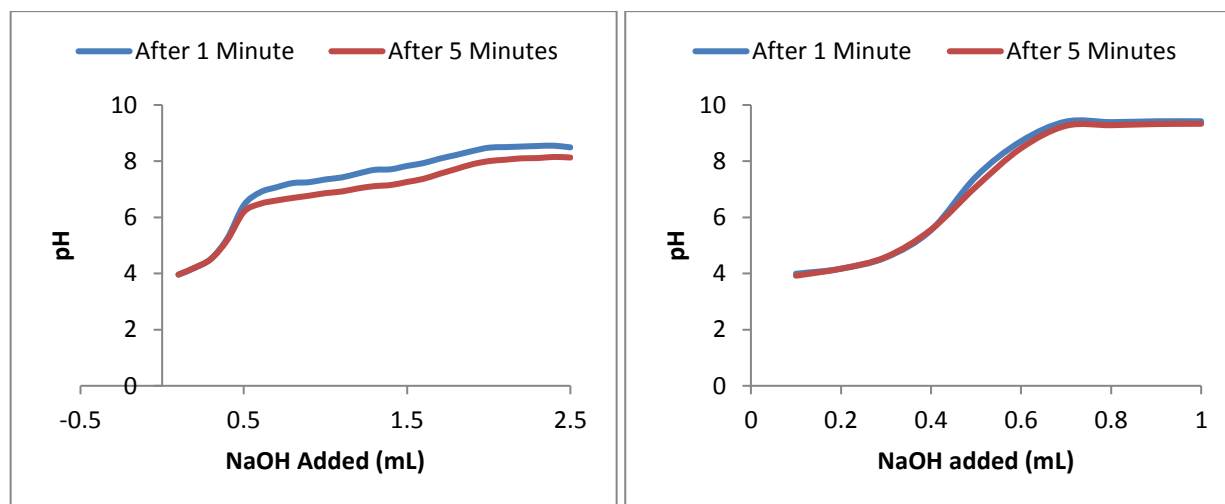


Figure 2-10: Titrations of JM21 AETMAC macroCTA (left) and JM61 APTAC macroCTA (right)

Table 2-4: Titration Data for MacroCTAs

Sample	Polymer Weight	Titrant	Endpoint	M_n	DP	Theoretical DP
JM21 AETMAC	0.0407 g	9.82 mM NaOH	1.7 mL	2438 g/mol	14 mer	18 mer
JM30 AETMAC	0.0099 g	9.82 mM NaOH	0.9 mL	2086 g/mol	12 mer	18 mer
JM31 AETMAC	0.0594 g	9.82 mM NaOH	2.9 mL	1120 g/mol	6 mer	18 mer
JM48 AETMAC	0.0146 g	10 mM NaOH	0.6 mL	2433 g/mol	13 mer	10 mer
JM50 AETMAC	0.0232 g	10 mM NaOH	1.2 mL	1933 g/mol	11 mer	10 mer
JM51 AETMAC	0.0337 g	10 mM NaOH	1.0 mL	3370 g/mol	20 mer	10 mer
JM61 APTAC	0.0189 g	10 mM NaOH	0.5 mL	3780 g/mol	20 mer	10 mer
JM81 APTAC	0.0730 g	9.82 mM NaOH	2.5 mL	2973 g/mol	16 mer	10 mer
JM83 APTAC	0.0474 g	23.1 mM NaOH	1.5 mL	1369 g/mol	7 mer	10 mer
JM87 APTAC	0.2293 g	25.0 mM NaOH	2.5 mL	3248 g/mol	15 mer	20 mer
JM90 APTAC	0.1559 g	25.0 mM NaOH	2.9 mL	2188 g/mol	9 mer	10 mer

The most effective way found to characterize macroCTAs is to use MALDI-TOF MS. Unlike other characterization techniques discussed so far, MALDI is capable of analyzing individual polymer chains instead of an average. This makes it possible to look at the number average molecular weight (M_n), weight average molecular weight (M_w), and dispersity (\mathcal{D}) of a sample using the following equations:

$$M_n = \frac{\sum N_i M_i}{\sum N_i} \quad (2-1)$$

$$M_w = \frac{\sum N_i M_i^2}{\sum N_i M_i} \quad (2-2)$$

$$\mathcal{D} = \frac{M_w}{M_n} \quad (2-3)$$

where N_i and M_i represent the signal peak area and corrected mass, respectively⁷⁰.

After much trial and error in sample preparation it was found that the combination of 1 μL of 10 mg/mL polymer solution with 3 μL of 10 mg/mL DHB solution applied on top and dried together produced the best spectra. The laser power needed to be substantially increased to maximize the signal intensity. Initial work was performed with 2-polyvinylpyridine (PVP) polymer standards, which were the

closest thing to a cationic polymer standard available. These standards produced spectra showing an envelope of peaks spaced 106 mass units apart, which corresponds to the molecular weight of one protonated repeating unit of PVP. A mass spectrum of a PVP standard with a reported M_n of 4880 u and M_w of 5460 u is shown in Figure 2-11.

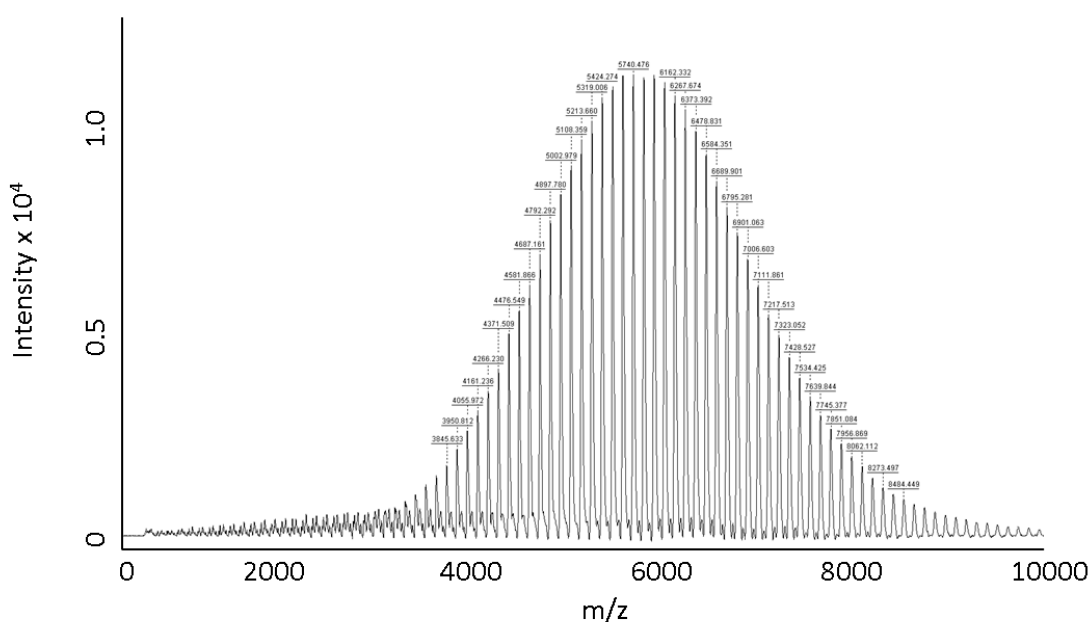


Figure 2-11: A MALDI-TOF mass spectrum of 2-polyvinylpyridine

The cationic macroCTA polymers synthesized by RAFT also had mass spectra that showed an envelope of peaks, but the spectra were more complex. There were four series of peaks within the envelope, and the interval between them was larger than expected. A spectrum of JM158 AETMAC and JM90 APTAC macroCTAs are shown in Figure 2-12.

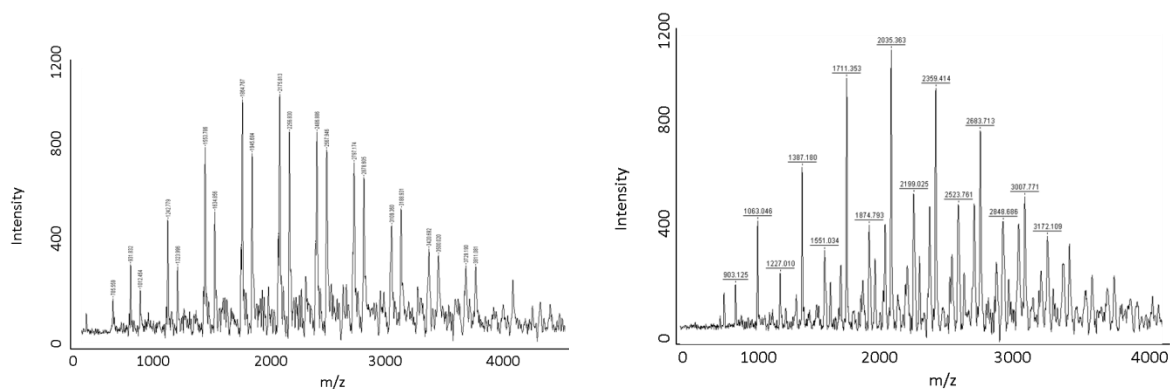


Figure 2-12: MALDI-TOF spectra of JM158 AETMAC (left) and JM90 APTAC (right) macroCTAs

The mass difference between peaks in a series is 311 u for AETMAC and 324 u for APTAC, which is greater than the 158 u for AETMAC without a chloride counter ion or 171 u for APTAC without a chloride counter ion. However, the spacing does correspond to an AETMAC-DHB or APTAC-DHB adduct. Adduct formation is not common in MALDI, but has been seen before in the literature⁷¹. Looking at the m/z for the series of peaks reveals that one series corresponds to polymer chains with their end-groups intact, one series corresponds to polymer chains that had lost the R-group, one series corresponds to polymer chains that had lost the Z-group, and one series where both end-groups were lost. The most prominent series were chains with either both end-groups intact and chains with no Z-group. The Z-group contains the trithiocarbonate that is designed to easily fragment, so it is not surprising that the energy from the laser during the MALDI process leads to fragmentation. This has been seen before with RAFT polymers and other types of controlled polymer syntheses⁷². Several batches of macroCTA were analyzed using MALDI-TOF MS, the results are shown in Table 2-5.

Table 2-5: MacroCTAs Characterized by MALDI-TOF MS

Sample ID	Polymer	M _n	M _w	Đ	DP
JM32	AETMAC	1083	1124	1.04	5
JM40	AETMAC	877	905	1.03	4
JM48	AETMAC	954	1006	1.05	4.5
JM157	AETMAC	1018	1071	1.05	5
JM158	AETMAC	1435	1497	1.04	7
KB2	AETMAC	889	915	1.03	4
JM68	APTAC	1079	1121	1.04	5
JM90	APTAC	1349	1412	1.05	6
JRM3	APTAC	1073	1118	1.04	5
KB1	APTAC	1196	1271	1.06	6

The degrees of polymerization found by NMR are consistently higher than those found by MALDI-TOF MS. This could be due to monomer still present in the samples making the NMR integration over-estimate the polymer peaks, or there could be mass discrimination in the MALDI-TOF. Other researchers have shown that mass discrimination is a problem with the analysis of polymers by MALDI-TOF MS, especially for polydisperse samples⁷³. Studies suggest that higher mass components are underrepresented compared to lower mass components⁷⁴. It is also possible that the DHB-adducts only form on lower molecular weight polymer chains.

2.3.2.2 Diblock Copolymers

Diblock copolymers are notoriously difficult to characterize, and cationic polymer are even more so. In addition, the diblock copolymer chains aggregate to form supramolecular latex nanoparticle structures through self-assembly. There is evidence of this in the NMR data. If a sample of diblock copolymer is lyophilized, the NMR spectrum is dependent on the solvent the sample is reconstituted in. Figure 2-13 shows JM142 EAAETMAC dissolved in D₂O. The solid polymer was not very soluble, and the water peak dominates the polymer signals. However, you can see the quaternary amine peak from the macroCTA at 3.12 ppm.

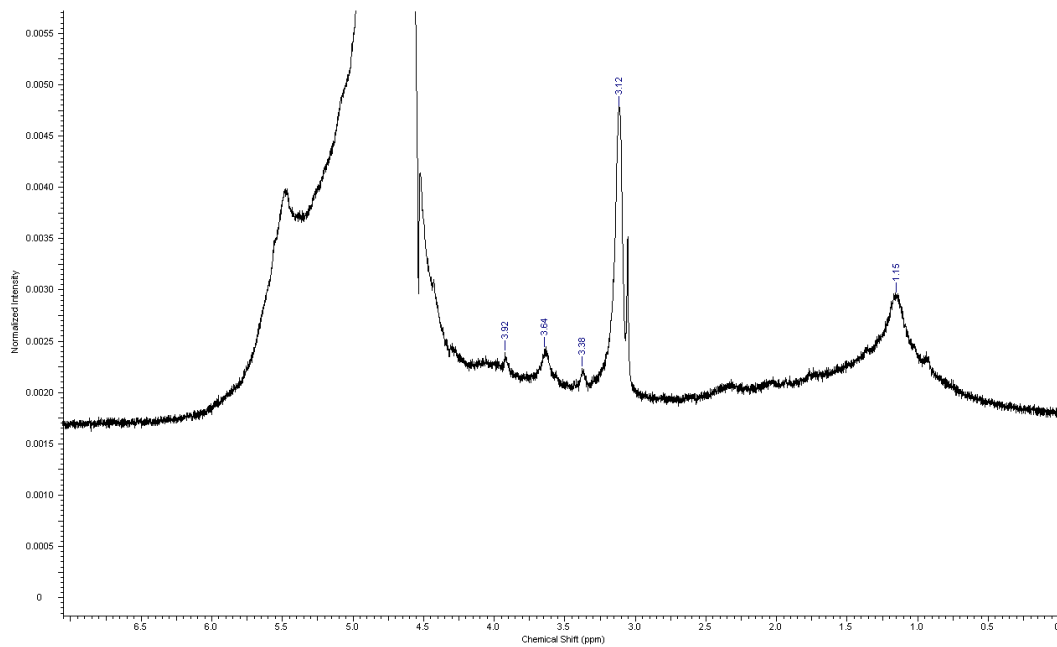


Figure 2-13: ¹H NMR spectrum of JM142 EAAETMAC in D₂O

The spectrum looks much different in CDCl₃, as shown in Figure 2-14. Signals from the ethyl acrylate are clearly seen at 4.08 and 1.22 ppm, and the quaternary amine at 3.12 is not present.

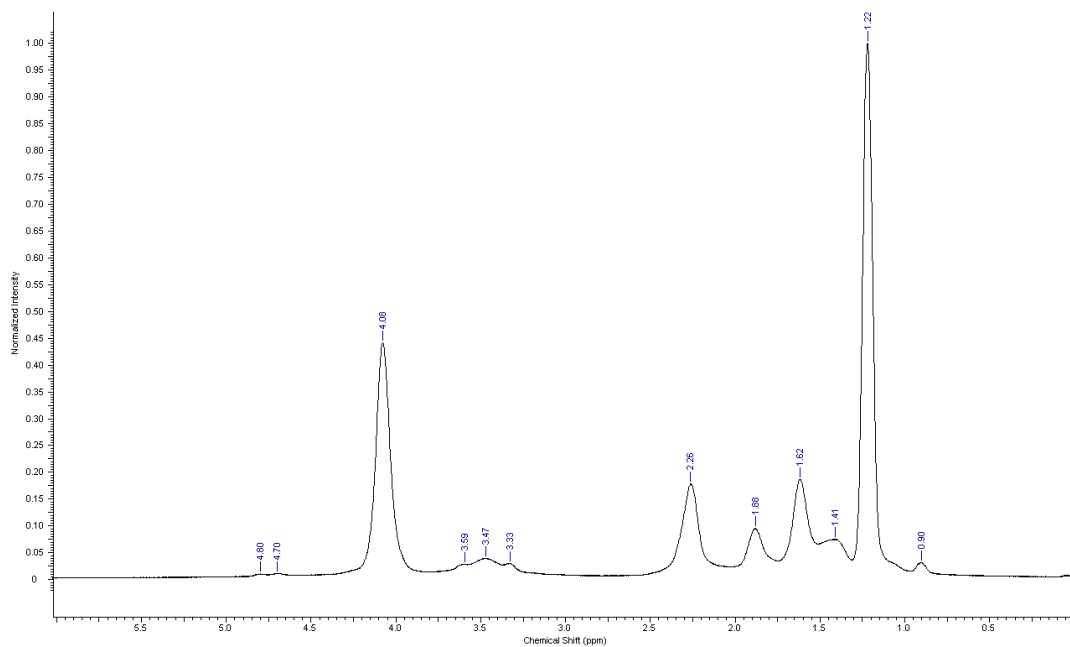


Figure 2-14: ¹H spectrum of JM142 EAAETMAC in CDCl₃.

The fact that one block is visible in one solvent but not the other suggests that the latex structure is dynamic and can form inverse micelles in organic solvent to shield the hydrophilic block. If the latex nanoparticles were a cross-linked structure they would not be able to behave so dynamically.

In order to try and investigate individual polymer chains, samples of the diblock copolymers were lyophilized and reconstituted in polar organic solvents in an attempt to solubilize both the hydrophilic and hydrophobic blocks. Methanol, ethanol, and acetonitrile were attempted, and methanol appeared to be the most effective for the most samples. Some of the milky white, more hydrophobic samples did not redissolve after lyophilization. Electropherograms showed a sharp peak that appeared at the same migration time as neutral DMSO, and a second, broad peak that had a longer migration time. This is shown for KB4B MAAETMAC, KB4D EAAETMAC, and KB4F BAAETMAC nanoparticle in Figure 2-13. There seems to be a larger component of homopolymer in the butyl acrylate sample than in the ethyl or methyl acrylate samples. However, without known standards for comparison quantitative data could not be obtained.

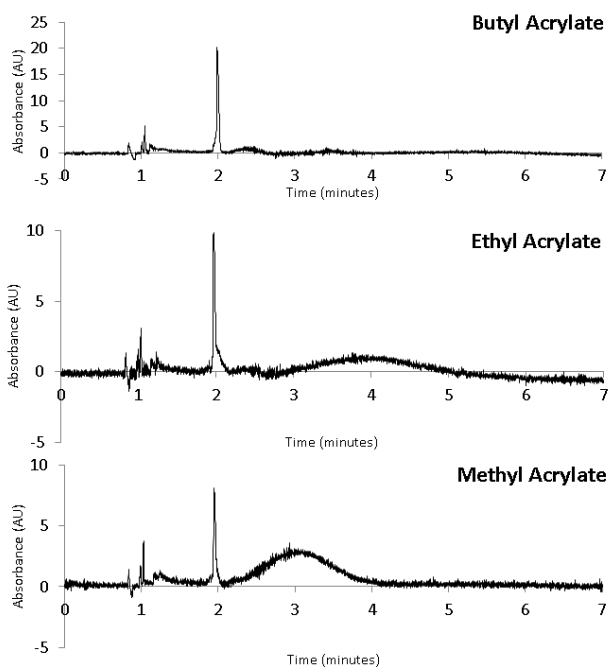


Figure 2-15: Non-Aqueous CE of KB4F BAAETMAC, KB4D EAAETMAC, and KB4B MAAETMAC nanoparticles using 10 mM ammonium acetate in methanol as BGE

Other important parameters to measure are the nanoparticle size and zeta potential. Two methods for measuring particle size were used: dynamic light scattering (DLS) and diffusion NMR. DLS instrumentation is easy to use, but samples must be carefully filtered to exclude dust particles, and the right concentration must be chosen so that enough scattering is detected but aggregation does not take place. A concentration of 0.01% wt/wt was found to produce enough scattering for data analysis, but the standard deviations of the measurements were quite high.

Diffusion NMR uses similar mathematical principles to transform a measured diffusion constant to a radius. A series of pulsed gradient steps are carried out, and the signal decays as the molecules diffuse away from where they started. Diffusion measurements were carried out on KB3F MAAPTAC nanoparticles in CDCl_3 , acetone- d_6 , and D_2O at 0.3%, 0.1%, and 0.01% wt/wt. The signal attenuation was found to be independent of observation time, which suggests that individual diblock copolymer chains are not exchanging in and out of the nanoparticles on the NMR timescale. Signal attenuation was also found to be independent of concentration, suggesting that particle/particle interactions are negligible.

The signal at 3.2 ppm from the quaternary amine on the hydrophilic block was chosen for analysis because it is present in all nanoparticles, as can be seen in Figure 2-16:

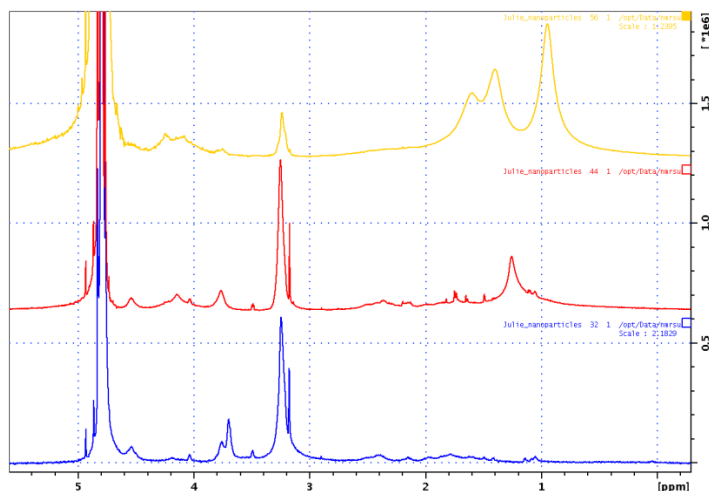


Figure 2-16: NMR spectra of JM132 BAAETMAC (top, yellow), JM136 EAAETMAC (middle, red), and JM137 MAAETMAC (bottom, blue) nanoparticles.

The signal attenuations were analyzed with a fitting routine and Monte-Carlo error analysis in MATLAB R2016a. The best fit was a biexponential fit, as seen in Figure 2-17. It is most apparent in the JM137 MAAETMAC sample.

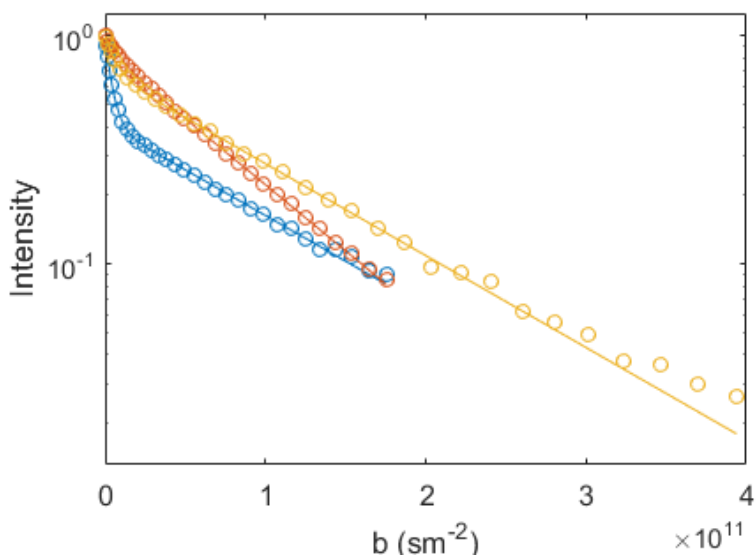


Figure 2-17: Signal attenuation for JM132 BAAETMAC (yellow), JM136 EAAETMAC (red), and JM137 MAAETMAC (blue) nanoparticles showing a biexponential fit.

The two exponential fits can then be transformed into diffusion coefficients through the Stejskal-Tanner equation, and the diffusion coefficients can be used to calculate the hydrodynamic radii with the Stokes-Einstein-Sutherland equation. These results are shown graphically in Figure 2-18. In each case there is a component with a slower diffusion coefficient and a component with a faster diffusion coefficient. Since diffusion and size are inversely proportional, this means that each sample contains a larger species and a smaller species. The larger structure is believed to be the latex nanoparticles, and the smaller piece could either be unreacted macroCTA or small copolymer chains that are not incorporated into the larger structure. There appeared to be a higher percentage of this smaller component in the more hydrophilic methyl acrylate nanoparticles.

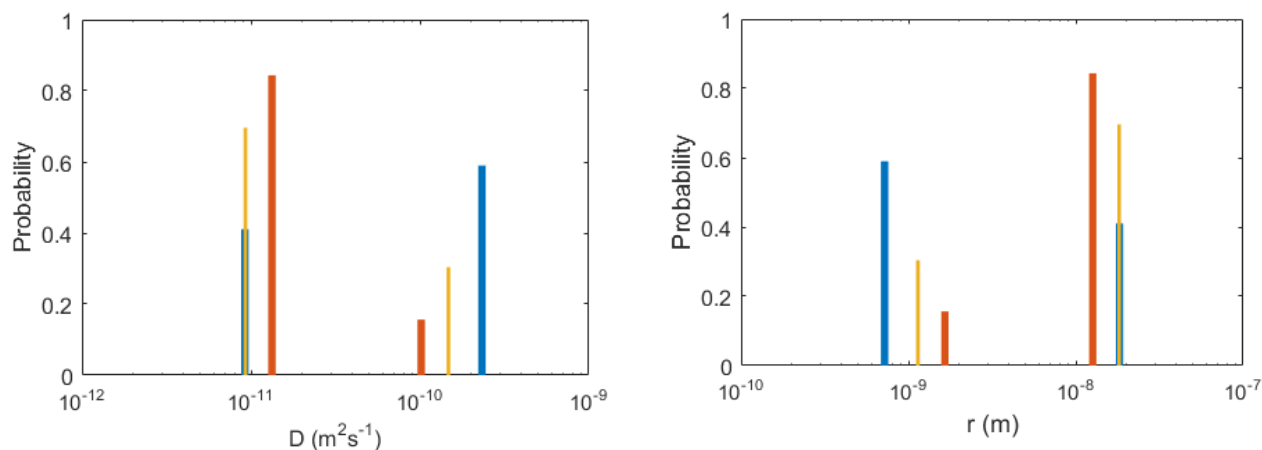


Figure 2-18: Diffusion coefficients (left) and hydrodynamic radii (right) of JM132 BAAETMAC (yellow), JM136 EAAETMAC (red), and JM137 MAAETMAC (blue) nanoparticles

The zeta potential and sizes found by both DLS and diffusion NMR for 10 nanoparticle samples are listed in Table 2-6. The sizes are consistently larger for DLS measurements. In general the fraction of smaller component found by diffusion NMR is greater for methyl acrylate nanoparticles. This makes sense because methyl acrylate is the most hydrophilic and have the greatest chance of being solubilized in water.

Table 2-6: Nanoparticle Size Characterization

Nanoparticle	Zeta Potential (mV)	Z-Average Diameter (DLS)	Average Nanoparticle Diameter (diffusion NMR)	Fraction of Smaller NMR Component
JM132 BAAETMAC	50.77	98.82	36.2 (0.92)	0.304 (0.007)
KB4F BAAETMAC	44.33	95.66	20.8 (0.51)	0.190 (0.015)
KB3A BAAPTAC	33.39	67.7	34.0 (0.10)	0.318 (0.001)
KB3D BAAPTAC	41.02	82.07	32.2 (0.41)	0.250 (0.013)
JM136 EAAETMAC	44.78	109.6	55.4 (0.91)	0.525 (0.004)
JM142 EAAETMAC	46.51	58.99	39.2 (0.20)	0.076 (0.003)
KB4D EAAETMAC	41.02	103.5	25.2 (0.10)	0.157 (0.005)
KB3C MAAPTAC	46.51	68.53	41.6 (0.82)	0.35 (0.009)
JM137 MAAETMAC	40.20	85.46	36.4 (0.51)	0.59 (0.002)
KB3F MAAPTAC	52.85	41.34	30.2 (0.41)	0.464 (0.006)

The values in parentheses are standard deviations.

Polymers are difficult to image with electron microscopy because there is little contrast between the organic sample and the carbon coated copper grid, and they can easily burn in the electron beam. Several attempts were made at the University of South Australia, and although most either burned or formed large aggregates, a successful image was taken of JM136 EAAETMAC. The size of the imaged nanoparticles is quite similar to the size obtained by diffusion NMR.

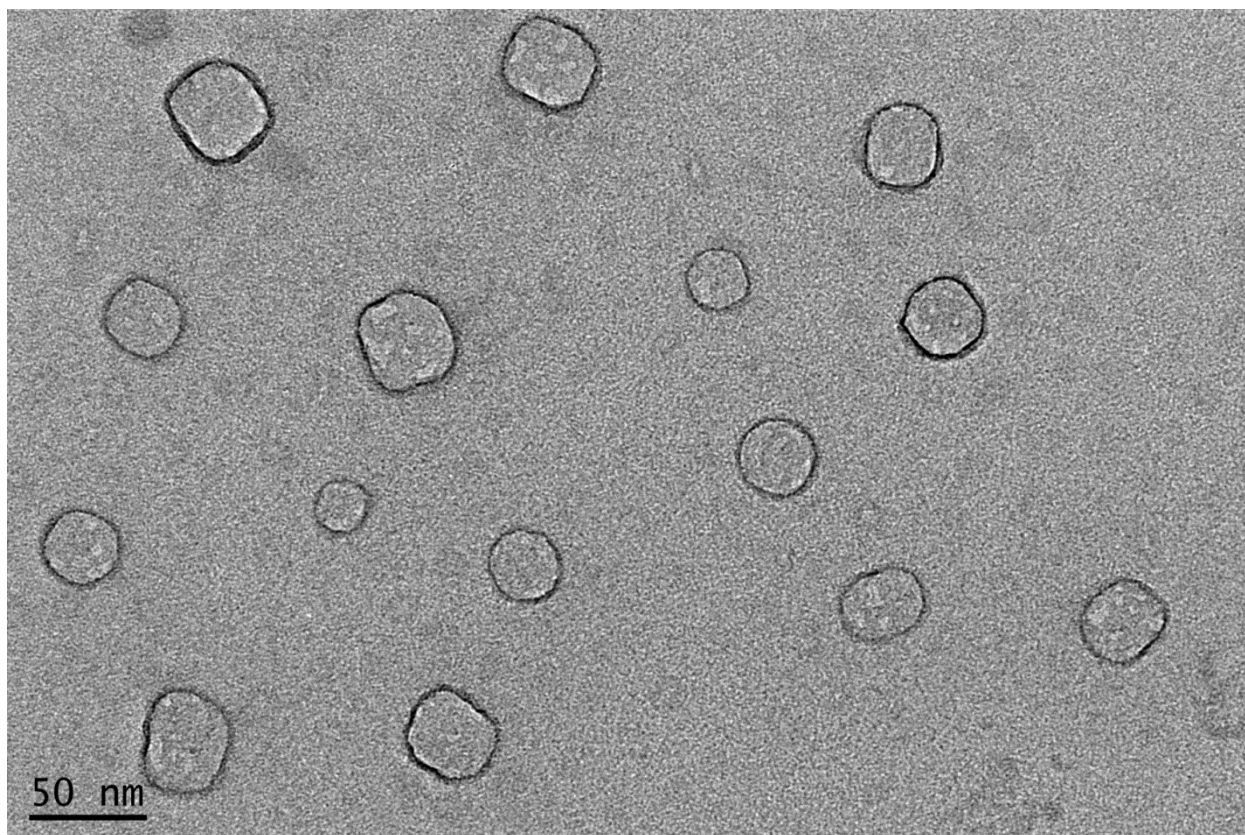


Figure 2-19: TEM Image of JM136 EAAETMAC nanoparticle.

2.4 Conclusions

RAFT polymerization is an effective method to synthesize cationic polymers and diblock copolymers. The CTA described by Ferguson worked well for the synthesis of AETMAC or APTAC macroCTA, which appeared to proceed in a straightforward manner. Diblock copolymers are more

challenging to synthesize, especially with more hydrophobic monomers. Successful nanoparticles were synthesized from BAAETMAC, EAAETMAC, MAAETMAC, BAAPTAC, and MAAPTAC diblock copolymers. Styrene, phenyl ethyl acrylate, and hexyl acrylate monomers were too hydrophobic to successfully polymerize in the aqueous environment.

Several methods were explored to characterize both the macroCTAs and diblock copolymers. MALDI-TOF was an effective way to assess the molecular weight and dispersity of a sample of macroCTA, and ^1H NMR could be used to assess the DP. DLS and diffusion NMR were used to investigate the latex nanoparticle size, and diffusion NMR suggests that the nanoparticles range in size from 21 to 55 nm in diameter. Non-aqueous CE revealed non-ionic homopolymer is present, which is likely trapped within the hydrophobic core.

Much has been learned, but there are still many things that would be helpful to know. Both diffusion NMR and non-aqueous CE suggest that the nanoparticle solutions also contain additional species, which could be hydrophobic homopolymer, residual macroCTA, or polymer chains not incorporated into the nanoparticle structure. More work is needed to truly understand these additional components and how they affect EKC systems. It is difficult to distinguish between individual copolymer chains and the supramolecular nanoparticle structure. Further work needs to be done to isolate the copolymer chains and find their M_n , M_w , and Đ , as well as figure out how many polymer chains are part of a latex nanoparticle.

In the following chapters the polymers synthesized and characterized as described in Chapter 2 will be used to carry out electrokinetic chromatography.

Chapter 3: Development of a Cationic Capillary Coating

3.1 Introduction

The cationic latex nanoparticles described in Chapter 2 were developed for use as PSPs in EKC for the simultaneous and rapid separation of anionic and neutral explosive compounds and residues. The cationic materials are expected to adsorb to the fused silica capillary walls, modifying the capillary so that it has a positive zeta potential and produces an anodic EOF. The anodic EOF should facilitate rapid separation and analysis of the anionic analytes. Previous studies with anionic nanoparticles have shown good separations of nonionic analytes but little to no interactions with ionic analytes, suggesting that cationic latex nanoparticle PSPs would not alter the migration and separation of anionic analytes. Thus, the purpose of a cationic PSP is two-fold: it should adsorb to the wall to create an anodic EOF for the rapid separation of anions, and act as a PSP to separate neutral compounds.

Unfortunately, significant complications were confronted during initial studies with the cationic nanoparticle PSPs. In these experiments, the method of Bushey and Jorgenson⁷⁵ was used to evaluate the mobility and selectivity of the PSPs by analyzing a homologous series of ketones and acetone. Acetone is not retained and is used as an EOF marker, and the alkyl phenyl ketones are employed as nonionic probe solutes with regular increases in hydrophobicity. In the absence of interactions between the nonionic analytes and the PSP they will all reach the detector together with a migration time identical to acetone.

When the cationic nanoparticles described in Chapter 2 were introduced into the BGE as a PSP and flushed through silica capillaries, they did adsorb to the capillary surface and reverse the EOF; acetone had a rapid migration velocity in the direction of the anode. The nanoparticles are also able to separate the alkyl phenyl ketones. However, the peak shapes were broader than expected, as shown in

Figure 3-1. Jared Baker, a visiting researcher, used these nanoparticles to separate ions in the summer of 2014 and observed some severe peak tailing for several anions.

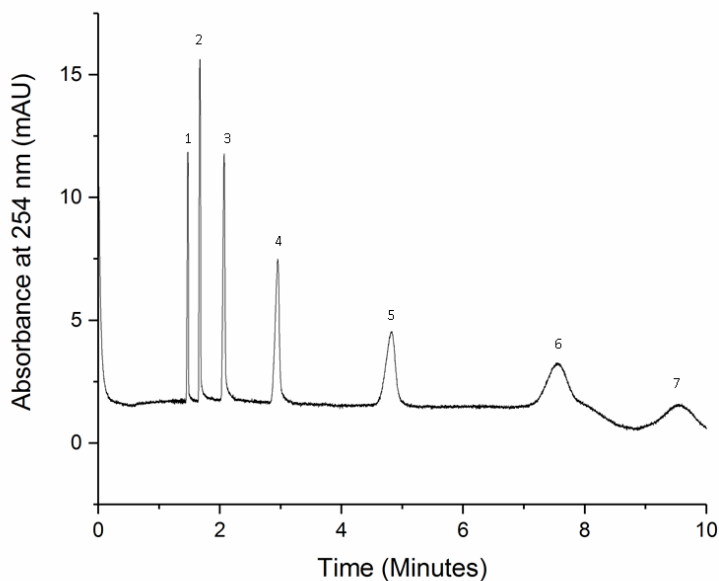


Figure 3-1: Unexpected band broadening in alkyl phenyl ketones: 1 – acetone, 2 – acetophenone, 3 – propiophenone, 4 – butyrophenone, 5 – valerophenone, 6 – hexanophenone, 7 – heptanophenone.

I developed a hypothesis that the nanoparticles adsorbed to the capillary surface were forming a stationary phase that was interacting with analytes in solution, contributing to the observed excessive band broadening. To test this hypothesis, a new capillary was prepared by flushing with cationic nanoparticles, then flushing with a background electrolyte that contained only buffer. Under these conditions, adsorbed nanoparticles render the capillary walls cationic and generate anodic EOF. Without the nanoparticle PSP present in the BGE, all nonionic compounds should migrate together and coelute with acetone. Instead, when the ketones were injected and analyzed under these conditions, multiple broad and asymmetrical peaks were observed, as shown in Figure 3-2. This experiment

confirmed my hypothesis that both retention and band broadening is a result of interactions between analytes and surface adsorbed nanoparticles.

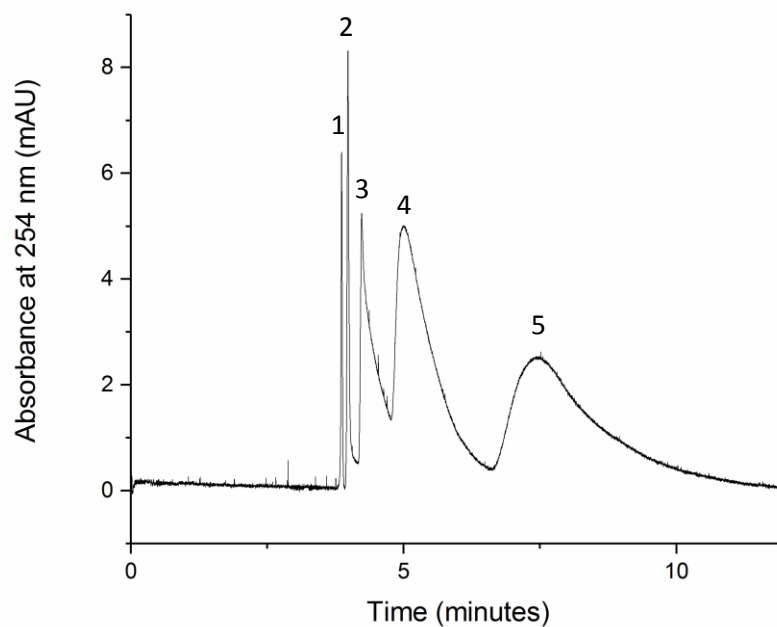


Figure 3-2: An injection of six alkyl phenyl ketones showed unexpected retention when PSP was not present in solution, suggesting interactions were taking place at the capillary wall. The peaks are believed to be 1- acetone/acetophenone, 2 – propiophenone/butyrophenone, 3 – valerophenone, 4 – hexanophenone, 5 – heptanophenone.

It is apparent that during EKC experiments two types of interactions are taking place; stationary phase retention at the capillary surface and pseudo-stationary phase retention in solution. These two types of interactions are most pertinent to more hydrophobic compounds, which explain why the broadening is most apparent in the more hydrophobic ketones.

The hypothesis of the work described in this chapter is that this problem can be combatted or eliminated by coating the surface of the capillary with a non-retentive cationic polymer coating before the nanoparticles PSP is introduced. This cationic coating must produce a robust and stable anodic EOF

and prevent adsorption of the cationic nanoparticles, but not show affinity for hydrophobic analytes. To achieve this goal, a new cationic homopolymer based on the same chemistry as the one of the cationic macroCTAs, poly[(2-acryloyloxy)ethyl]trimethyl ammonium chloride (PAETMAC) was synthesized and used as a cationic capillary coating in conjunction with cationic latex nanoparticles as PSP. This chapter describes the synthesis, characterization, and coating performance of PAETMAC, and compares its performance to that of commercially available cationic polymer coating materials.

3.2 Experimental

3.2.1 Synthesis

The synthesis of PAETMAC is essentially the same as the synthesis of a macroCTA as described in Chapter 2, but with a higher concentration of monomer to produce polymers with a higher degree of polymerization. A target of 50 repeating units was chosen to provide plenty of cationic sites for adsorption to the capillary surface but without creating a polymer that was difficult to work with as a solution. An initial batch, labeled JM159, was synthesized on 9/30/14 and used extensively. Three later batches were synthesized on 9/28/16 (JRM30), 11/7/16 (JRM32), and 11/22/16 (JRM35) to investigate batch-to-batch reproducibility.

To synthesize PAETMAC, 1 mmol of 2-[[[(butylsulfanyl)carbonothioyl]sulfanyl]propanoic acid CTA, 0.1 mmol 4,4'-azobis(4-cyanovaleric acid) initiator, and 50 mmol AETMAC were combined in 20 mL of deionized water. The AETMAC solution was washed with dichloromethane to remove the inhibitor prior to use. The system was sparged with nitrogen gas for 20 minutes, then the heat was set to 70° C and allowed to react for 6 hours. The details for the synthesis of each of the four batches are shown in Table 3-1. During two syntheses, 1 mL aliquots of the reaction mixture were removed and lyophilized for

¹H NMR analysis. Two of the batches were dialyzed with 500 MWCO dialysis tubing in 4 L of deionized water.

Table 3-1 Synthetic conditions for four batches of PAETMAC

Batch Name	CTA	Initiator	AETMAC (80% solution)	Aliquots Taken?	Dialyzed?
JM159	0.2425 g of JM5	0.0280 g	12.306 g	Yes	Yes
JRM30	0.2439 g of JRM8	0.0284 g	12.127 g	No	Yes
JRM32	0.2430 g of JRM8	0.0284 g	12.224 g	No	No
JRM35	0.2449 g of JRM8	0.0318 g	12.230 g	Yes	No

3.2.2 Characterization

The polymers were characterized by ¹H NMR spectroscopy, MALDI-TOF MS, and zeta potential measurement. D₂O was used as the NMR solvent and spectra were acquired on the Agilent 400 MHz spectrometer using the standard parameters. For MALDI-TOF analysis 10 mg/mL solutions in 70/30 0.1% TFA in water/acetonitrile of each polymer were prepared, as well as a 10 mg/mL solution of 2,5-dihydroxybenzene as a matrix. Spots were applied as 1 µL of polymer solution followed by 3 µL of DHB solution that were allowed to dry together. Spectra were acquired with a Bruker microFlex instrument equipped with a 337 nm nitrogen laser. Zeta potential measurements were taken on 5% polymer solutions in 10 mM Tris buffer that were filtered through a 0.45 µm filter and analyzed in Malvern disposable folded capillary cells.

3.2.3 Capillary Coating for CE and EKC

CE and EKC runs were performed on an Agilent 3D CE instrument equipped with an onboard UV detector and controlled by ChemStation software. Fused silica capillaries of 50 µm inner diameter were cut to 34 cm and a window was burned 8.5 cm from the end for an effective length of 26.5 cm. Capillaries were flushed with 1 M sodium hydroxide for 60 minutes, water for 2 minutes, 5% wt/wt

cationic polymer solution for 10 minutes, water for 2 minutes, and background electrolyte (BGE) for 10 minutes. Background electrolyte consisted of 10 mM Tris buffer that was adjusted to the desired pH with acetic acid. In most experiments 150 μ L of 1.0 M acetic acid was diluted to 10 mL with 10 mM Tris for a pH of 5. For EKC experiments 0.3% wt/wt of JM142 EAAETMAC nanoparticles were added as PSP by diluting 130 μ L of stock JM142 EAAETMAC solution to 5 mL with Tris-Acetate buffer.

Three commercial cationic polymers were also tested for EOF, retention, and peak shape during EKC. Each polymer was obtained from Sigma-Aldrich. Hexadimethrine Bromide (HDM), Sigma-Aldrich part number 107689-10G, included no description of its molecular weight. This polymer is commercially marketed as Polybrene. Poly(diallyldimethylammonium chloride) (PDADMAC), Sigma-Aldrich part number 409014-1L, has a reported M_w range from 100,000 – 200,000 g/mol. Polyethylenimine (PEI), Sigma-Aldrich part number 408727-1L, has a reported M_w of 25,000 g/mol as measured by light scattering. 5 wt% aqueous solutions were made by dissolving the appropriate amount of polymer in water. Capillaries were prepared in the same way as capillaries treated with PAETMAC.

3.3 Results and Discussion

3.3.1 Polymer synthesis and characterization

The initial synthesis of JM159 PAETMAC polymer had a yield of 1.6228 g after dialysis. The second batch, JRM30, was also dialyzed, and 0.5961 g was recovered from the tubing. This was the remainder of the 500 MWCO tubing, so the next two batches were not dialyzed to avoid significant loss from larger pore tubing. The third batch, JRM32, had a yield of 14.5909 g and the fourth batch, JRM35, had a yield of 9.3356 g. The dialyzed batches were yellow crystals, but the undialyzed batches were

thick yellow gels. The dramatically greater yields suggest that a large amount of material is being lost during the dialysis process, even with a low molecular weight cutoff.

Each batch of PAETMAC was analyzed by MALDI-TOF MS; the overlaid spectra are shown in Figure 3-3.

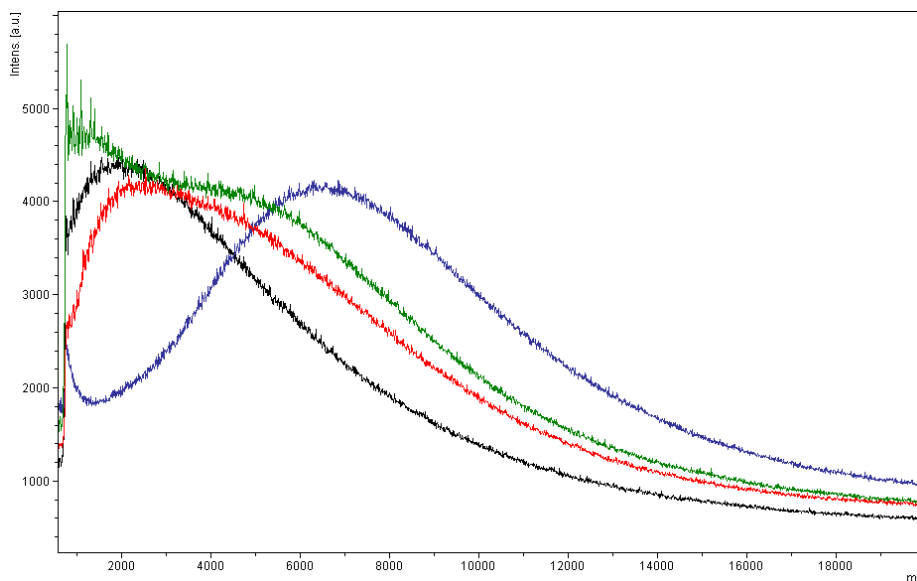


Figure 3-3: MALDI-TOF MS spectra of four batches of PAETMAC. Blue – JM159, Red – JRM30, Green – JRM32, Black – JRM35.

The three later batches appear to have a greater percentage of smaller polymer chains than the original JM159, and the dialyzed JRM30 showed less low molecular weight material than the two undialyzed batches. The ^1H NMR and zeta potential measurement results as shown in Table 3-2. The zeta potential is clearly positive, indicating the polymers are indeed cationic.

Table 3-2: Properties of four batches of PAETMAC polymer.

Polymer	JM159	JRM30	JRM32	JRM35
DP by NMR	248	57	38	38
M_n by NMR	14,500	5,100	3,500	3,300
Zeta Potential	+47.1	+18.5	+20.9	+24.0

Each characterization technique showed that JM159 had a much higher degree of polymerization than the other three batches. A different synthetic batch of chain transfer agent was

used for the later three batches because all of the original batch had been used up. Aliquots were taken every hour during the synthesis of JM159 and JRM35. The % conversion of the first PAETMAC batch steadily rose from 48% at hour 3 to 98% at hour 6, much like the macroCTAs discussed in Chapter 2. JRM35 had a % conversion that remained steady at 76% for all 6 hours, suggesting that the reaction kinetics for the later three batches were much different. It is possible that the first batch of CTA was less active than the second, resulting in a higher DP when the same ratio of CTA to monomer was used.

3.3.2 PAETMAC Treated Capillaries

An initial coating test was performed by flushing a 34 cm capillary with a solution of JM159 in water for 10 minutes. The capillary was then flushed with 10 mM Tris-HCl buffer adjusted to pH 7.2, which is the standard buffer our lab uses for EKC experiments. A series of 100 injections of acetone were performed to look at the magnitude and repeatability of the EOF, which was calculated to be $-4.2 \times 10^{-4} \text{ cm}^2/\text{V}\cdot\text{s}$ with an RSD of 2.4%. When the six alkyl phenyl ketones were injected a sharp peak with a small shoulder was observed, as shown in Figure 3-4. This is what should be observed if there is no significant wall retention.

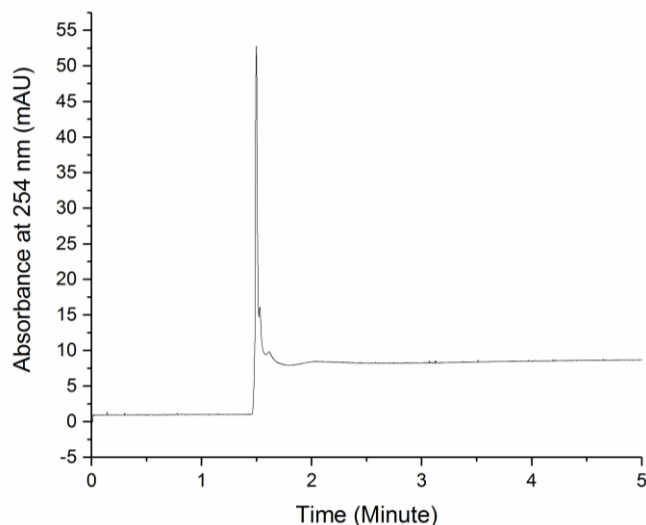


Figure 3-4: Retention is no longer observed with a PAETMAC coating

Since the initial results looked promising, a pH study was carried out. A new buffer system, Tris-Acetate, was chosen for this study because Tris-HCl would not provide buffer capacity in the acidic pH range. While Tris-Acetate is not the most common buffer, it is used in the literature⁷⁶ and provides buffering capacity from Tris in the basic range and from acetate in the acidic range. Acetic acid was added to a 10 mM solution of Tris to create Tris-Acetate buffers at pH 4, 5, 6, 7, and 8. Ohm's Law plots were made to check for Joule heating by varying the applied voltage and measuring the current. If Joule heating is occurring a plot of voltage vs current would deviate from linearity, but all five pH levels had an $R^2 > 0.99$. The plots are shown in Figure 3-5. The similar currents generated by each buffer also demonstrate that the conductivity, and therefore ionic strength, are similar for these five buffers.

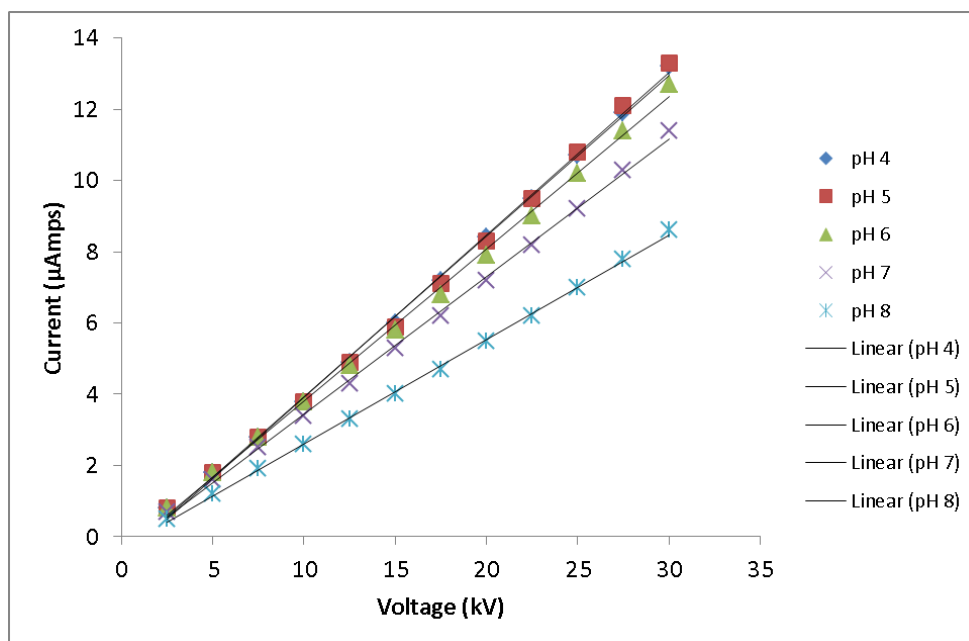


Figure 3-5: Ohm's Law plots for Tris-Acetate buffers at pH 4, 5, 6, 7, and 8.

100 injections of acetone were performed at each pH level, and the results are shown in Figure 3-6. The EOF magnitude was relatively consistent across the pH range studied, although the variance increased at pH 8. The EOF for each injection over time is shown in Figure 3-7. At acidic pH there

appears to be an equilibration period of about 20 injections where the EOF increases and then stabilizes in magnitude. At pH 7 a slight trend can be seen, and at pH 8 the EOF shows a continuous drift toward a lower magnitude over time. This could be caused by hydrolysis and exposure of residual silanol groups at the capillary surface, or by polymer instability. The titration experiments discussed in Chapter 2 showed that AETMAC macroCTAs are unstable at basic pH, and this study is further evidence of this fact. Quaternary amine polymers have been shown to degrade to tertiary amines at basic pH⁷⁷.

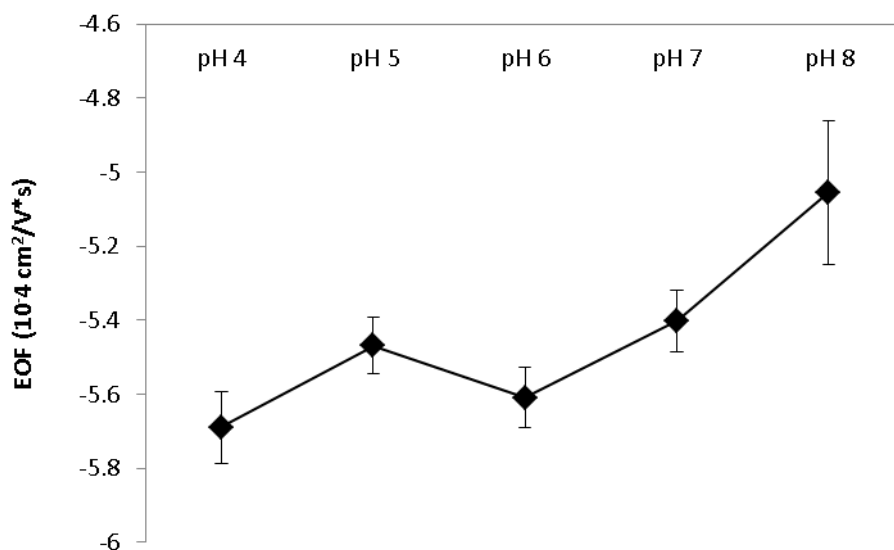


Figure 3-6: The average EOF and standard deviation for 100 injections at pH 4, 5, 6, 7, and 8.

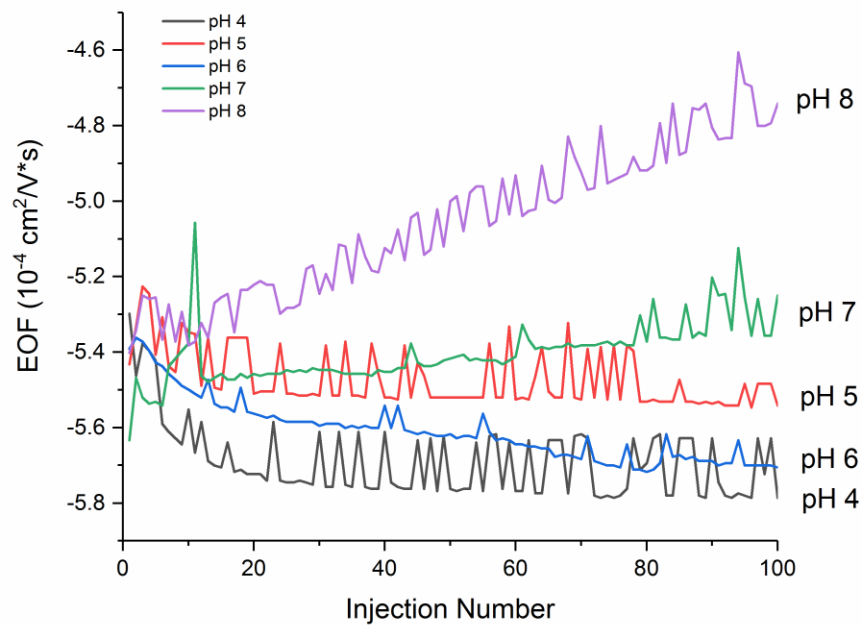


Figure 3-7: The EOF for each of a series of 100 injections at pH 4, 5, 6, 7, and 8.

The coating appeared to work well for CE applications, so it was tested with the addition of a PSP. JM142 EAAETMAC was used with a 48.5 cm capillary, 10 mM pH 5 Tris-Acetate buffer and 0.3% wt/wt PSP to separate the mix of alkyl phenyl ketones, which were considerably sharper. The best electropherogram is presented in Figure 3-8:

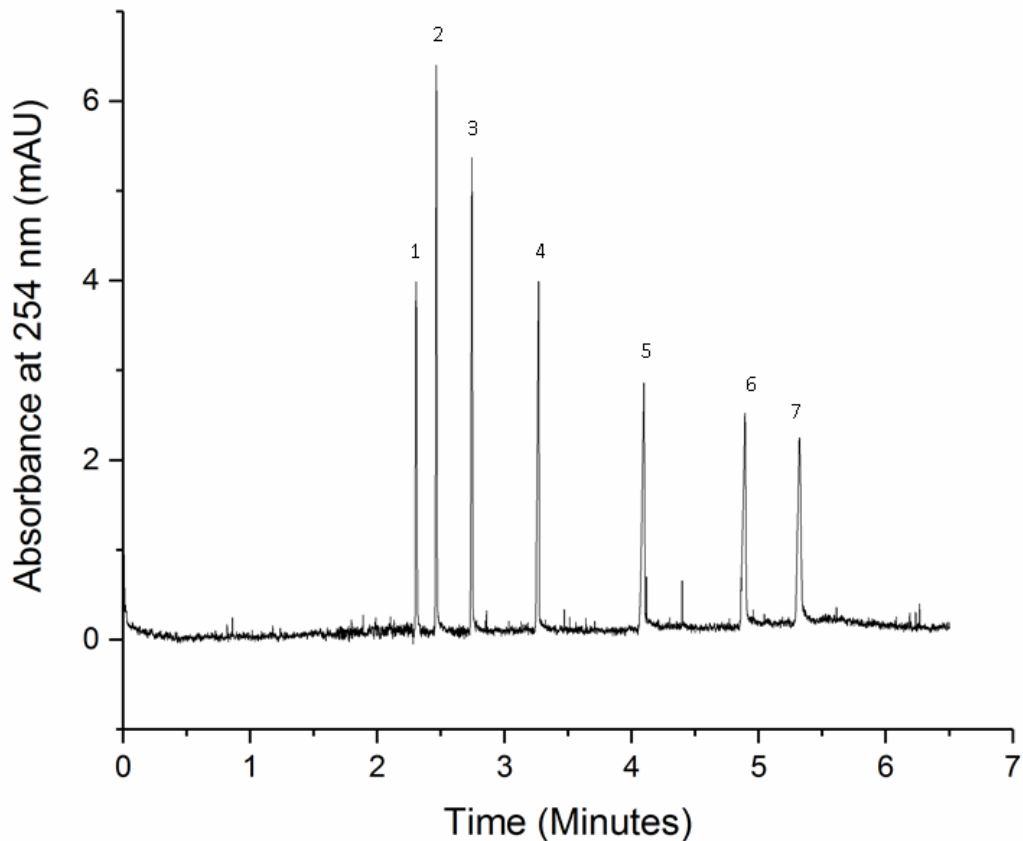


Figure 3-8: Alkyl phenyl ketones with excellent peak shapes: 1 – acetone, 2 – acetophenone, 3 – propiophenone, 4 – butyrophenone, 5 – valerophenone, 6 – hexanophenone, 7 – heptanophenone.

With more repetitions it became clear that some fronting was typical, and this is explored further in Chapter 4. Even with the fronting, peak shapes are dramatically improved relative to those in capillaries treated with nanoparticles. PAETMAC batch JM159 was used to treat capillaries used in the LSER studies described in Chapter 4, and many of the explosives separations in Chapter 5.

Three additional batches of PAETMAC polymer were synthesized later to investigate the batch-to-batch reproducibility. In each case the polymer appeared to adsorb to the capillary and produce an anodic EOF. However, there was quite a bit of variability in the EOF, as shown in Table 3-3. The lack of reproducibility is concerning, and implies that we do not have good control over the synthesis.

Table 3-3: EOF Produced by Different Batches of PAETMAC

Batch	Molecular Weight g/mol	EOF ($10^{-4} \text{ cm}^2/\text{V*s}$)	RSD
JM159	14,500	-5.5	1.4%
JRM30	5,100	-2.6	36%
JRM32	3,500	-4.3	13%
JRM35	3,300	-7.0	4.9%

3.3.3 Commercial Cationic Polymer Treated Capillaries

The same sequence of injections were done with the three commercial cationic polymers as well, using a pH 5 10 mM Tris-Acetate BGE. The average EOF and RSD are shown in Table 3-4 along with the molecular weights, and the EOF with each injection is shown in Figure 3-9.

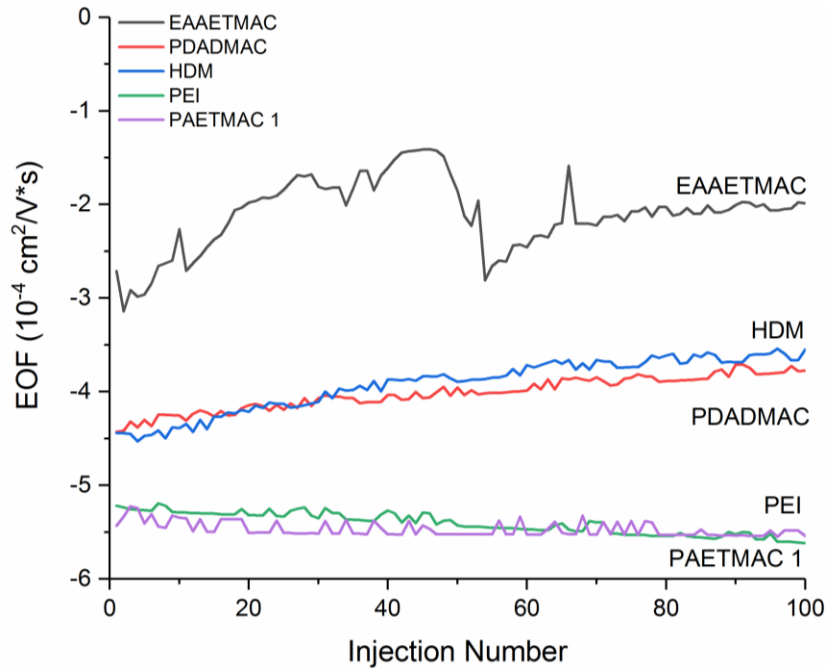


Figure 3-9: The EOF for each injection for three commercial cationic polymers, JRM159 PAETMAC, and JM142 EAAETMAC cationic latex nanoparticles.

Table 3-4: EOF generated by different cationic capillary coatings

Polymer	Molecular Weight g/mol	EOF (10^{-4} cm ² /V*s)	RSD
PAETMAC	M _n : 14,500	-5.7	1.7%
EAAETMAC	Unknown	-2.1	16%
PEI	M _w : 25,000	-5.4	2.1%
PDADMAC	M _w : 100,000 – 200,000	-4.0	4.4%
HDM	Not Provided	-3.9	7.1%

No clear trend was observed between molecular weight and EOF. PAETMAC is comparable to PEI, while PDADMAC and HDM are similar to each other. PEI produces a stable EOF, but PDADMAC and HDM show a trend of reduced EOF with time. EAAETMAC nanoparticles produce the least stable coating, which may be due to a lower charge density on the nanoparticles or conformational effects with the adsorbed amphiphilic copolymer.

3.3.4 Effect on EKC Peak Shapes

While it is important to produce a strong anodic EOF, the other important goal of a cationic capillary coating is to improve peak shapes during EKC. To test the effect of the different coatings a series of 10 injections of the six alkyl phenyl ketones was performed on a capillary coated with each cationic polymer. As a comparison, one capillary was coated with JM142 EAAETMAC nanoparticles following the same procedure. A pH 5 10 mM Tris-Acetate BGE with JRM142 EAAETMAC at 0.3 weight % as the PSP was used for all experiments. A representative electropherogram for each treatment is shown in Figure 3-10.

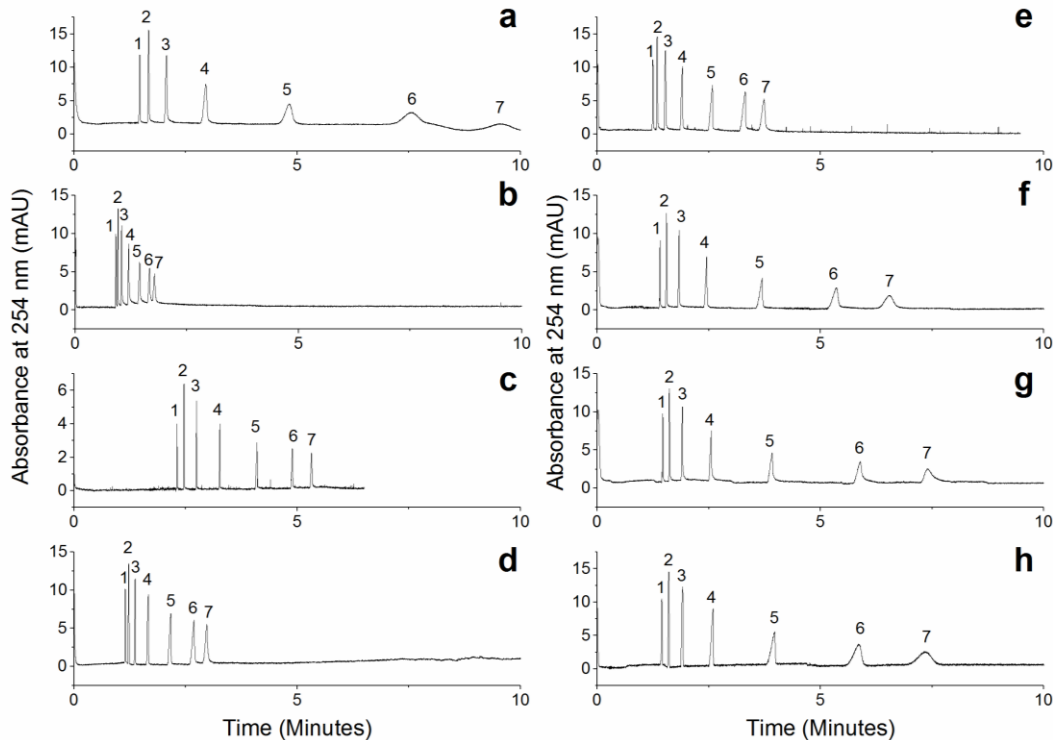


Figure 3-10: Six alkyl phenyl ketones 1 – acetone, 2 – acetophenone, 3 – propiophenone, 4 – butyrophenone, 5 – valerophenone, 6 – hexanophenone, 7 – heptanophenone separated by JM142 EAAETMAC nanoparticles and capillaries treated with 8 different cationic polymers: a) JRM142 EAAETMAC nanoparticles, b) PEI, c) JRM159 PAETMAC, d) JRM35 PAETMAC, e) JRM32 PAETMAC, f) PDADMAC, g) HDM, and h) JRM30 PAETMAC.

The average N for each compound is shown in Table 3-5, listed by coatings that produced the strongest EOF to the weakest. The EAAETMAC nanoparticles showed a loss of efficiency starting with butyrophenone. The other coatings showed that low to intermediate hydrophobicity analytes have plate counts consistent with acetone. However, the four coatings with the weakest EOF show significant decreases in plate counts for the more hydrophobic compounds, starting with valerophenone for PDADMAC and JRM30 PAETMAC, hexanophenone for JRM32, and heptanophenone for HDM. This may be caused by adsorption of nanoparticles to an incomplete cationic polymer coating, or in the case of HDM, by hydrophobic interactions with the polymer itself.

Table 3-5: Theoretical Plate Counts Using Different Cationic Capillary Coatings

Polymer	EOF	Acetone 10 ³	Aceto- phenone 10 ³	Propio- phenone 10 ³	Butyro- phenone 10 ³	Valero- phenone 10 ³	Hexano- phenone 10 ³	Heptano- phenone 10 ³
PAETMAC 4	-7.0	63 (5.6)	55 (4.9)	52 (5.0)	53 (7.3)	46 (5.1)	43 (4.6)	35 (5.3)
PEI	-5.4	42 (1.2)	33 (0.4)	32 (0.9)	40 (1.4)	45 (2.0)	47 (1.3)	47 (3.6)
PAETMAC 3	-4.3	37 (1.8)	37 (4.0)	34 (3.4)	38 (2.3)	38 (3.0)	27 (3.6)	19 (3.0)
PDADMAC	-4.0	52 (6.0)	46 (6.6)	49 (7.3)	50 (3.5)	32 (3.7)	20 (4.0)	11 (4.2)
HDM	-3.9	60 (7.7)	52 (5.8)	50 (5.5)	52 (2.9)	41 (2.8)	35 (4.8)	22 (1.8)
PAETMAC 2	-2.6	40 (1.6)	34 (2.0)	38 (1.5)	41 (1.8)	25 (1.9)	14 (1.8)	8 (1.8)
EAAETMAC	-2.1	66 (5.8)	59 (3.0)	47 (3.6)	24 (2.0)	12 (0.8)	7 (0.5)	5 (1.4)

The values in parentheses are standard deviations

3.4 Conclusions

Adding a separate cationic polymer as a capillary coating improves the EKC performance when a cationic latex nanoparticle is used as a PSP. While there is some variability in the synthesis, all four batches of PAETMAC produce strong anodic EOF and a coated capillary has good repeatability over 100 injections at acidic or neutral pH. Better control over the synthesis is necessary to create reproducible batches of polymer, but dialysis was shown not to be necessary for good performance. The PAETMAC polymers perform as well or better than the commercial cationic polymers PEI, PDADMAC, and HDM. No correlation was found between the EOF and polymer molecular weight or zeta potential for either PAETMAC or the commercial polymers. PAETMAC coated capillaries were used for all the experiments discussed in Chapters 4 and 5.

Chapter 4: Evaluation of Cationic Latex Nanoparticles as Pseudo-Stationary Phases

4.1 Introduction

The pseudo-stationary phase is the heart of electrokinetic chromatography, as this is what gives the technique its ability to separate neutral compounds. Unlike a GC capillary or HPLC column, a PSP can be changed by simply flushing the CE capillary. All PSPs must have a charged group to impart mobility when a voltage is applied, and functional groups that can interact with the target analytes. PSPs can be surfactant micelles⁷⁸, vesicles⁷⁹, liposomes⁸⁰, microemulsions⁸¹, carbon nanotubes and fullerenes³¹, or polymers⁸². Polymers PSPs have the advantage of a wide range of monomer functionalities that can provide a variety of different selectivities.

With so many options to choose from, it is important to be able to quantify the mobility and selectivity of a given material. LSER is a useful model for quantifying the different types of intermolecular interactions happening between analytes and a PSP during a separation. Several research groups have used LSER to characterize PSPs⁸³⁻⁸⁷. Principal Component Analysis (PCA) has been applied to LSER results to classify PSPs into categories by selectivity⁸⁸, which showed that PSPs cluster as a function of their chemical nature and that hydrogen bond acidity, hydrogen bond basicity, and hydrophobicity are the main contributions to the principle components.

This chapter will describe the use of the cationic latex nanoparticles synthesized in Chapter 2 as PSPs for EKC. The PAETMAC cationic polymer was shown to be an effective capillary coating in Chapter 3, so PAETMAC coated capillaries were used for the experiments described in this chapter in conjunction with the cationic latex nanoparticle PSPs. The selectivity and retention of alkyl phenyl ketones and 39 solutes used in the LSER model will be discussed.

4.2 Experimental

EKC experiments were performed on an Agilent ^{3D}CE instrument with onboard UV detection and controlled by ChemStation software. Fused silica capillaries were flushed with 1 M sodium hydroxide for three hours prior to their first use, then flushed with water for two minutes, 5% JM159 PAETMAC polymer for 10 minutes, water for 2 minutes, then BGE for 10 minutes. The capillary was flushed for two minutes with BGE between injections.

To characterize the retention and selectivity of a PSP, one must determine t_0 , t_r , and t_{PSP} . While t_0 is easily determined by using a neutral marker like acetone, DMSO, or mesityl oxide, t_{PSP} is more difficult because it is harder to find a completely retained compound. The method of Bushey and Jorgenson⁷⁵ can be used to evaluate the mobility of a PSP by analyzing a homologous series of six alkyl phenyl ketones and acetone. Acetone is not retained and is used as an EOF marker. The log of the retention factor for each ketone is plotted against the carbon number of the alkyl chain, and the Goal Seek function in Microsoft Excel is used to iteratively calculate the t_{PSP} that leads to a line of best fit. The slope of this line can be used to calculate the methylene selectivity, which is a measure of how a PSP can separate hydrophobic compounds. Comparing t_0 to t_{PSP} will reveal the migration window for a given system.

A PSP optimization study was performed on a 65.8 cm capillary, 60 cm effective length, at 25° C where the concentration of, buffer, PSP, and applied voltage was systematically varied. Tris-Acetate buffer was made at 10 mM, 25 mM, and 50 mM; KB3A BAAPTAC PSP was added at 0.1, 0.3, and 0.5% wt/wt, and voltage was applied at -20, -25, and -30 kV. An alkyl phenyl ketone stock mixture was made by combining 200 μ L of acetophenone, propiophenone, butyrophenone, valerophenone, hexanophenone, and heptanophenone. A working mix was prepared by diluting 24 μ L to 1 mL with

acetone for a concentration of 4000 ppm. An alkyl phenyl ketone standard was prepared for analysis by adding 15 μ L of working mix to 1 mL of BGE for a concentration of 60 ppm.

LSER experiments were performed on 48.5 cm capillaries, 40 cm effective length, at 25° C and -20 kV applied voltage. The BGE consisted of 10 mM Tris adjusted to pH 7.2 with hydrochloric acid and 0.3% wt/wt of the nanoparticle being studied. A set of 39 compounds with known solute descriptors were analyzed for each nanoparticle, these are listed in Table 4-1. These compounds contain a variety of functional groups to avoid cross-correlation between descriptors, and there are enough of them to obtain an exhaustive fit⁸⁹. This list includes 8 derivatives of benzene to compare the polar group selectivity. Each compound was run individually to estimate its retention for a given nanoparticle, then mixtures between three and eight compounds were prepared so that no compounds co-migrated. These mixtures were run five times each for each nanoparticle to find the retention factors. Alkyl phenyl ketones were run between each LSER mixture to monitor changes in the system. Linear regression analyses were performed using Microsoft Excel 2010. The log of the retention factor for each replicate was used as the Y variable and the LSER solute descriptors were used as the X variables. LSER data on the anionic PSPs BAAMPS, EAAMPS, MAAMPS, and SDS was provided by Dr. Jesse Hyslop.

Table 4-1: LSER Solutes and Descriptors

Solute	V	E	S	A	B
1-Methylnapthalene	1.226	1.344	0.9	0	0.2
1-Napthol	1.1441	1.52	1.08	0.61	0.4
3,5-Dimethylphenol	1.057	0.82	0.84	0.57	0.36
3-Bromophenol	0.95	1.06	1.15	0.7	0.16
3-Chlorophenol	0.898	0.909	1.06	0.69	0.15
3-Methyl Benzyl Alcohol	1.057	0.815	0.9	0.33	0.59
4-Bromophenol	0.95	1.08	1.17	0.67	0.2
4-Chloroacetophenone	1.136	0.955	1.09	0	0.44
4-Chloroaniline	0.939	1.06	1.13	0.3	0.31
4-Chlorophenol	0.898	0.915	1.08	0.67	0.2
4-Chlorotoluene	0.98	0.705	0.67	0	0.07
4-Ethylphenol	1.057	0.8	0.9	0.55	0.36
4-Fluorophenol	0.793	0.67	0.97	0.63	0.23
4-Nitroaniline	0.9904	1.22	1.91	0.42	0.38
4-Nitrotoluene	1.032	0.87	1.11	0	0.28
Acetophenone	1.014	0.818	1.01	0	0.48
Anisole	0.916	0.708	0.75	0	0.29
Benzene	0.716	0.61	0.52	0	0.14
Benzonitrile	0.871	0.742	1.11	0	0.33
Benzyl Alcohol	0.916	0.803	0.87	0.33	0.56
Biphenyl	1.324	1.36	0.99	0	0.22
Chlorobenzene	0.839	0.718	0.65	0	0.07
Ethylbenzene	0.998	0.613	0.51	0	0.15
Ethylbenzoate	1.214	0.689	0.85	0	0.46
Indole	0.946	1.2	1.12	0.44	0.22
Iodobenzene	0.975	1.188	0.82	0	0.12
M-Cresol	0.916	0.822	0.88	0.57	0.34
Methyl Benzoate	1.073	0.733	0.85	0	0.46
Methyl-o-Toluate	1.214	0.772	0.87	0	0.43
Napthalene	1.085	1.36	0.92	0	0.2
Nitrobenzene	0.891	0.871	1.11	0	0.28
p-Cresol	0.916	0.82	0.87	0.57	0.31
Phenol	0.775	0.805	0.89	0.6	0.3
Phenyl Acetate	1.073	0.661	1.13	0	0.54
Propiophenone	1.155	0.804	0.95	0	0.51
Propylbenzene	1.139	0.604	0.5	0	0.15
p-Xylene	0.998	0.613	0.52	0	0.16
Resorcinol	0.834	0.98	1	1.1	0.58
Toluene	0.857	0.601	0.52	0	0.14

4.3 Results and Discussion

4.3.1 Homologous Series

A systematic study was performed to investigate the effect of buffer concentration, PSP concentration, and applied voltage on the separation of a homologous series of acetone and six alkyl phenyl ketones. A longer 68.5 cm capillary (60 cm effective length) was used to ensure all compounds were resolved. The results are shown in Table 4-2.

Table 4-2: Systematic variable changes on EKC Performance

Tris	PSP	Voltage	Current μ Amps	t_0	μ_{EOF}	t_{PSP}	μ_{PSP}	α_{CH3}	t_{PSP} / t_0
10 mM	0.30%	-20 kV	-4.0	7.430	-4.610	23.807	3.171	3.111	3.204
10 mM	0.30%	-25 kV	-5.2	5.928	-4.622	18.974	3.178	3.105	3.201
10 mM	0.30%	-30 kV	-6.3	4.913	-4.648	15.976	3.218	3.007	3.252
10 mM	0.50%	-20 kV	-4.2	7.365	-4.650	23.025	3.163	3.026	3.126
10 mM	0.50%	-25 kV	-5.3	5.884	-4.657	18.300	3.159	3.145	3.110
10 mM	0.50%	-30 kV	-6.3	4.853	-4.705	15.112	3.194	3.036	3.114
25 mM	0.10%	-20 kV	-8.3	8.228	-4.163	31.965	3.091	3.229	3.885
25 mM	0.10%	-25 kV	-10.5	6.508	-4.210	28.449	3.247	2.973	4.371
25 mM	0.10%	-30 kV	-12.9	5.358	-4.262	22.619	3.252	3.027	4.221
25 mM	0.30%	-20 kV	-8.9	8.446	-4.055	31.531	2.969	3.001	3.733
25 mM	0.30%	-25 kV	-11.3	6.428	-4.263	21.907	3.012	3.021	3.408
25 mM	0.30%	-30 kV	-13.8	5.558	-4.108	21.082	3.025	3.029	3.793
25 mM	0.50%	-20 kV	-9.2	8.419	-4.068	30.570	2.948	2.997	3.631
25 mM	0.50%	-25 kV	-11.6	6.659	-4.115	24.260	2.985	2.998	3.643
25 mM	0.50%	-30 kV	-14.1	5.505	-4.148	20.002	3.006	3.201	3.633
50 mM	0.10%	-20 kV	-15.5	8.814	-3.886	45.791	3.138	3.196	5.195
50 mM	0.10%	-25 kV	-19.9	7.065	-3.878	40.754	3.206	3.054	5.768
50 mM	0.10%	-30 kV	-24.7	5.719	-3.993	32.495	3.290	3.032	5.682
50 mM	0.30%	-20 kV	-17.2	8.718	-3.929	47.814	3.212	3.236	5.485
50 mM	0.30%	-25 kV	-22.0	6.763	-4.051	36.030	3.291	3.018	5.328
50 mM	0.30%	-30 kV	-27.4	5.607	-4.072	33.745	3.396	3.011	6.018
50 mM	0.50%	-20 kV	-17.0	8.685	-3.944	43.432	3.155	2.987	5.001
50 mM	0.50%	-25 kV	-22.0	6.821	-4.017	36.520	3.267	3.010	5.354
50 mM	0.50%	-30 kV	-27.3	5.587	-4.087	30.624	3.341	2.995	5.481

As the applied voltage is increased, the measured current also increases. Increasing the buffer concentration also increases the current because there is more electrolyte in the system. However, increasing the PSP concentration with a constant buffer concentration and applied voltage does not lead to a significant increase in current. The current must be controlled to prevent Joule heating, but cationic latex nanoparticles are not a significant contributor. This contrasts with surfactants micelle PSPs, where free surfactant contributes to high current and Joule heating when used at high concentrations. Increasing the applied voltage leads to faster analysis times, but also an increase in noise. Increasing the buffer concentration decreases the EOF, leading to longer analysis times. As the applied voltage is increased μ_{PSP} increases slightly.

The most important observation from this study is that the resolution of the homologous series is very dependent on PSP concentration. At low concentrations the peaks are clustered near t_0 , while at high concentrations they are clustered near t_{PSP} . This trend can be seen in Figure 4-1, which compares separations using 25 mM TA buffer at -25 kV using 0.1% (a), 0.3% (b), and 0.5% (c) PSP. The resolution between acetophenone and propiophenone increases from 16 with 0.1% to 30 with 0.5% PSP, while the resolution between hexanophenone and heptanophenone decreases from 18 with 0.1% to 16 with 0.5% PSP. This is important information because it suggests that the amount of PSP can be tailored to the hydrophobicity of the analytes being separated. EKC is one of the only techniques where the phase ratio can be adjusted so easily.

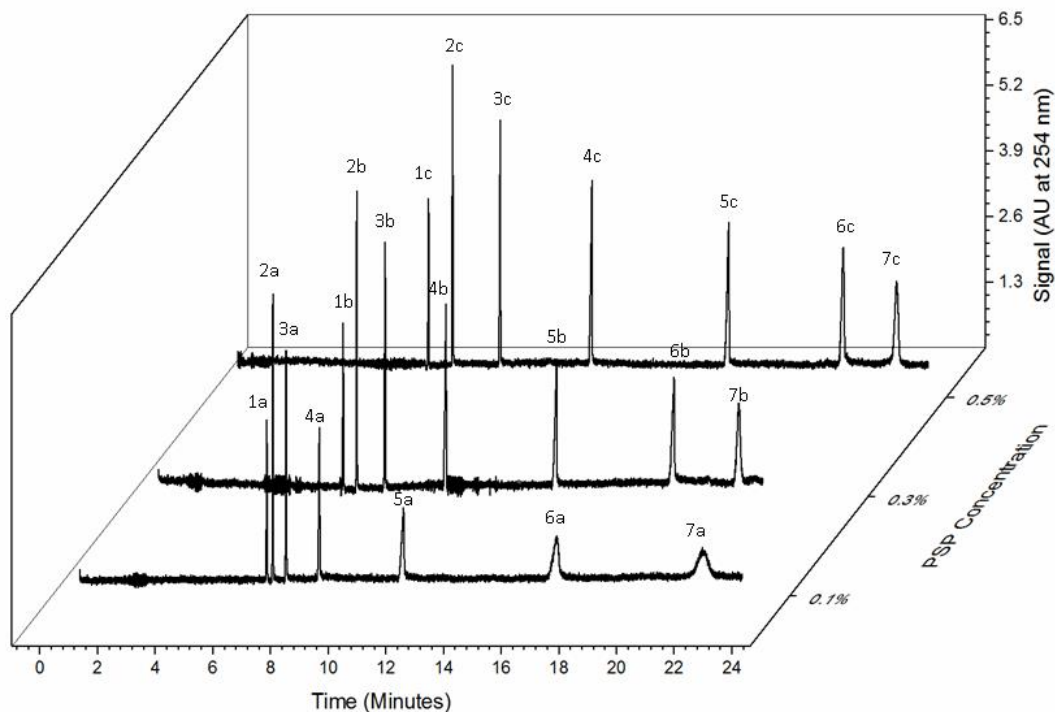


Figure 4-1: The separation of alkyl phenyl ketones 1 – acetone, 2 – acetophenone, 3 – propiophenone, 4 – butyrophenone, 5 – valerophenone, 6 – hexanophenone, and 7 – heptanophenone by a) 0.1%, b) 0.3%, or c) 0.5% KB3A BAAPTAC PSP in a 68.5 cm PAETMAC coated capillary.

Different nanoparticles were analyzed by looking at data from the homologous series of ketones as part of the LSER analysis using standard conditions of a 48.5 cm capillary, 40 cm effective length, 10 mM pH 7.2 Tris-HCl buffer, and 0.3% PSP concentration. The alkyl phenyl ketones were analyzed between blocks of LSER analytes to ensure the system was working properly, and to be able to calculate t_{PSP} for the $\log(k)$ calculations. These conditions were chosen to be consistent with previous work on anionic latex nanoparticles for the best comparison. The results are shown in Table 4-3.

Table 4-3: Comparison of μ_{eo} , μ_{PSP} , and α_{CH2} of Different Nanoparticles

Name	Chemistry	μ_{eo} (10^{-4} $(\text{cm}^2/\text{V}\cdot\text{s})$)	μ_{ep} (10^{-4} $(\text{cm}^2/\text{V}\cdot\text{s})$)	α_{CH2}	t_{PSP} / t_0	N	Replicates
JM132	BAAETMAC	-4.7 ± 0.4	3.45 ± 0.05	3.22 ± 0.07	4.1 ± 0.9	118000 ± 17000	n = 10
KB4F	BAAETMAC	-5.8 ± 0.1	3.31 ± 0.06	2.85 ± 0.08	2.34 ± 0.08	263000 ± 43000	n = 10
KB3D	BAAPTAC	-4.4 ± 0.2	3.51 ± 0.08	2.95 ± 0.09	4.9 ± 0.3	284000 ± 42000	n = 7
KB3A	BAAPTAC	-5.1 ± 0.2	3.3 ± 0.1	3.14 ± 0.09	2.86 ± 0.06	179000 ± 58000	n = 10
JM136	EAAETMAC	-4.5 ± 0.2	3.29 ± 0.05	3.01 ± 0.11	3.7 ± 0.4	120000 ± 29000	n = 8
KB4D	EAAETMAC	-5.28 ± 0.08	3.36 ± 0.02	2.78 ± 0.06	2.75 ± 0.08	225000 ± 18000	n = 6
JM142	EAAETMAC	-4.84 ± 0.09	3.17 ± 0.06	2.92 ± 0.06	2.9 ± 0.1	142000 ± 30000	n = 12
KB3C	MAAPTAC	-4.56 ± 0.1	3.37 ± 0.06	2.56 ± 0.03	3.9 ± 0.2	214000 ± 26000	n = 11
JM137	MAAETMAC	-4.67 ± 0.05	3.32 ± 0.04	2.53 ± 0.03	3.5 ± 0.1	150000 ± 26000	n = 6
KB3F	MAAPTAC	-4.4 ± 0.1	3.5 ± 0.1	2.56 ± 0.07	4.9 ± 0.2	206000 ± 33000	n = 4

The EOF is a function of the cationic capillary coating more than the PSP, and no clear trend can be seen. All cationic latex nanoparticles studied had electrophoretic mobilities opposite that of the EOF with a magnitude between 3.0 and 3.5 10^{-4} $\text{cm}^2/\text{V}\cdot\text{s}$. No clear trend could be found with regards to nanoparticle chemistry, diameter, zeta potential, or fraction of the smaller component detected by diffusion NMR. The migration window t_{PSP}/t_0 was proportional to μ_{eo} , where a strong EOF led to a narrower migration window but a faster analysis time. Methylene selectivity is discussed below.

A repeatability study was performed on a 34 cm JRM30 PAETMAC coated capillary using JM142 EAAETMAC as PSP. 100 injections of the alkyl phenyl ketones were performed to look at the reproducibility of the retention factors and the number of theoretical plates generated by a given nanoparticle. The results are listed in Table 4-4 and shown graphically in Figure 4-2. The retention factors remained steady over the course of the 100 injections, and showed more variability in the

strongly retained, hydrophobic compounds. The methylene selectivity remained steady at 2.91 ± 0.035 with an RSD of 1.2%. The efficiency of the system had more variation, with the smallest RSD at 27%. After about 50 injections the efficiency abruptly decreased, which can be seen in Figure 4-2.

Table 4-4: Repeatability Study with Alkyl Phenyl Ketones

Compound	Retention Factor	RSD	Number of Theoretical Plates	RSD
Acetophenone	0.099 ± 0.0012	1.2%	$170,000 \pm 53,000$	30%
Propiophenone	0.316 ± 0.0031	1.0%	$120,000 \pm 39,000$	31%
Butyrophenone	0.87 ± 0.015	1.7%	$61,000 \pm 17,000$	27%
Valerophenone	2.56 ± 0.070	2.7%	$36,000 \pm 13,000$	37%
Hexanophenone	7.7 ± 0.32	4.1%	$33,000 \pm 17,000$	50%
Heptanophenone	20 ± 1.4	6.8%	$35,000 \pm 26,000$	74%

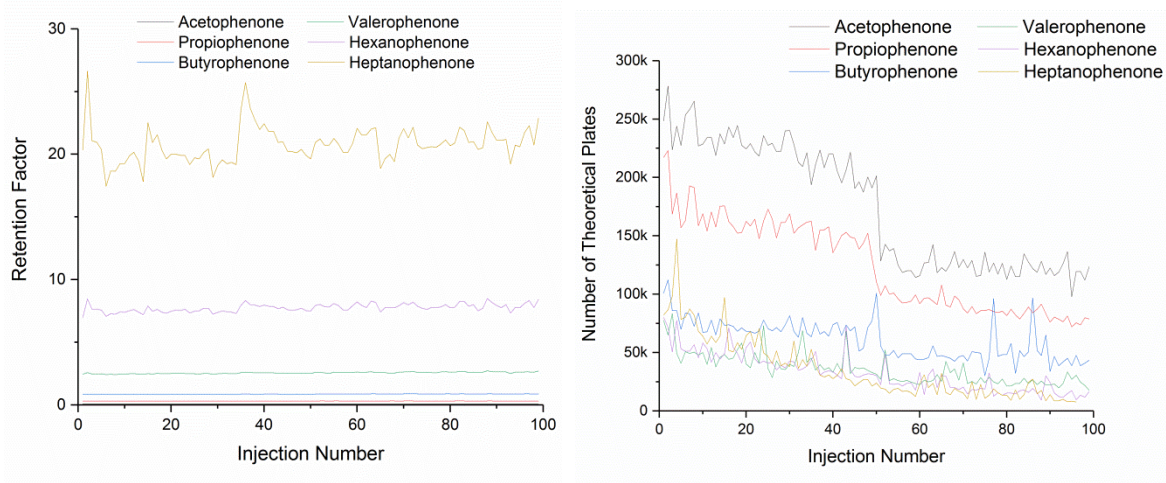


Figure 4-2: The retention factor and number of theoretical plates for the six alkyl phenyl ketones over the course of 100 injections.

4.3.2 Selectivity

There are two types of selectivity in EKC systems: hydrophobic and polar group selectivity. The hydrophobic selectivity is represented by the methylene selectivity (α_{CH_2}) that was calculated from the slope of a plot of retention factor vs carbon number for the series of alkyl phenyl ketones described earlier. As the hydrophobic core gets more hydrophobic from methyl to ethyl to butyl, the methylene

selectivity increases. When comparing a group of nanoparticles with the same core chemistry, larger nanoparticles have greater methylene selectivity. This is seen the most in butyl acrylate nanoparticles, to a lesser extent with ethyl nanoparticles, and there is no clear trend with methyl nanoparticles. This trend is shown graphically in Figure 4-3.

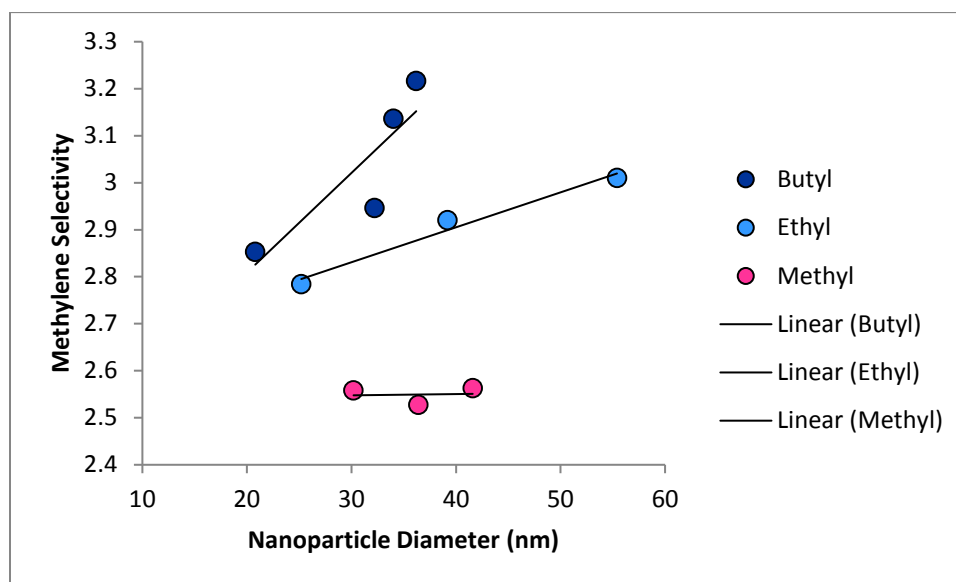


Figure 4-3: Nanoparticle size vs methylene selectivity.

These results compare favorably to the methylene selectivities for anionic nanoparticles with the same core chemistries but with an AMPS shell. The average methylene selectivity for a given core chemistry comparing cationic latex nanoparticles and anionic latex nanoparticles is shown in Table 4-5, using data from BAAMPS, EAAMPS, and MAAMPS data generated by Hungngai (Jane) Chuk and Jesse Hyslop. Results for the surfactants SDS and CTAB are also shown. Methylene selectivity is similar between methyl acrylate nanoparticles and surfactants, and both types of nanoparticles have increased selectivity for hydrophobic compounds. This seems counter-intuitive because the surfactants have longer carbon chains than butyl acrylate, but there are likely many more butyl acrylate pendant chains per nanoparticle than there are hydrocarbon tails per surfactant micelle.

Table 4-5: Methylene selectivities of cationic and anionic latex nanoparticles

	Cationic	Replicates	Anionic	Replicates
Butyl Acrylate	3.0 ± 0.17	37 (4 particles)	3.2 ± 0.16	37 (2 particles)
Ethyl Acrylate	2.9 ± 0.11	27 (3 particles)	2.9 ± 0.11	25 (2 particles)
Methyl Acrylate	2.55 ± 0.041	21 (3 particles)	2.5 ± 0.11	15 (2 particles)
50 mM Surfactant	2.58 ± 0.086	13 (CTAB)	2.57 ± 0.079	13 (SDS)

Polar group selectivity compares the retention of benzene to the retention of various substituted benzenes by calculating the ratio of $k_{\text{substituted}}/k_{\text{benzene}}$.⁹⁰ Compounds retained less than benzene will be less than one, and compounds retained more will have a value greater than one. The polar selectivity for benzyl alcohol (-CH₂OH), phenol (-OH), acetophenone (-C=OCH₃), phenyl acetate (-OC=OCH₃), benzonitrile (-CN), anisole (-OCH₃), nitrobenzene (-NO₂), toluene (-CH₃), chlorobenzene (-Cl), and iodobenzene (-I) for each nanoparticle. The results are shown in Table 4-6.

Table 4-6: Polar Group Selectivity for Cationic Latex Nanoparticles

Compound	JM132 BA	KB4F BA	KB3D BA	KB3A BA	JM136 EA	JM142 EA	KB4D EA	KB3C MA	JM137 MA	KB3F MA
Benzyl Alcohol	0.045 (0.001)	0.097 (0.001)	0.09 (0.023)	0.14 (0.022)	0.07 (0.015)	0.01 (0.011)	0.2 (0.12)	0.2 (0.16)	0.16 (0.056)	0.105 (0.001)
Phenol	0.155 (0.001)	0.292 (0.003)	0.235 (0.004)	0.431 (0.001)	0.240 (0.003)	0.20 (0.037)	0.3 (0.19)	0.316 (0.004)	0.40 (0.068)	0.324 (0.005)
Acetophenone	0.325 (0.003)	0.406 (0.008)	0.362 (0.006)	0.69 (0.053)	0.355 (0.009)	0.303 (0.001)	0.52 (0.021)	0.49 (0.010)	0.44 (0.062)	0.503 (0.004)
Phenyl Acetate	0.338 (0.005)	0.425 (0.005)	0.413 (0.007)	0.770 (0.001)	0.430 (0.006)	0.35 (0.041)	0.15 (0.035)	0.71 (0.012)	0.6 (0.13)	0.59 (0.014)
Benzonitrile	0.440 (0.006)	0.50 (0.011)	0.465 (0.004)	0.899 (0.002)	0.48 (0.010)	0.35 (0.031)	0.90 (0.085)	0.8 (0.19)	0.6 (0.12)	0.67 (0.014)
Anisole	1.30 (0.067)	1.36 (0.019)	1.35 (0.048)	2.19 (0.017)	1.5 (0.33)	0.91 (0.034)	1.56 (0.036)	1.49 (0.023)	0.9 (0.13)	1.474 (0.008)
Nitrobenzene	1.02 (0.024)	1.20 (0.024)	1.18 (0.023)	2.2 (0.21)	1.10 (0.015)	0.83 (0.055)	1.6 (0.24)	1.63 (0.038)	1.4 (0.23)	1.50 (0.015)
Toluene	3.02 (0.026)	2.89 (0.014)	2.89 (0.027)	6.8 (0.14)	2.57 (0.065)	2.7 (0.68)	4.1 (0.15)	2.94 (0.075)	2.3 (0.34)	2.42 (0.085)
Chlorobenzene	5.30 (0.087)	4.94 (0.065)	4.9 (0.17)	10.63 (0.036)	4.66 (0.065)	5 (1.1)	7.1 (0.57)	5.2 (0.12)	4.2 (0.67)	4.52 (0.098)
Iodobenzene	20 (1.6)	15.5 (0.46)	16.2 (0.75)	31.9 (0.26)	13.7 (0.23)	9.9 (0.61)	23.2 (0.37)	16.4 (0.82)	14 (3.0)	13.0 (0.51)

The values in parentheses are standard deviations

In each case benzyl alcohol, phenol, acetophenone, phenyl acetate, and benzonitrile were retained less than benzene while toluene, chlorobenzene, and iodobenzene were more retained than benzene. Anisole and nitrobenzene were both close enough in retention to benzene that they were retained more than benzene in some cases and less in others, and their retention order was not consistent. These results suggest that alcohols and ketones are more soluble in the BGE, where hydrogen bonding with water is more favorable. Methyl groups and halides interact much more with the hydrophobic core of the nanoparticles. Retention factors in general were greater for butyl acrylate nanoparticles, which gave them a larger spread of polar group selectivity values than methyl acrylate nanoparticles. The migration order is similar to the SDBS vesicles described in reference 77.

The polar group selectivity of cationic latex nanoparticles was compared to that of anionic latex nanoparticles and the surfactants SDS and CTAB, as shown in Table 4-7. The selectivities were similar for cationic and anionic latex nanoparticles, but the surfactants were much different. Notable differences are that acetophenone, phenyl acetate, and benzonitrile are much more retained by SDS than any of the nanoparticle chemistries, and phenol is retained more strongly by CTAB than any of the other PSPs studied. Although CTAB, APTAC, and AETMAC all have quaternary amine functional groups, the environment of the head group and micellar structure must be significantly different from the cationic shell of the nanoparticles.

Table 4-7: Polar Group Selectivity Comparison between PSPs

	Cationic BA	Cationic EA	Cationic MA	Anion BA	Anionic EA	Anion MA	SDS	CTAB
Benzyl Alcohol	0.08 (0.026)	0.080 (0.084)	0.14 (0.088)	0.053 (0.005)	0.17 (0.096)	0.115 (0.003)	0.528 (0.004)	0.419 (0.002)
Phenol	0.23 (0.058)	0.4 (0.35)	0.35 (0.052)	0.158 (0.009)	0.4 (0.18)	0.32 (0.010)	0.582 (0.005)	1.60 (0.015)
Acetophenone	0.36 (0.035)	0.3 (0.17)	0.48 (0.044)	0.34 (0.014)	0.5 (0.11)	0.45 (0.016)	2.16 (0.048)	0.76 (0.034)
Phenyl acetate	0.39 (0.040)	0.2 (0.16)	0.6 (0.10)	0.35 (0.030)	0.7 (0.22)	0.569 (0.004)	1.39 (0.016)	0.818 (0.008)
Benzonitrile	0.47 (0.026)	0.5 (0.3)	0.7 (0.14)	0.38 (0.016)	0.8 (0.24)	0.63 (0.013)	1.41 (0.013)	0.660 (0.005)
Anisole	1.34 (0.053)	1.1 (0.6)	1.3 (0.28)	1.2 (0.26)	1.8 (0.45)	1.24 (0.013)	3.37 (0.033)	1.56 (0.014)
Nitrobenzene	1.13 (0.088)	1.0 (0.6)	1.5 (0.15)	1.0 (0.11)	1.6 (0.43)	1.34 (0.027)	1.65 (0.041)	1.183 (0.007)
Toluene	2.93 (0.064)	3.0 (0.9)	2.6 (0.34)	2.4 (0.85)	3.5 (0.82)	2.10 (0.024)	2.57 (0.044)	3.06 (0.068)
Chlorobenzene	5.0 (0.22)	6 (2.0)	4.6 (0.54)	5.5 (0.72)	6 (1.4)	3.94 (0.078)	6.38 (0.039)	4.33 (0.024)
Iodobenzene	17 (1.8)	13 (8.2)	14 (2.3)	17 (2.4)	19 (4.5)	10.9 (0.11)	7.91 (0.071)	15.1 (0.87)

The values in parenthesis are standard deviations

4.3.3 Linear Solvation Energy Relationships

LSE analysis was performed on 10 different nanoparticles: two BAAETMAC, two BAAPTAC, three EAAETMAC, one MAAETMAC, and two MAAPTAC. Unfortunately, all EAAPTAC syntheses were not successful or did not produce enough polymer for analysis. The results are shown in Table 4-8. The two dominant terms in all cases are v and b ; the McGowen characteristic volume and the hydrogen bond basicity, or ability to accept a hydrogen bond. The large positive v term suggests that it is easier to form a cavity in the PSP than the aqueous BGE, and the large negative b term suggests that the BGE is a much better hydrogen bond donor than the PSP. The e , s , and a terms are all much smaller in magnitude, which is observed in nearly all LSE analyses of EKC PSPs⁹¹. The coefficient c is a system constant that

captures the phase ratio and any forces not accounted for by the other five terms. In each case c is smaller than v and b but larger than e , s , and a ; which suggests that there may be something else going on not reflected in the current LSER model.

Table 4-8: LSER Results for 10 Cationic Latex Nanoparticles

	Chemistry	c	v	e	s	a	b	R²
JM132	BAAETMAC	-2.5 (0.11)	3.5 (0.13)	0.71 (0.077)	-0.46 (0.067)	-0.45 (0.050)	-3.8 (0.10)	0.955
KB4F	BAAETMAC	-2.86 (0.045)	3.68 (0.064)	0.21 (0.044)	-0.06 (0.026)	-0.20 (0.019)	-3.98 (0.079)	0.999
KB3D	BAAPTAC	-2.72 (0.066)	3.62 (0.094)	0.37 (0.064)	-0.16 (0.039)	-0.35 (0.028)	-3.9 (0.12)	0.997
KB3A	BAAPTAC	-3.0 (0.20)	3.6 (0.23)	0.7 (0.14)	-0.31 (0.12)	-0.29 (0.092)	-4.2 (0.19)	0.866
JM136	EAAETMAC	-3.0 (0.10)	3.6 (0.12)	0.84 (0.07)	-0.36 (0.058)	-0.23 (0.044)	-3.73 (0.094)	0.956
KB4D	EAAETMAC	-2.7 (0.13)	3.3 (0.15)	0.89 (0.090)	-0.66 (0.079)	-0.11 (0.059)	-3.3 (0.12)	0.926
JM142	EAAETMAC	-2.4 (0.25)	3.5 (0.28)	0.7 (0.17)	-0.7 (0.15)	-0.2 (0.11)	-4.1 (0.23)	0.816
KB3C	MAAPTAC	-2.70 (0.069)	3.18 (0.098)	0.46 (0.067)	-0.02 (0.04)	-0.32 (0.029)	-3.3 (0.12)	0.996
JM137	MAAETMAC	-2.02 (0.091)	2.4 (0.11)	0.85 (0.064)	-0.24 (0.056)	-0.19 (0.042)	-2.95 (0.087)	0.945
KB3F	MAAPTAC	-2.72 (0.071)	2.89 (0.082)	0.69 (0.049)	-0.17 (0.043)	-0.22 (0.032)	-3.15 (0.067)	0.970

Values in parenthesis are standard errors.

To help look for trends a large composite analysis was run combining the data from all nanoparticles with butyl acrylate cores, all nanoparticles with ethyl acrylate cores, all nanoparticles with methyl acrylate cores, all nanoparticles with AETMAC shells, and all nanoparticles with APTAC shells. The results are listed in Table 4-9 and shown graphically in Figures 4-4 and 4-5 for easier visualization.

Table 4-9: Composite LSER Results

	c	v	e	s	a	b	R ²
All BA	-2.69 (0.073)	3.37 (0.084)	0.71 (0.051)	-0.40 (0.044)	-0.27 (0.034)	-3.70 (0.069)	0.911
All EA	-2.7 (0.11)	3.5 (0.12)	0.81 (0.74)	-0.57 (0.064)	-0.17 (0.048)	-3.7 (0.10)	0.870
All MA	-2.45 (0.069)	2.73 (0.080)	0.74 (0.048)	-0.18 (0.042)	-0.22 (0.031)	-3.13 (0.066)	0.915
All AETMAC	-2.53 (0.067)	3.22 (0.078)	0.78 (0.047)	-0.47 (0.041)	-0.21 (0.030)	-3.54 (0.063)	0.883
All APTAC	-2.72 (0.066)	3.17 (0.076)	0.70 (0.046)	-0.25 (0.040)	-0.25 (0.030)	-3.52 (0.063)	0.918

Values in parentheses are standard errors.

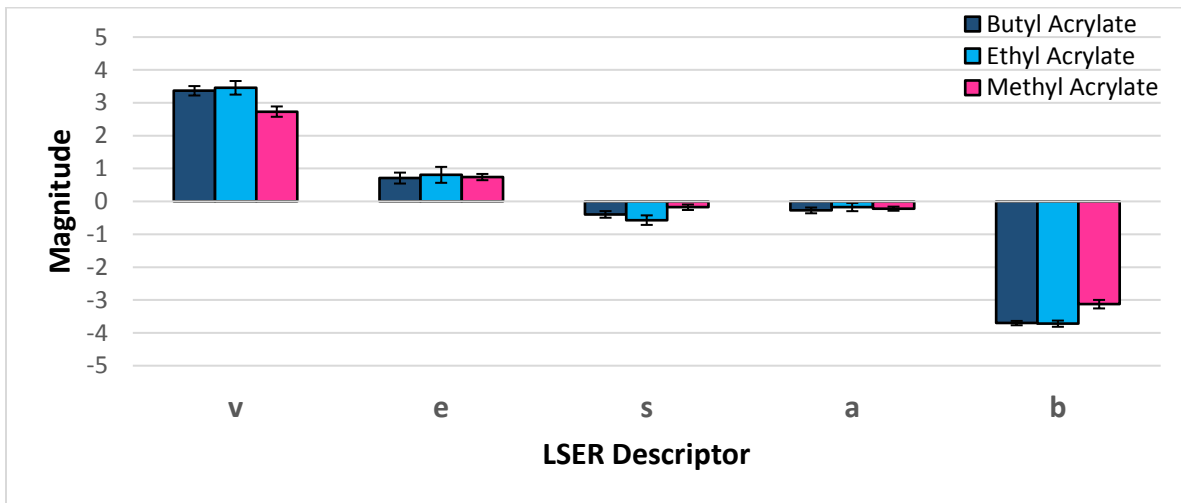


Figure 4-4: Composite LSER Analysis to compare hydrophobic cores

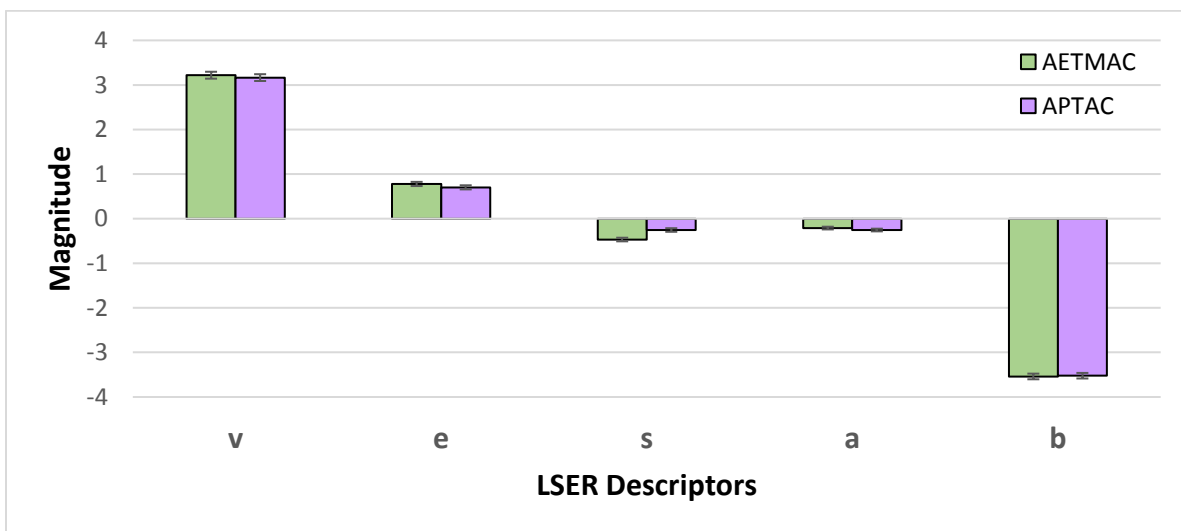


Figure 4-5: Composite LSER analysis to compare hydrophilic shells

This analysis reveals that the two different shells are not significantly different, but that nanoparticles with methyl acrylate cores are significantly different than nanoparticles with either ethyl acrylate or butyl acrylate cores. The addition of a second carbon to the hydrophobic pendent chain appears to make a dramatic difference in the solvation characteristics, but increasing the length of the chain further does not.

The LSER values for other PSPs from the literature are presented in Table 4-10 for comparison:

Table 4-10: Comparison to other LSER studies of PSPs

	v	e	s	a	b
BAAA ³⁹ (anionic latex nanoparticle)	3.29 (0.24)	0.61 (0.16)	-0.40 (0.14)	-0.41 (0.11)	-3.94 (0.22)
BAAMPS ³⁹ (anionic latex nanoparticle)	3.02 (0.24)	0.70 (0.14)	-0.53 (0.13)	-0.32 (0.10)	-3.27 (0.19)
EA AMPS ³⁹ (anionic latex nanoparticle)	2.19 (0.40)	0.75 (0.23)	-0.47 (0.28)	-0.24 (0.15)	-2.96 (0.31)
SDS ³⁹ (anionic surfactant)	2.9 (0.2)	0.5 (0.10)	-0.5 (0.14)	-0.2 (0.11)	-2.33 (0.04)
CTAB (cationic surfactant)	3.41 (0.05)	0.76 (0.03)	-0.46 (0.03)	1.03 (0.02)	-2.94 (0.05)
C16TEAB ⁹² (cationic surfactant)	3.23 (0.18)	0.63 (0.11)	-0.33 (0.09)	1.06 (0.07)	-2.83 (0.14)
C16MPDB ⁹² (cationic surfactant)	2.43 (0.23)	0.42 (0.14)	-0.15 (0.12)	0.95 (0.09)	-2.85 (0.19)
Nanodisc ⁹³ (lipid bilayer in polymer belt)	3.04 (0.10)	0.60 (0.07)	-0.36 (0.05)	0.57 (0.04)	-3.26 (0.08)

The values in parentheses are standard errors

The cationic latex nanoparticles appear to have more in common with anionic latex nanoparticles than they do with cationic surfactants. The most striking difference is in the a term, which represents hydrogen bond donating ability. Cationic surfactants typically have a positive a term^{87,88,94}, which matches what was seen for the three cationic surfactants and the nanodiscs with quaternary ammonium head groups. However, the cationic nanoparticles have a small and negative a term, similar to SDS and anionic nanoparticles. Work with phospholipids suggests that water molecules form a clathrate structure around trimethylammonium head groups⁹⁵⁻⁹⁷, where the water molecules can hydrogen bond

to each other rather than with the nitrogen atom because the hydrophobic methyl groups are in the way. This clathrate structure is a different environment compared to the bulk BGE, which is why there is a significant difference in the two LSER terms related to hydrogen bonding in LSER. The fact that the a term is different for cationic latex nanoparticles suggests that either the clathrate structure does not form, or that it does not play a significant role in retention during EKC.

4.4 Conclusions

In this chapter the cationic latex nanoparticles were evaluated as PSPs for EKC. Analyzing the data from the homologous series of alkyl phenyl ketones and the set of 39 LSER solutes has revealed several important aspects of retention. Methylene selectivity is driven by the hydrophobicity of the nanoparticle core and the size of the nanoparticle, with the greatest methylene selectivity seen in the largest butyl acrylate nanoparticles. Polar group selectivity is driven by the ability to donate or accept hydrogen bonds, solute size, and solute polarizability. Iodobenzene was the most retained compound of the substituted benzenes studied, and also has the largest E value of 1.188. Water is a better hydrogen bond donor and acceptor than any of the PSPs, so compounds that can both donate and accept a hydrogen bond, like benzyl alcohol, are barely retained by any of the PSPs studied.

A surprising finding from the LSER studies was that cationic latex nanoparticles have a small and negative a term. Surfactant micelles and lipid bilayers are well understood structures that consist of a polar head group and a non-polar tail. Water is excluded from the hydrophobic core. Most hydrophilic analytes cannot penetrate the Stern layer to reach the core, which means selectivity is driven by the chemistry of the headgroup. Latex nanoparticles, however, show selectivity that is influenced primarily by the different core chemistries. Cationic nanoparticles with quaternary amines and anionic nanoparticles with sulfonate groups behave nearly identically, and cationic latex nanoparticles behave more like anionic latex nanoparticles than cationic surfactants. For this to happen, the solutes must be

able to penetrate through the cationic shell of the latex nanoparticle and interact with the hydrophobic core. This work suggests that latex nanoparticles are not just polymeric versions of surfactant micelles. Water might not be completely excluded from the hydrophobic domain, facilitating transport of analytes to the core. The most hydrophobic monomer, butyl acrylate, has a much shorter carbon chain than the hydrocarbon tails of the surfactants studied here, and the acrylate functional group is much more hydrophilic. The cationic block is not behaving in the same way as a quaternary ammonium headgroup on a surfactant.

The results found in this chapter can be used to select an appropriate nanoparticle for a given analysis. The separation of hydrophobic compounds like PAHs would require a large butyl acrylate for the methylene selectivity, while the separation of more polar compounds might work better with methyl acrylate. Explosives compounds contain many polar nitro groups, so a methyl acrylate would likely be the most appropriate choice. This will be explored further in Chapter 5.

Chapter 5: A Method for the Separation of Explosives

5.1 Introduction

Many analytical techniques have been used to detect and quantify explosives; including chromatography⁹⁸, spectroscopy⁹⁹, trained dogs¹⁰⁰, and sensors¹⁰¹. An ideal detector must be both sensitive and selective. It needs to detect trace levels of explosives while avoiding both false positives and false negatives. There is no one universal detector that works 100% of the time, so different detection methods are employed for different applications.

There are several scenarios where the detection of explosives is important. Incoming shipments on cargo ships or passenger luggage needs to be screened without opening every container. People must be screened in places like airports and military checkpoints, and environmental samples need to be analyzed near former military sites. There are two basic types of detection: bulk, and vapor or particle detection. Methods for detecting bulk explosives inside containers include x-ray scattering, dispersive x-ray diffraction, computed tomography (CT), nuclear magnetic resonance spectroscopy (NMR), electron spin resonance (ESR) spectroscopy, nuclear quadrupole resonance (NQR) spectroscopy, microwave spectroscopy, Raman spectroscopy, thermal neutron activation (TNA), fast neutron activation (FNA), neutron elastic scatter (NES), and associated particle imaging (API).⁷ These techniques can be interfaced to improve performance; such as with the XENIS instrument that combines the high quality images produced with X-rays with the TNA's specificity for nitrogen⁷. Techniques like infrared (IR) and UV-Vis spectroscopy cannot be used in these cases because they do not penetrate the containers.

Vapor detection is advantageous because it is a contactless detection method, but is challenging due to the low vapor pressure of some explosive compounds. Commercial explosive formulations often include taggents, compounds with high vapor pressure to allow them to be detected more easily. Vapor generators include continuous flow, pulsed flow, thermal desorption, and systems that use gas

chromatographs to generate vapors¹⁰². Particulates can be collected from people or surfaces using swabs or other adsorbent materials. This is more invasive than vapor collection, but captures material with lower volatility. Gas and liquid chromatography can be used to separate analytes and interfaced with various detectors including electron capture detectors (ECD), thermal energy analyzers (TEA), mass spectrometers (MS), and ion mobility spectrometers (IMS).

IMS is one of the most widely used techniques for screening in airports. There are several commercial instruments currently in use, including the Ionscan[®] made by Smiths Detection and the Itemizer[®] made by Ion Track Instruments. An IMS instrument consists of an ion source, an ion gate, a drift tube, and a detector. Analytes are ionized in the source, which is typically a ⁶³Ni foil but can also be corona discharge, photoionization, or electrospray, and sent through the ion gate as a discrete packet. A series of conducting rings in the drift tube establishes an electric field. Analytes move through the drift tube to the detector on the other side, which is usually a Faraday plate. The resulting spectrum is a plot of ion current vs ion drift time. Reagent gases can be added to create adducts to increase specificity. Explosives are fairly electronegative and are detected in negative ion mode as [M-H]⁻, [M · NO₃]⁻, and [M · Cl]⁻. Adduct formation is sensitive to humidity and temperature, so the conditions must be carefully controlled¹⁰³. False positives are also possible when compounds with similar drift times found in cosmetics, personal care products, and household cleaners are picked up by the swabs¹⁰⁴.

Environmental samples like water or soil can also be analyzed to detect spent munitions or landmines. Ammunition is not always disposed of in an environmentally friendly manner, and wastewater from their manufacture can be discharged into rivers and streams. Landmines are a serious problem in Afghanistan, Angola, Bosnia, Cambodia, Croatia, Egypt, Iran, Iraq, and Mozambique, which each have millions of unexploded landmines. Detection methods include manual prodding, metal detectors, and ground penetrating radar. About 80% of landmines contain TNT and its related

impurities. The isomers of dinitrotoluene and dinitrobenzene have much higher vapor pressures than TNT itself, so it is possible to detect landmines by analyzing vapor¹⁰⁵.

Samples can be taken and brought to a lab for separation and analysis. Gas chromatography-mass spectrometry (GC-MS), high performance liquid chromatography (HPLC), and ion chromatography (IC) are common analytical techniques that can be used for the analysis of explosives residues. EPA method 8330 uses HPLC to analyze nitroaromatic and nitramine compounds, and IC is useful for inorganic ions. These are well-developed analytical techniques, but they do have disadvantages. GC can only analyze compounds that can withstand the high temperatures involved. HPLC is time consuming and uses large volumes of organic solvents. In addition, multiple methodologies must be used to assess the full range of compounds.

CE is a complimentary technique to ion chromatography that is often used for the analysis of ionic analytes found in explosives residues, especially from IEDs. Important ions for detection include the oxidizers nitrate, chlorate, and perchlorate; plus product ions such as thiocyanate. Breadmore and coworkers have done extensive work in this area and have developed specialized instrumentation using a miniaturized blue LED detector⁵⁵, conductivity detection⁵⁶, or sequential injection⁵⁷ to separate and detect anions and cations found in IED residues. The method developed by Breadmore's group was adapted for use as a complimentary method to ion chromatography by the French police¹⁰⁶. CE has also been used to analyze ions found in incendiary devices¹⁰⁷, acid-aluminum mixtures⁶⁰, and consumer fireworks¹⁰⁸. Kobrin and coworkers developed a portable CE system to bring into the field for preliminary fingerprinting of explosives through conductivity detection and principal component analysis⁶¹. Many inorganic anions are not visible by the UV detector that comes on commercial CE instruments, but an alternative is capacitively-coupled contactless conductivity detection (C4D).

Commercial instruments such as the TraceDec or home-built systems can be interfaced with commercial CE instruments or lab-on-a-chip microfluidics systems^{109–111}.

EKC was first used to separate gunshot and explosives residues by Northrop, Martire, and MacCrehan⁴⁹ in 1991 using SDS, borate buffer, and tetraalkyl ammonium salts to enhance the separation of inorganic ions. They looked at a mix of 26 compounds and were able to separate most of them, with the exception of mononitrotoluene and dinitrotoluene isomers and used multiple UV wavelengths to identify compounds. Mussenbrock and Kleiböhmer¹¹² were able to separate 22 out of 24 target analytes using a mixed surfactant BGE with SDS and SB-12 in 1995. Oehler¹¹³ separated 14 nitroaromatic and nitramine compounds using SDS in 15 minutes in 1997, and in 1998 Bailey¹¹⁴ used capillary electrochromatography with 1.5 μm octyldecylsilica particles to separate 14 nitroaromatic and nitramine compounds in 8 minutes. More recently perfluorooctanoic acid (PFOA) was used as a PSP for the analysis of nitroaromatic explosives in environmental samples by ESI-MS⁵⁴ and MEKC was used for to separate peroxide-based explosives⁵³.

UV detection is not the best for explosives, especially nitamines which do not absorb UV very well. An alternate detection approach is indirect detection, where the absence of the background is detected instead of the presence of the analyte. Indirect detection methods include vacancy chromatography, amperometric detection, and fluorescence quenching¹¹⁵. Hilmi, Luong, and Nguyen¹¹⁶ used EKC and amperometric detection to analyze nitrotoluenes. Laser induced fluorescence can be used to detect the fluorescence quenching of nitroaromatic and nitramine compounds. Kennedy, Caddy, and Douse¹¹⁷ in 1997 used indirect fluorescence detection to detect 8 high explosives separated by SDS and using fluorescein as a fluorophore. Goodpaster and McGuffin¹¹⁸ used pyrene as a fluorophore for fluorescence quenching detection.

Both CE and EKC have shown promise for the analysis of different types of explosives compounds, and since they use the same instrumentation, it should be possible to combine the two. The nanoparticles synthesized in Chapter 2 and characterized in Chapter 4, in conjunction with the cationic capillary coating discussed in Chapter 3, were used to separate a mixture of anions and nitroaromatic and nitramine neutral compounds commonly found in explosives residues. The anions are detected by conductivity detection and the nitroaromatics are detected by UV detection. Although not fully investigated here, this technique should be compatible with a more sensitive fluorescence quenching detection system as well.

5.2 Experimental

The neutral compounds 2-amino-4,6-dinitrotoluene (2-AM), 4-amino-2,6-dinitrotoluene (4-AM), 3,5-dinitroaniline (DNA), 1,3-dinitrobenzene (DNB), 2,4-dinitrotoluene (2,4-DNT), 2,6-dinitrotoluene (2,6-DNT), HMX, nitrobenzene (NB), nitroglycerin (NYG), 2-nitrotoluene (2-NT), 3-nitrotoluene (3-NT), 4-nitrotoluene (4-NT), PETN, RDX, Tetryl (TET), 1,3,5-trinitrobenzene (TNB), and 2,4,6-trinitrotoluene (TNT) were chosen because they are listed under EPA Method 833B: Nitroaromatics, Nitramines, and Nitrate Esters by High Performance Liquid Chromatography. Standards were purchased from Restek Corporation as 1000 µg/mL solutions in acetonitrile. Individual standards were used to insure the correct identification, and two premade mixtures from Restek were used to look at the separation. The anions thiocyanate, chlorate, perchlorate, nitrite, and azide were chosen because they are ions that often appear in explosives residues but do not commonly appear in background samples¹¹⁹. Chloride and sulfate are usually found in environmental samples, and nitrate could be from either explosives or as a background ion. Anion standards were prepared by heating the sodium salt in a 100° C oven overnight to remove residual water, then dissolving the anhydrous salt in deionized water. Benzenesulfonic acid was used as an internal standard, and was prepared in deionized water.

Several different studies were performed using either anions, nitroaromatics, or both groups of analytes. In the spring of 2014 the retention factors of the 15 nitroaromatic compounds were calculated using the anionic surfactant SDS, the anionic nanoparticles LH11 MAAMPS, LH109 EAAMPS, and LH111 BAAMPS, the cationic surfactant CTAB, and the cationic nanoparticles JM137 MAAETMAC, JM136 EAAETMAC, and JM132 MAAETMAC. The anionic PSPs were used with a 10 mM borate BGE, and the cationic PSPs were used with Tris-HCl BGE at pH 7.2. All EKC experiments were carried out in 48.5 cm capillaries with 20 kV applied voltage. This early work was performed before the cationic capillary coatings were developed, which resulted in broad, inefficient separations. Each nitroaromatic compound was analyzed individually to determine its migration time, then between three and five blocks containing three to seven compounds were run five times to get repeatability data. The retention factor was calculated using equation 1-16. A commercially prepared standard of 17 nitroaromatic and nitramine compounds was run to evaluate the separation under the studied conditions. Compounds were identified by their retention factor and UV spectra.

After the PAETMAC coating was developed, more experiments were performed in the spring of 2015 with JM137 MAAETMAC, JM136 EAAETMAC, JM142 EAAETMAC, and JM132 BAAETMAC with 48.5 cm JM159 PAETMAC coated capillaries using 10 mM Tris-Acetate buffer at pH 5. To prepare this buffer 1.5 mL of 1.0 M acetic acid and 0.1211 g of Tris were dissolved in 100 mL of Nanopure water and filtered with a 0.45 μm nylon filter. In the spring of 2016 six nanoparticles synthesized by Kim Brown, KB3A BAAPTAC, KB3C MAAPTAC, KB3F MAAPTAC, KB4C EAAETMAC, KB4D EAAETMAC, and KB4F BAAETMAC were used with either 34 cm, 48.5 cm, or 68.5 cm PAETMAC coated capillaries and pH 5 Tris-Acetate buffer. In the spring of 2017 these nanoparticles were used with Tris-Acetate buffer and differing amounts of acetonitrile.

Anions were analyzed using a TraceDec capacitively coupled contactless conductivity detector (C4D). This detector consists of a box containing the electronics and a sensor that comes attached to a special CE cassette. The capillary passes through the sensor 10 cm from the outlet end. To maximize the signal, settings were configured as follows: Frequency: High, Voltage: 0 dB, Gain: 200%. The offset was adjusted each day to make the signal between 500 and 1000 mV. More concentrated BGE required a higher offset. Anion standards were run either individually for identification or as a mixture to evaluate the separation.

The final, optimized conditions were a 48.5 cm PAETMAC coated capillary and a BGE consisting of 25 mM pH 5 Tris-Acetate buffer with 20% acetonitrile, bringing the Tris-Acetate to 20 mM. KB3F MAAPTAC was added at 0.4% wt/wt. Calibration curves were made under these conditions using blocks of four compounds at 5, 10, 25, 50, and 100 ppm with 50 ppm internal standard. Each concentration was run in triplicate. Four different calibration curves were generated using external standard calibration, normalized external standard calibration, internal standard calibration, and normalized internal standard calibration. The standard deviation of the 10 ppm standards was used to calculate the limit of detection (LOD) and limit of quantitation (LOQ).

5.3 Results and Discussion

5.3.1 Nitroaromatic and Nitramine Compounds

The goal of the initial study in 2014 was to look for differences in selectivity between the common surfactants SDS and CTAB, anionic and cationic nanoparticles, and the three different core chemistries methyl acrylate, ethyl acrylate, and butyl acrylate. The plan was to run everything under identical conditions, however, SDS did not work well in the Tris-HCl buffer and the cationic nanoparticles did not work well in the borate buffer. To compromise, the anionic PSPs were used with a 10 mM borate buffer and the cationic PSPs were used with a Tris-HCl buffer at pH 7.2. The retention factors for

each compound by each PSP were calculated, and the average and standard deviations are listed in

Table 5-1.

Table 5-1: Retention Factors for Nitro Compounds Separated by Different PSPs

Anionic PSPs				
Analyte	Surfactant	Methyl Acrylate	Ethyl Acrylate	Butyl Acrylate
2-AM	3.4 (0.17)	0.37 (0.024)	2.90 (0.020)	2.56 (0.14)
4-AM	4.2 (0.23)	0.419 (0.0030)	4.51 (0.022)	3.63 (0.031)
DNA	1.91 (0.078)	0.197 (0.0019)	1.54 (0.018)	1.453 (0.0046)
DNB	0.95 (0.033)	0.07 (0.011)	0.46 (0.011)	0.417 (0.0028)
2,4-DNT	2.22 (0.093)	0.18 (0.015)	1.35 (0.020)	1.332 (0.0091)
2,6-DNT	2.5 (0.11)	0.21 (0.018)	1.92 (0.021)	1.94 (0.020)
HMX	0.43 (0.016)	0.238 (0.0088)	1.17 (0.017)	0.743 (0.014)
NB	1.10 (0.045)	0.051 (0.0064)	0.44 (0.018)	0.490 (0.0059)
2-NT	2.7 (0.12)	0.114 (0.0016)	1.29 (0.019)	1.531 (0.0088)
3-NT	3.1 (0.15)	0.135 (0.0071)	1.33 (0.023)	1.198 (0.0040)
4-NT	3.0 (0.15)	0.13 (0.013)	1.30 (0.018)	1.46 (0.013)
RDX	0.53 (0.019)	0.089 (0.012)	0.47 (0.015)	0.382 (0.0045)
Tetryl	1.67 (0.062)	0.8 (0.21)	9.88 (0.031)	5.42 (0.018)
TNB	0.57 (0.019)	0.09 (0.015)	0.77 (0.016)	0.650 (0.0044)
TNT	1.44 (0.053)	0.32 (0.017)	3.52 (0.018)	2.81 (0.0067)
Cationic PSPs				
Analyte	Surfactant	Methyl Acrylate	Ethyl Acrylate	Butyl Acrylate
2-AM	27 (1.6)	0.70 (0.011)	0.81 (0.015)	1.73 (0.012)
4-AM	42 (3.0)	0.91 (0.027)	1.23 (0.087)	2.278 (0.0025)
DNA	20.7 (0.74)	0.428 (0.0069)	0.452 (0.0067)	0.49 (one rep)
DNB	2.19 (0.023)	0.136 (0.0028)	0.136 (0.0029)	0.295 (0.0042)
2,4-DNT	6.2 (0.14)	0.0327 (0.0063)	0.44 (0.013)	0.922 (0.0063)
2,6-DNT	7.2 (0.12)	0.433 (0.0039)	0.57 (0.028)	1.29 (0.033)
HMX	23 (1.4)	0.509 (0.0039)	0.370 (0.0058)	0.594 (0.0045)
NB	1.75 (0.017)	0.105 (0.0019)	0.127 (0.0050)	0.334 (0.0032)
2-NT	5.9 (0.11)	0.261 (0.0044)	0.39 (0.018)	1.03 (0.032)
3-NT	6.22 (0.093)	0.269 (0.0042)	0.379 (0.0032)	1.066 (0.0071)
4-NT	6.3 (0.12)	0.278 (0.0020)	0.399 (0.0074)	0.97 (0.012)
RDX	7.6 (0.19)	0.162 (0.0030)	0.141 (0.0016)	0.279 (0.0019)
Tetryl	27 (1.6)	1.59 (0.025)	1.99 (0.026)	3.54 (0.024)
TNB	4.02 (0.069)	0.225 (0.0044)	0.224 (0.0027)	0.431 (0.0054)
TNT	2.83 (0.037)	0.774 (0.0012)	0.887 (0.0088)	1.791 (0.0054)

These results suggest that compounds are retained more strongly by nanoparticles with butyl acrylate cores than for ethyl or methyl acrylate cores. Cationic and anionic nanoparticles with the same

core had very similar retention factors, which is consistent with the findings in Chapter 4. The two surfactants had very different selectivities compared to the nanoparticles. Some trends regarding structure and retention can be observed for the acrylate nanoparticles. Increasing the number of nitro groups on an analyte increases retention, which can be seen by the increase in retention factor from nitrotoluene to dinitrotoluene to trinitrotoluene. This was seen with all three core chemistries. Adding a methyl group increases retention more than adding a nitro group, as can be seen by the increase in retention factor 1,3,5-trinitrobenzene to the nitrotoluene isomers. The presence of an aniline group increases retention as well, as can be seen from the large retention factors of 2-AM and 4-AM. PETN is the most strongly retained compound in each case studied, and contains four nitro groups and four methylene groups.

This study was repeated with the cationic nanoparticles in July 2015 with JM159 PAETMAC coated capillaries to see what effect the coating had on the separation of nitroaromatic compounds. The Tris-Acetate buffer at pH 5 was used instead of Tris-HCl at pH 7.2. The efficiency and signal to noise ratio improved with the PAETMAC coated capillaries, as shown in Figure 5-1 comparing a separation performed with JM136 EAAETMAC nanoparticles using nanoparticle coated and PAETMAC coated capillaries. The retention factors obtained with PAETMAC coated capillaries are shown in Table 5-2, and electropherograms of a separation are shown for JM137 MAAETMAC, JM136 EAAETMAC, and JM132 BAAETMAC in Figure 5-2.

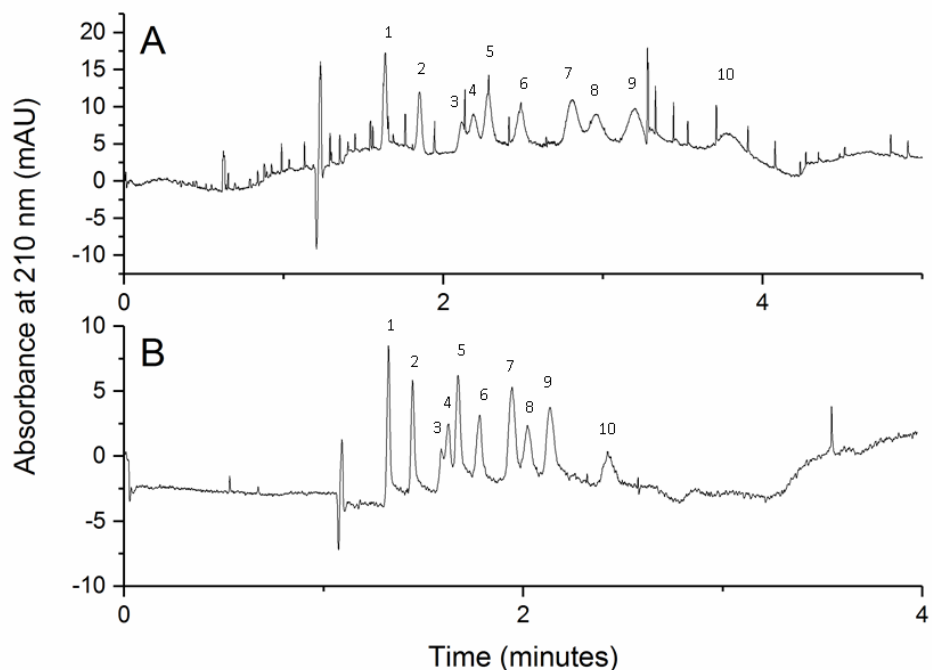


Figure 5-1: The separation of 1 – RDX/NB/DNB, 2 – TNB, 3 – 4-NT, 4 – 3-NT/2-NT, 5 – HMX/2,4-DNT, 6 – DNA, 7 – 2AM, 8 – TNT, 9 – 4AM, 10 – TET using 0.3% JM136 EAAETMAC cationic latex nanoparticles in a pH 5 Tris-Acetate BGE with 34 cm capillaries coated with A) EAAETMAC nanoparticles, or B) JM159 PAETMAC cationic polymer.

Table 5-2: Nitroaromatic Compounds with Cationic Nanoparticles and PAETMAC Coated Capillaries

Analyte	Methyl Acrylate	Ethyl Acrylate	Butyl Acrylate
2-AM	4.5 (0.62)	2.2 (0.19)	1.9 (0.15)
4-AM	6.8 (0.29)	3.2 (0.36)	3.1 (0.39)
DNA	2.8 (0.31)	1.20 (0.097)	1.38 (0.094)
DNB	0.899 (0.0087)	0.41 (0.050)	0.38 (0.034)
2,4-DNT	2.19 (0.022)	1.1 (0.11)	1.12 (0.077)
2,6-DNT	2.85 (0.070)	1.5 (0.12)	2.5 (0.22)
HMX	3.55 (0.088)	1.1 (0.11)	0.69 (0.054)
NB	0.682 (0.0066)	0.41 (0.050)	0.43 (0.036)
2-NT	1.6 (0.16)	1.07 (0.074)	1.5 (0.11)
3-NT	1.58 (0.026)	1.05 (0.088)	1.17 (0.086)
4-NT	1.76 (0.031)	0.92 (0.075)	1.11 (0.074)
RDX	1.05 (0.011)	0.41 (0.050)	0.35 (0.034)
Tetryl	12 (3.4)	6.0 (0.91)	5.5 (0.74)
TNB	1.54 (0.015)	0.66 (0.071)	0.56 (0.044)
TNT	5.97 (0.097)	2.7 (0.35)	2.3 (0.18)

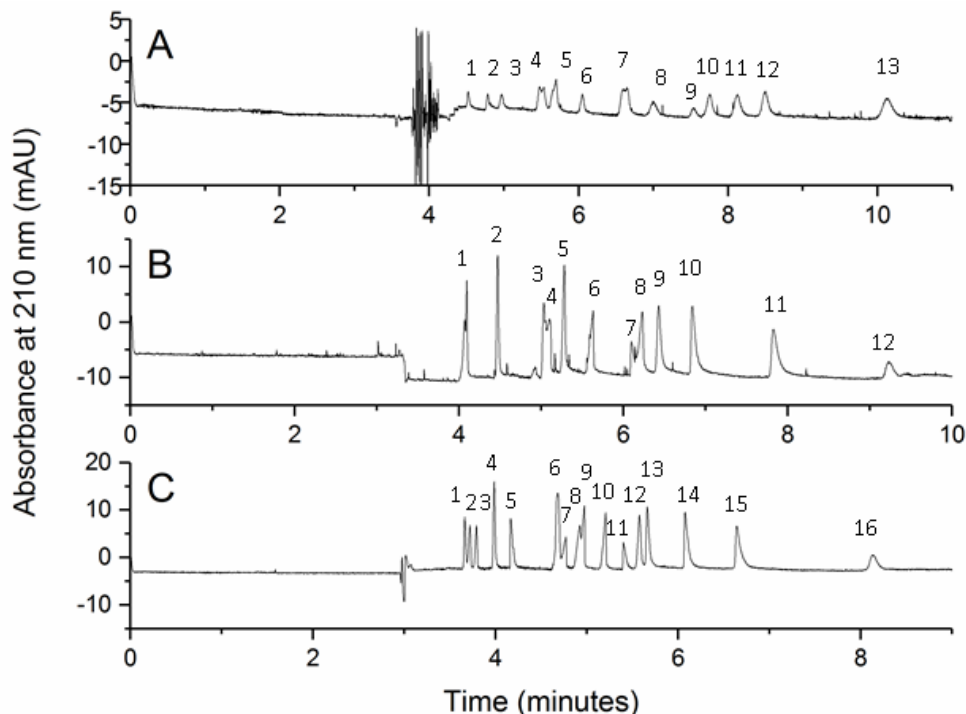


Figure 5-2: The separation of the 8330B list of nitroaromatic and nitramine compounds using 0.3% of A) JM137 MAAETMAC (1 – NB, 2 – DNB, 3 – RDX, 4 – TNB/3-NT, 5 – 2-NT/4-NT, 6 – 2,4-DNT, 7 – DNA/2,6-DNT, 8 – HMX, 9 – 2AM, 10 – TNT, 11 – 4AM, 12 – TET, 13 – PETN), B) JM136 EAAETMAC (1 – RDX/NB/DNB, 2 – TNB, 3 – 2-NT/4-NT, 4 – 3-NT, 5 – HMX, 6 – DNA/2,4-DNT, 7 – 2,6-DNT, 8 – 2AM, 9 – TNT, 10 – 4AM, 11 – TET, 12 – PETN), and C) JM132 BAAETMAC (1 – RDX, 2 – DNB, 3 – NB, 4 – TNB, 5 – HMX, 6 – 2,4-DNT, 7 – 4-NT, 8 – 2-NT, 9 – 3-NT, 10 – 2,6-DNT, 11 – NYG, 12 – 2AM, 13 – TNT, 14 – 4AM, 15 – TET, 16 – PETN) cationic latex nanoparticles in a pH 5 Tris-Acetate BGE in 48.5 cmJM159 PAETMAC coated capillaries.

To correctly assign compounds in the 17 compound mixture, the absorbance at three different wavelengths were monitored: 210 nm, 254 nm, and 320 nm. All the explosives absorbed at 210 nm, most absorbed somewhat at 254 nm, and only mono and dinitrotoluene compounds absorbed at 320 nm. 1,3-dinitroaniline showed a negative peak at 320 nm. The electropherograms presented in this chapter show only the 210 nm trace for clarity, but all wavelengths were used for analyte assignments. There is some ambiguity in the assignments when resolution is poor or compounds co-migrate. The absorbance at different wavelengths is presented in Table 5-3.

Table 5-3: Absorbance of 100 ppm standards at three different wavelengths

Explosive	Absorbance at 210 nm (mAU)	Absorbance at 254 nm (mAU)	Absorbance at 320 nm (mAU)
2-AM	17.8	13.5	0
4-AM	25.5	14.3	0.68
DNA	34.5	23.9	-1.0
DNB	20.8	34.0	1.5
2,4-DNT	11.8	16.7	2.2
2,6-DNT	15.0	9.0	1.8
HMX	19.4	7.9	0
NB	13.7	11.7	2.7
2-NT	17.4	6.8	3.1
4-NT	8.2	0.56	2.2
RDX	16.1	8.2	0
Tetryl	17.7	10.3	1.8
TNB	28.5	19.4	0.35
TNT	14.3	11.4	0.96
NYG	9.1	0	0

There are some disadvantages to using retention factors to compare the separation of these compounds by different PSPs. One is that the calculation involves the EOF, which can change slightly from run to run. A small change in EOF has a larger effect on strongly eluted compounds that spend more time migrating, which leads to more uncertainty. In addition, t_{PSP} is needed for the calculation, and since this value is calculated based on the retention of the homologous series of alkyl phenyl ketones any changes run to run are not reflected. In Table 5-2 the methyl acrylate nanoparticle appears to have the greatest retention, which is inconsistent with the earlier work.

An alternative approach to compare migrations is to use an internal standard and calculate normalized mobilities using the equation¹²⁰

$$\Delta\mu = \mu_{analyte} - \mu_{IS} = \left(\frac{L_D L_T}{V} \left(\frac{1}{t_{analyte}} - \frac{1}{t_0} \right) \right) - \left(\frac{L_D L_T}{V} \left(\frac{1}{t_{IS}} - \frac{1}{t_0} \right) \right) \quad (5-1)$$

where $\Delta\mu$ is the normalized mobility, μ_{analyte} and μ_{IS} are the mobilities of the analyte and internal standard, respectively, L_D is the capillary length to the detector, L_T is the total capillary length, V is the applied voltage, t_{analyte} , t_0 , and t_{IS} are the migration times of the analyte, an unretained compound, and the internal standard, respectively. A change in the EOF will affect both the analyte and the IS, leading to a more reproducible metric. The sign of the mobility depends on retention relative to the internal standard: an analyte that reaches the detector before the internal standard will have a positive $\Delta\mu$, while an analyte that reaches the detector after the internal standard will have a negative $\Delta\mu$. Benzene sulfonic acid was chosen as an internal standard because the aromatic ring makes it visible by UV detection and the low pK_a of the sulfonate group should make it visible to the conductivity detector. The molecular structure is shown in Figure 5-3. In practice, the IS appears as a negative peak on the C4D and absorbs at 210 nm on the UV detector. The IS peak appears after the anions but before acetone and the other neutral compounds.

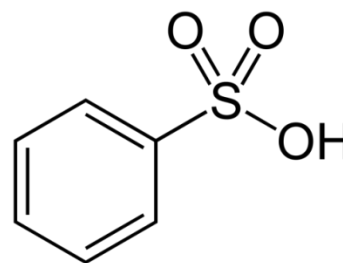


Figure 5-3: Benzene sulfonic acid was used as an internal standard.

The BAAPTAC nanoparticle KB3A was used extensively to optimize conditions for the separation of nitroaromatic compounds. Resolution is difficult to achieve between very similar compounds, such as the three isomers of nitrotoluene. A 68.5 cm PAETMAC coated capillary was used in conjunction with KB3A BAAPTAC nanoparticles to try and improve resolution. It did, at the expense of a longer analysis time. As mentioned in Chapter 4, the amount of PSP in the BGE has an important role in retention and resolution. KB3A was added to the pH 5 Tris-Acetate BGE at 0.1%, 0.3%, and 0.5%. Resolution improved as the percentage of PSP increased, as can be seen in Figure 5-4.

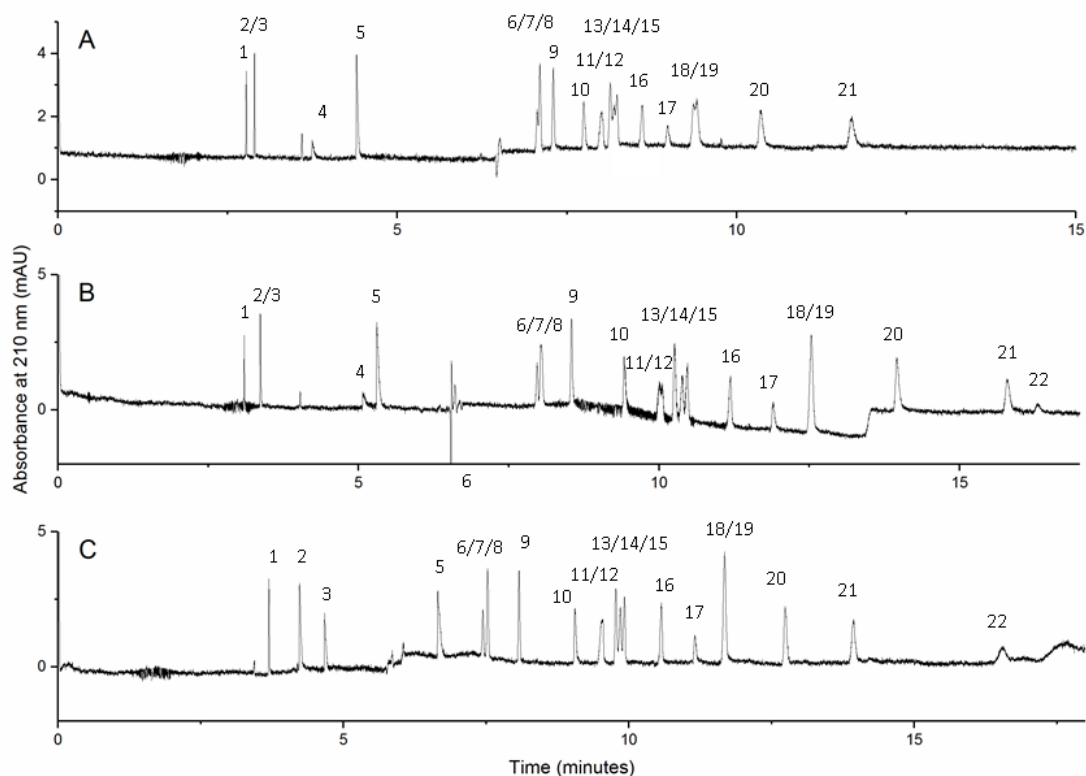


Figure 5-4: The separation of 1 – NO_2^- , 2 – NO_3^- , 3 – N_3^- , 4 – SCN^- , 5 – IS, 6 – RDX, 7- DNB, 8 – NB, 9 – TNB, 10 – HMX, 11 – 2-NT, 12 – 4-NT, 13 – DNA, 14 – 3-NT, 15 – 2,4-DNT, 16 – 2,6-DNT, 17 – NYG, 18 – 2AM, 19 – TNT, 20 – 4AM, 21 – TET, 22 – PETN using A) 0.1%, B) 0.3%, and C) 0.5% of KB3A BAAPTAC in a pH 5 Tris-Acetate BGE in 48.5 cmJM159 PAETMAC coated capillaries.

Increasing the amount of PSP in solution improved the resolution for co-migrating compounds, which can be seen for analytes 6/7/8 and 13/14/15 in Figure 5-4. However, the selectivity was not changed by the increased capillary length. Different concentrations of BGE and PSP were tried, and higher concentrations of buffer reduced the EOF and improved the separation. Using 25 mM Tris-Acetate buffer and 0.5% PSP made it so a 34 cm capillary could be used instead of a 68.5 cm capillary. This significantly decreased the analysis time, as shown in Figure 5-5.

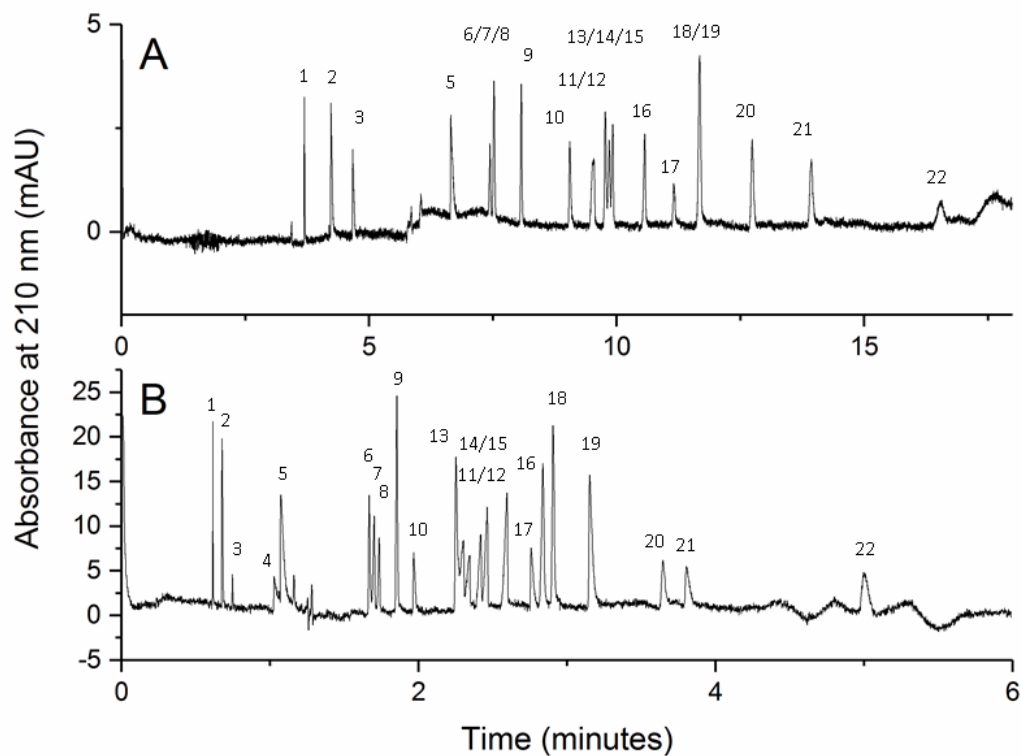


Figure 5-5: The separation of 1 – NO_2^- , 2 – NO_3^- , 3 – N_3^- , 4 – SCN^- , 5 – IS, 6 – RDX, 7- DNB, 8 – NB, 9 – TNB, 10 – HMX, 11 – 2-NT, 12 – 4-NT, 13 – DNA, 14 – 3-NT, 15 – 2,4-DNT, 16 – 2,6-DNT, 17 – NYG, 18 – 2AM, 19 – TNT, 20 – 4AM, 21 – TET, 22 – PETN using 0.5% KB3A in 25 mM pH 5 Tris-Acetate BGE with A) 68.5 cm and B) 34 cm JM159 PAETMAC coated capillaries.

The other nanoparticles synthesized by Kim Brown were used to analyze nitroaromatic compounds and nitroglycerin in four blocks of four compounds, and their normalized mobilities and retention factors were calculated. Six nanoparticles were compared: KB3C MAAPTAC, KB3F MAAPTAC, KB4C EAAETMAC, KB4D EAAETMAC, KB3A BAAPTAC, and KB3D BAAPTAC. The normalized mobilities are shown in Table 5-4, and the retention factors are shown in Table 5-5. These were all analyzed with 0.5%

PSP in the BGE because more PSP led to better resolution for the isomers. Electropherograms are shown in Figures 5-6.

Table 5-4: Normalized Mobilities for Nitroaromatic Compounds

Compound	KB3F MAAPTAC	KB3C MAAPTAC	KB4C EAAETMAC	KB4D EAAETMAC	KB3A BAAPTAC	KB3D BAAPTAC
2-AM	-4.28 (0.013)	-3.732 (0.0028)	-4.42 (0.031)	-3.93 (0.015)	-4.18 (0.018)	-3.742 (0.0054)
4-AM	-4.484 (0.0050)	-3.887 (0.0025)	-4.66 (0.015)	-4.18 (0.017)	-4.465 (0.0033)	-3.573 (0.0064)
DNA	-3.898 (0.0049)	-3.4458 (0.00088)	-4.042 (0.0046)	-3.40 (0.036)	-3.715 (0.0011)	-3.157 (0.0025)
DNB	-2.95 (0.012)	-2.689 (0.0016)	-3.05 (0.029)	-2.50 (0.015)	-2.42 (0.012)	-2.191 (0.0050)
2,4-DNT	-3.48 (0.046)	-3.325 (0.0026)	-3.93 (0.014)	-3.35 (0.015)	-3.564 (0.0043)	-2.778 (0.0066)
2,6-DNT	-3.965 (0.0065)	-3.516 (0.0024)	-4.22 (0.015)	-3.65 (0.014)	-3.949 (0.0045)	-3.12 (0.010)
HMX	-3.95 (0.012)	-3.477 (0.0032)	-3.85 (0.038)	-3.36 (0.015)	-3.68 (0.018)	-3.314 (0.0061)
NB	-2.799 (0.0080)	-2.545 (0.0013)	-3.06 (0.013)	-2.50 (0.015)	-2.494 (0.0048)	-2.152 (0.0058)
2-NT	-3.595 (0.0098)	-3.170 (0.0019)	-3.90 (0.029)	-3.36 (0.015)	-3.01 (0.010)	-3.046 (0.0024)
3-NT	-3.739 (0.0051)	-3.2139 (0.00094)	-3.974 (0.0040)	-3.42 (0.045)	-3.4704 (0.00090)	-3.026 (0.0061)
4-NT	-3.53 (0.012)	-3.151 (0.0011)	-3.869 (0.0064)		-3.617 (0.0054)	-3.023 (0.0011)
RDX	-3.081 (0.0048)	-2.761 (0.0017)	-3.142 (0.0060)	-2.593 (0.0048)	-2.322 (0.0019)	-2.165 (0.0018)
Tetryl	-4.77 (0.059)	-4.123 (0.0019)	-4.930 (0.0068)	-4.51 (0.011)	-4.805 (0.0049)	-3.9551 (0.00079)
TNB	-3.34 (0.042)	-3.082 (0.0012)	-3.476 (0.0068)	-2.86 (0.012)	-2.810 (0.0049)	-2.3728 (0.00031)
TNT	-4.38 (0.0061)	-3.8371 (0.00086)	-4.548 (0.0044)	-3.988 (0.0048)	-4.210 (0.0023)	-3.573 (0.0064)
NYG	-4.22 (0.052)	-3.746 (0.0013)	-4.466 (0.0070)		-4.135 (0.0054)	-3.4246 (0.00099)

Table 5-5: Retention Factors for Nitroaromatic Compounds

Compound	KB3F MAAPTAC	KB3C MAAPTAC	KB4C EAAETMAC	KB4D EAAETMAC	KB3A BAAPTAC	KB3D BAAPTAC
2-AM	2.536 (0.0032)	2.778 (0.0037)	3.21 (0.050)	2.170 (0.0084)	2.44 (0.066)	3.503 (0.0093)
4-AM	3.32 (0.012)	3.562 (0.0071)	4.412 (0.0042)	2.7 (0.30)	3.212 (0.0060)	2.572 (0.0045)
DNA	1.540 (0.0068)	1.720 (0.0029)	1.717 (0.0020)	1.14 (0.053)	1.526 (0.0042)	1.531 (0.0034)
DNB	0.532 (0.001)	0.612 (0.0013)	0.553 (0.0083)	0.404 (0.0016)	0.44 (0.014)	0.555 (0.0014)
2,4-DNT	0.99 (0.040)	1.437 (0.0026)	1.517 (0.0024)	0.9 (0.24)	1.271 (0.0011)	0.995 (0.0019)
2,6-DNT	1.660 (0.0028)	1.896 (0.0015)	2.182 (0.0024)	1.3 (0.25)	1.828 (0.0013)	1.46 (0.011)
HMX	1.673 (0.0037)	1.844 (0.0073)	1.47 (0.023)	1.122 (0.0037)	1.47 (0.034)	1.956 (0.0024)
NB	0.429 (0.0019)	0.4810 (0.00082)	0.539 (0.0015)	0.3 (0.23)	0.4683 (0.00077)	0.4804 (0.00040)
2-NT	1.090 (0.0016)	1.192 (0.0022)	1.54 (0.022)	1.122 (0.0037)	0.80 (0.024)	1.348 (0.0029)
3-NT	1.264 (0.0056)	1.239 (0.0022)	1.579 (0.0030)	1.17 (0.050)	1.220 (0.0031)	1.402 (0.0018)
4-NT	1.031 (0.0042)	1.14 (0.015)	1.406 (0.0062)		1.397 (0.0045)	1.336 (0.0033)
RDX	0.608 (0.0028)	0.664 (0.0014)	0.5878 (0.00044)	0.4516 (0.00031)	0.414 (0.0013)	0.488 (0.0017)
Tetryl	6.2 (0.32)	6.18 (0.053)	8.23 (0.054)	5.00 (0.052)	5.27 (0.023)	4.90 (0.012)
TNB	0.85 (0.038)	1.04 (0.015)	0.889 (0.0033)	0.642 (0.0059)	0.688 (0.017)	0.643 (0.0012)
TNT	2.85 (0.010)	3.268 (0.0068)	3.533 (0.0069)	2.7 (0.30)	2.506 (0.0043)	2.447 (0.0047)
NYG	2.40 (0.096)	2.75 (0.029)	3.122 (0.0078)		2.280 (0.0055)	2.159 (0.0034)

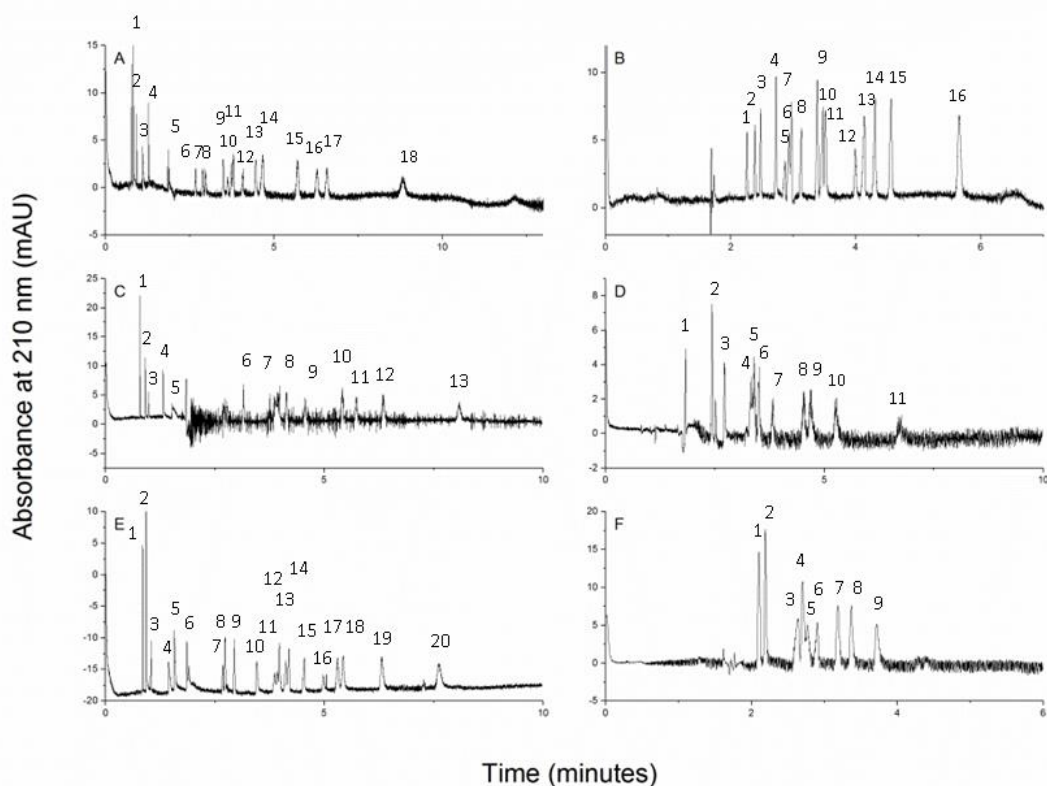


Figure 5-6: The separation of the 8330B list of nitroaromatic and nitramine compounds in a pH 5 Tris-Acetate BGE in 34 cmJM159 PAETMAC coated capillaries.using 0.5% of:

A) KB3C MAAPTAC: 1 – NO₂⁻, 2 – NO₃⁻, 3 – SCN⁻, 4 – N₃⁻, 5 – IS, 6 – NB, 7 – DNB, 8 – RDX, 9 – TNB, 10 – 4-NT/4-NT, 11 – 3-NT/2,4-DNT, 12 – HMX, 13 - DNA, 14 – 2,6-DNT, 15 – 2AM, 16 – TNT, 17 – 4AM, 18 –TET

B) KB3F MAAPTA: 1 – NB, 2 – DNB, 3 – RDX, 4 – TNB, 5 – 4-NT, 6 – 2-NT, 7 – 3-NT, 8 – 2,4-DNT,9 – HMX, 10 – DNA, 11 – 2,6-DNT, 12 – NYG, 13 – 2AM, 14 – TNT, 15 – 4AM, 16 – TET)

C) KB4C EAAETMAC: 1 – NO₂⁻, 2 – NO₃⁻, 3 – SCN⁻, 4 – N₃⁻, 5 – IS, 6 – NB/DNB/RDX/TNB, 7 – 2-NT/4-NT/3-NT/2,4-DNT, 8 – HMX/DNA, 9 – 2,6-DNT/NYG, 10 – 2AM, 11 – TNT, 12 – 4AM, 13 – TET

D) KB4D EAAETMAC: 1 – t₀, 2 – NB/DNB/RDX, 3 – TNB, 4 – 2-NT/4-NT, 5/6/7 – TNB/3-NT/2,4-DNT/HMX/DNA/2,6-DNT/NYG, 8 – 2AM, 9 – TNT, 10 – 4AM, 11 – TET

E) KB3D BAAPTAC: 1 – NO₂⁻, 2 – NO₃⁻, 3 – SCN⁻, 4 – N₃⁻, 5 – IS, 6 – t₀, 7 – RDX, 8 – DNB/NB, 9 – TNB, 10 – 2,4-DNT, 11-14 – 2-NT/3-NT/4-NT/2,6-DNT/DNA, 15 – HMX, 16 – NYG, 17 – 2-AM, 18 – TNT, 19 – 4AM, 20 – TET

F) KB4F BAAETMAC: 1 – RDX/NB/DNB, 2- TNB, 3-6 – NT/DNT/HMX/DNA/NYG, 7 – 2AM/TNT, 8 – 2AM, 9 – TET

The KB4 series of nanoparticles did not work particularly well. The electropherograms were very noisy and many of the nitroaromatic compounds were not separated. The KB2 macroCTA used in these syntheses was one of the smallest with a DP of 4, and KB4F BAAETMAC and KB4D EAAETMAC were the smallest nanoparticles of their core chemistries as characterized by diffusion NMR. The best performing nanoparticles were KB3A BAAPTAC and KB3F MAAPTAC. KB3F MAAPTAC was chosen for further study to optimize conditions for a joint separation of anions and nitroaromatic compounds.

5.3.2 Anions

In February 2014 the group acquired a TraceDec capacitively coupled contactless conductivity detector (C4D). As an early experiment, conditions used by Breadmore⁵⁷ were used to try and separate a mix of 10 anions: fluoride, chloride, azide, thiocyanate, nitrate, carbonate, chlorate, perchlorate, phosphate, and sulfate. While these conditions work well for anion separations by CE, when JM142 EAAETMAC PSP was added the UV baseline was not stable. The Tris-HCl at pH 7.2 BGE used for the LSER work could not be used here because chloride is a target analyte, so Tris-Acetate buffer was used as it worked well for both anions by C4D and nitroaromatics by UV.

Initial work with anions was done in a pH 5 Tris-Acetate buffer without PSP. The anions have quite high mobilities, and resolution was a problem. One way to improve resolution is to lengthen the capillary. Different capillary lengths of 34 cm, 48.5 cm, and 68.5 cm were tried and length did improve the resolution, which can be seen in Figure 5-7.

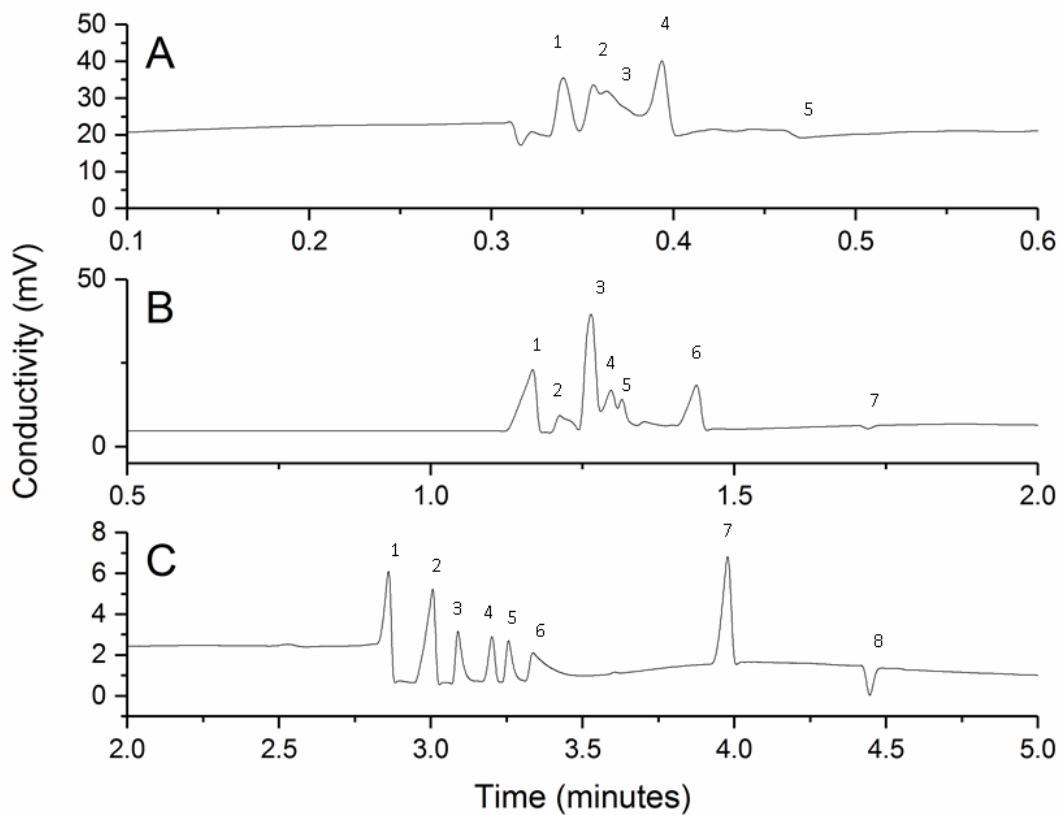


Figure 5-7: Anion resolution improves with increasing capillary length from
 A) 34 cm: 1 – Cl⁻/NO₂⁻, 2 – NO₃⁻/ClO₃⁻, 3 – ClO₄⁻/SCN⁻, 4 – N₃⁻, 5 – IS
 B) 48.5 cm, 1 – Cl⁻, 2 – NO₂⁻, 3 – NO₃⁻, 4 – ClO₃⁻, 5 – ClO₄⁻/SCN⁻, 6 – N₃⁻, 7 – IS
 C) 68.5 cm. 1 – Cl⁻, 2 – NO₂⁻, 3 – NO₃⁻, 4 – ClO₃⁻, 5 – ClO₄⁻, 6 – SCN⁻, 7 – N₃⁻, 8 – IS

The concentration of anions in the BGE affects the peak shape. Anions begin to front as the concentration gets too high, as seen in Figure 5-8. Fronting peaks make already poor resolution even worse, which is especially apparent in the 1000 ppm injection. Despite the worsening peak shape, peak areas still remained proportional to concentration. A seven point calibration curve with concentrations of 5, 10, 25, 50, 100, 250, and 500 ppm had R² values of 0.98 for chloride, 0.99 for chlorate, and 0.99 for azide.

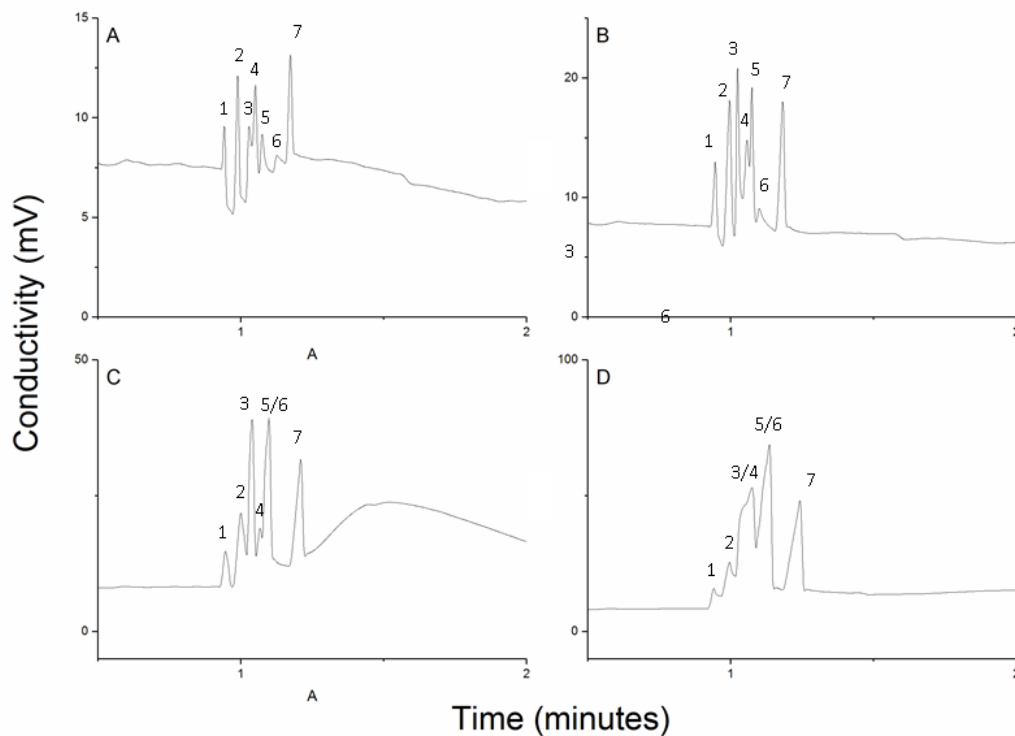


Figure 5-8: A mixture of: 1 – Cl^- , 2 – NO_2^- , 3 – NO_3^- , 4- ClO_3^- , 5 – ClO_4^- , 6 – SCN^- , 7 – N_3^- anions at A) 100 ppm, B) 250 ppm, C) 500 ppm, and D) 1000 ppm in pH 5 Tris-Acetate buffer in a 48.5 cm capillary with no PSP.

To accomplish the goal of a simultaneous separation of anions and nitroaromatic compounds, the cationic latex nanoparticles must be added to the BGE as a PSP. Most ions, including chloride, nitrate, nitrite, and chlorate continued to have sharp peak shapes and similar migration times when a PSP was added. However, thiocyanate and perchlorate began to broaden and have significant tailing, even when only 0.1% PSP was added to the BGE. As more PSP was added, peaks for these two anions became increasingly broad until the peak could not be seen. This is shown in Figure 5-9.

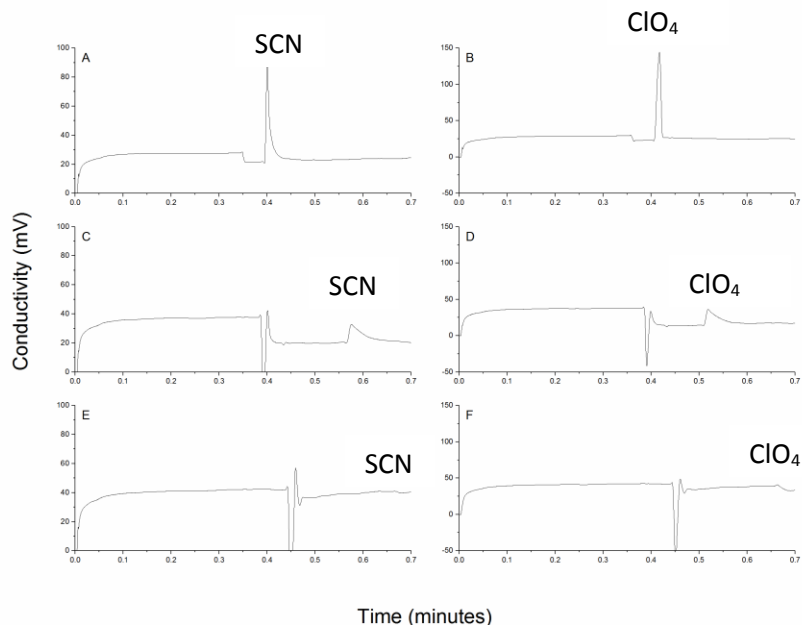


Figure 5-9: Thiocyanate and Perchlorate get broader A) 0% B) 0.3% C) 0.5% of KB3A BAPTAC PSP

These two anions are more hydrophobic than the other analytes in the list¹²¹, suggesting that these ions in particular were interacting with the hydrophobic core of the nanoparticles the way the neutral compounds do. To explore this further, a study was undertaken with 17 different anions which were run with pH 5 Tris-Acetate BGE alone, Tris-Acetate buffer with 0.078% JM30 PAETMAC to look for ionic interactions, and Tris-Acetate buffer with JM142 EAAETMAC PSP to look for hydrophobic interactions. Each anion was run as an individual standard in triplicate using a 34 cm JRM35 PAETMAC coated capillary. In some cases, no peak was observed on the C4D. The anion mobilities were calculated and are shown in Table 5-6.

Table 5-6: Anion Interactions with Polymers in Solution

Anion	TA Alone	RSD	TA + PAETMAC	RSD	TA + EAAETMAC	RSD
Azide	5.90 ± 0.024	0.40%	3.105 ± 0.0044	0.14%	4.595 ± 0.0046	0.01%
Benzenesulfonate	4.16 ± 0.014	0.33%	1.778 ± 0.0099	0.56%	2.857 ± 0.0032	0.11%
Bromide	9.52 ± 0.025	0.26%	4.49 ± 0.017	0.37%	5.06 ± 0.01	0.22%
Chlorate	8.07 ± 0.039	0.49%	5.06 ± 0.019	0.38%	5.49 ± 0.016	0.30%
Chloride	6.79 ± 0.018	0.26%	4.86 ± 0.032	0.65%	5.51 ± 0.024	0.44%
Citrate	4.72 ± 0.016	0.33%	4.97 ± 0.028	0.56%	Not Run	
Fluoride	5.36 ± 0.015	0.27%	4.00 ± 0.045	1.1%	4.40 ± 0.062	1.4%
Formate	5.9 ± 0.11	1.8%	4.67 ± 0.024	0.51%	Not Run	
Iodate	7.6 ± 0.56	7.3%	5.61 ± 0.033	0.58%	4.35 ± 0.013	0.30%
Iodide	6.51 ± 0.012	0.19%	4.66 ± 0.023	0.48%	5.041 ± 0.0091	0.18%
Nitrate	8.89 ± 0.046	0.52%	4.977 ± 0.0078	0.16%	5.55 ± 0.015	0.27%
Nitrite	9.03 ± 0.014	0.15%	4.88 ± 0.018	0.38%	5.598 ± 0.0066	0.12%
Perchlorate	8.1 ± 0.12	1.5%	5.04 ± 0.012	0.24%	5.73 ± 0.24	0.42%
Phosphate	4.419 ± 0.0075	0.17%	3.58 ± 0.052	1.5%	Not Run	
Propanesulfonate	4.344 ± 0.0063	0.14%	3.25 ± 0.019	0.59%	3.80 ± 0.024	0.86%
Sulfate	6.21 ± 0.068	1.1%	5.042 ± 0.0069	0.13%	Not Run	
Thiocyanate	8.20 ± 0.026	0.31%	N.D.	N.D.	4.12 ± 0.023	0.56%

In order to analyze these ions the capillary must be coated with a cationic additive of some kind, which makes it difficult to isolate whether interactions are taking place with the polymers at the capillary surface or polymers in solution. This particular study was not conclusive, and further research should be done to understand the interactions between anions and polymer additives.

5.3.3 Optimizing Conditions for the Simultaneous Separation of Anions and Nitro Compounds

To simultaneously separate anions and neutral compounds by EKC, the interactions between the hydrophobic anions and the PSP must be mitigated. One way to do this is to add an organic modifier to the BGE to decrease retention of hydrophobic compounds. To investigate this further, acetonitrile was added to the BGE and individual standards of perchlorate and thiocyanate were analyzed with increasing concentrations of KB3F MAAPTAC PSP. Although the organic modifier did not completely remove the hydrophobic interactions, peak shapes did improve, as seen in Figure 5-10. Tailing is still

observed with both peaks, but more PSP can be added without the peaks broadening to the extent that they disappear. Up to 0.4% PSP can be used in conjunction with 20% acetonitrile.

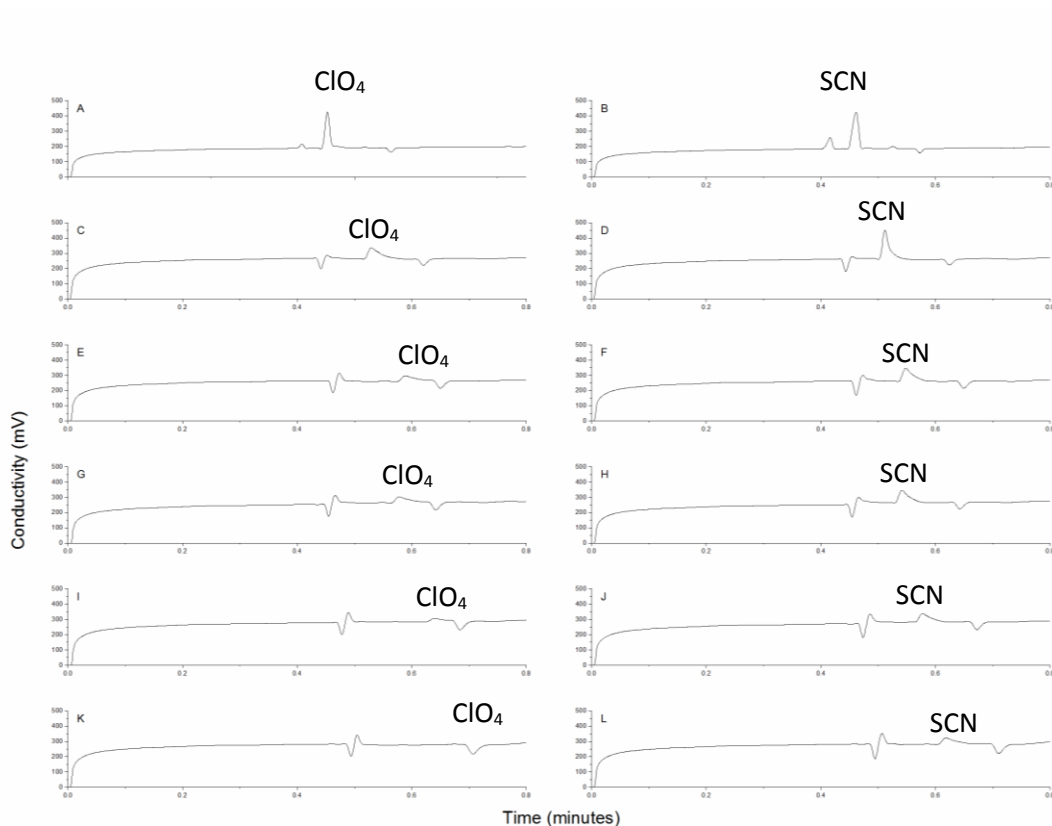


Figure 5-10: Hydrophobic anions on a 34 cm PAETMAC coated capillary with 20 mM Tris-Acetate buffer, 20% acetonitrile, and A) ClO_4^- with 0% PSP, B) SCN^- with 0% PSP, C) ClO_4^- with 0.1% PSP, D) SCN^- with 0.1% PSP, E) ClO_4^- with 0.2% PSP, F) SCN^- with 0.2% PSP, G) ClO_4^- with 0.3% PSP, H) SCN^- with 0.3% PSP, I) ClO_4^- with 0.4%, J) SCN^- with 0.4% PSP, K) ClO_4^- with 0.5%, and L) SCN^- with 0.5% PSP

Adding acetonitrile to the BGE also affects the retention of the nitro compounds. Compounds are less retained in the presence of the organic modifier, and the migration order of the analytes changes. The retention of 2,4-DNT decreases as acetonitrile is added, causing it to migrate faster than most other analytes when 20% acetonitrile is added. All compounds have faster migration times, but TNB and NYG are affected less than other compounds, causing them to appear later in the migration order when 20% acetonitrile is added. Adding additional PSP to the BGE increases retention, as shown

in Figure 5-11. The analyses shown in Figure 5-11 were performed on a 34 cm capillary, and there is a noticeable loss of resolution. Because retention is reduced, a longer capillary can be used without a dramatic increase in analysis time. Figure 5-12 shows the separation of analytes with a 48.5 cm capillary with 10% and 20% acetonitrile. The analysis still takes less than 10 minutes, and most compounds reach the detector before six minutes.

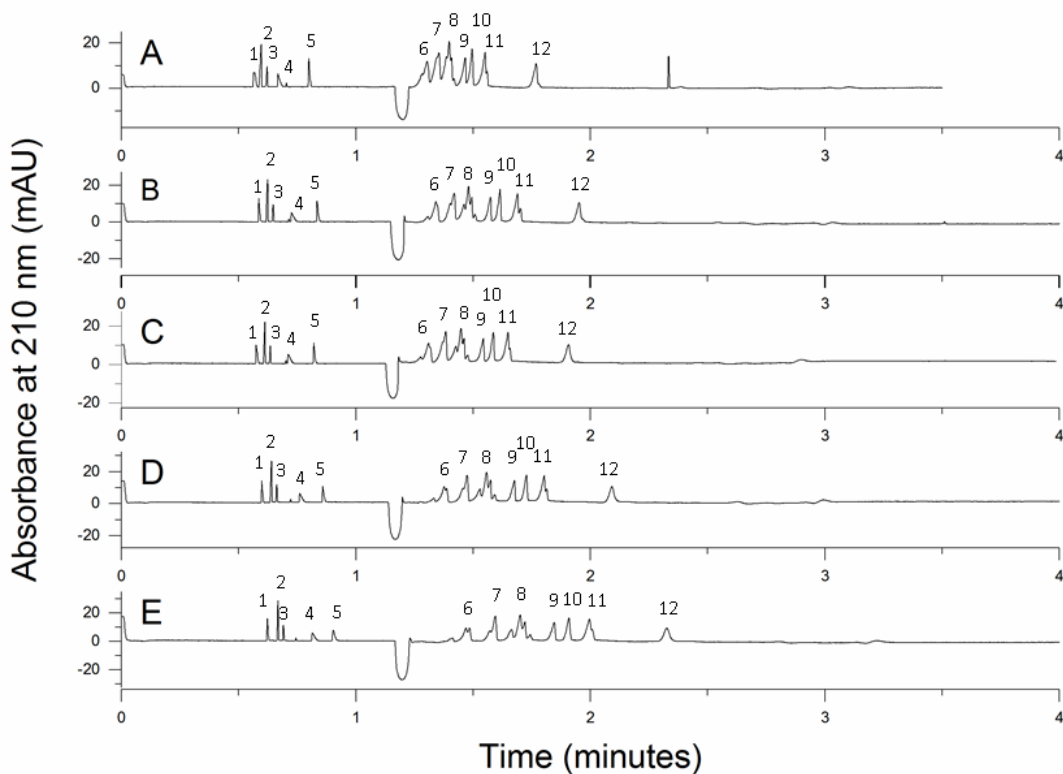


Figure 5-11: A mixture of 1 – NO_2^- , 2 – NO_3^- , 3 – N_3^- , 4 – SCN^- , 5 – IS, 6 – NB/DNB/RDX, 7 – 2-NT/3-NT/4-NT, 8 – TNB, 2,4-DNT/HMX/DNA/2,6-DNT, 9 – 2AM, 10 – 4 AM, 11 – TNT/NYG, 12 – TET in 20 mM pH 5 Tris-Acetate buffer with 20% acetonitrile in a 34 cm capillary with KB3F as PSP at A) 0.1% wt/wt, B) 0.2% wt/wt, C) 0.3% wt/wt, D) 0.4% wt/wt, and E) 0.5% wt/wt.

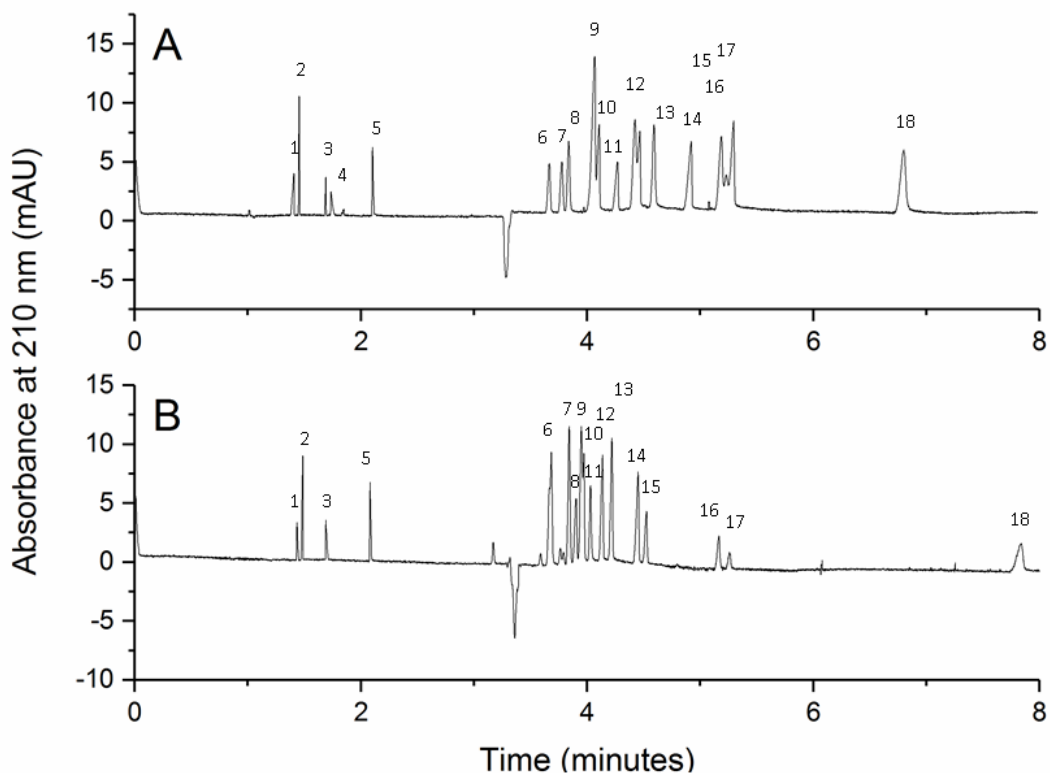


Figure 5-12: A mixture of A) 1 – NO_2^- , 2 – NO_3^- , 3 – N_3^- , 4 – SCN^- , 5 – IS, 6 – NB, 7 – DNB 8 – RDX, 9 – TNB/2-NT/4-NT, 10 – 3-NT, 11 – 2,4-DNT, 12 – HMX/DNA, 13 – 2,6-DNT, 14 – 2AM, 15 – TNT, 16 – NYG, 17 – 4AM, 18 – TET in 20 mM pH 5 Tris-Acetate buffer in a 48.5 cm capillary with 0.2% KB3F and 10% acetonitrile and

B) 1 – NO_2^- , 2 – NO_3^- , 3 – N_3^- , 5 – IS, 6 – NB/DNB/RDX, 7-10 – 2-NT/3-NT/4-NT/TNB, 11 – 2,4-DNT, 13 – HMX, 14 – DNA, 13 – 2,6-DNT, 14 – 2AM, 15 – 4 AM, 16 – TNT, 17 – NYG, 18 – TET in 20 mM pH 5 Tris-Acetate buffer in a 48.5 cm capillary with 0.2% KB3F 20% acetonitrile

The following conditions were chosen for further study: 48.5 cm PAETMAC coated capillary, pH 5, 25 mM Tris-Acetate buffer with 20% acetonitrile added, which dilutes the buffer to 20 mM Tris-Acetate, and KB3F MAAPTAC as a PSP at 0.4%, which was the maximum amount where perchlorate could still be seen. Using these conditions, the limit of detection, limit of quantitation, and calibration curves were constructed for the 16 nitro compounds and four nitrogen anions.

Standards at 5, 10, 25, 50, and 100 ppm with 50 ppm internal standard were run in triplicate in blocks of four compounds each to determine the limit of detection, limit of quantitation, and construct a calibration curve for each compound. There are four possible ways to construct a calibration curve from these data: external standard calibration, normalized external standard calibration, internal standard calibration, and normalized internal standard calibration. In external standard calibration the concentration is plotted on the X-axis and the peak area is plotted on the Y-axis. In CE and EKC, a compound with a slower migration velocity will spend more time travelling past the detector, and therefore the area will be larger for late migrating compounds¹²². To compensate for this, the peak area can be divided by the migration time to calculate the normalized peak area. Plotting the normalized peak area against concentration will create the normalized external standard calibration curve. Other significant sources of variation can come from the CE injection. Comparing the analyte to an internal standard injected at the same time will compensate for injection variation because the discrepancy will affect both peaks, improving precision when area repeatability is poor¹²³. An internal standard calibration curve is the ratio of the analyte and internal standard concentrations on the X-axis and the ratio of the analyte and internal standard peak areas on the Y-axis. The normalized internal standard calibration curve uses the ratio of the two normalized peak areas. The four high explosives were plotted using each of the four methods, as shown in Figure 5-13. The R^2 values for each method are listed in Table 5-6.

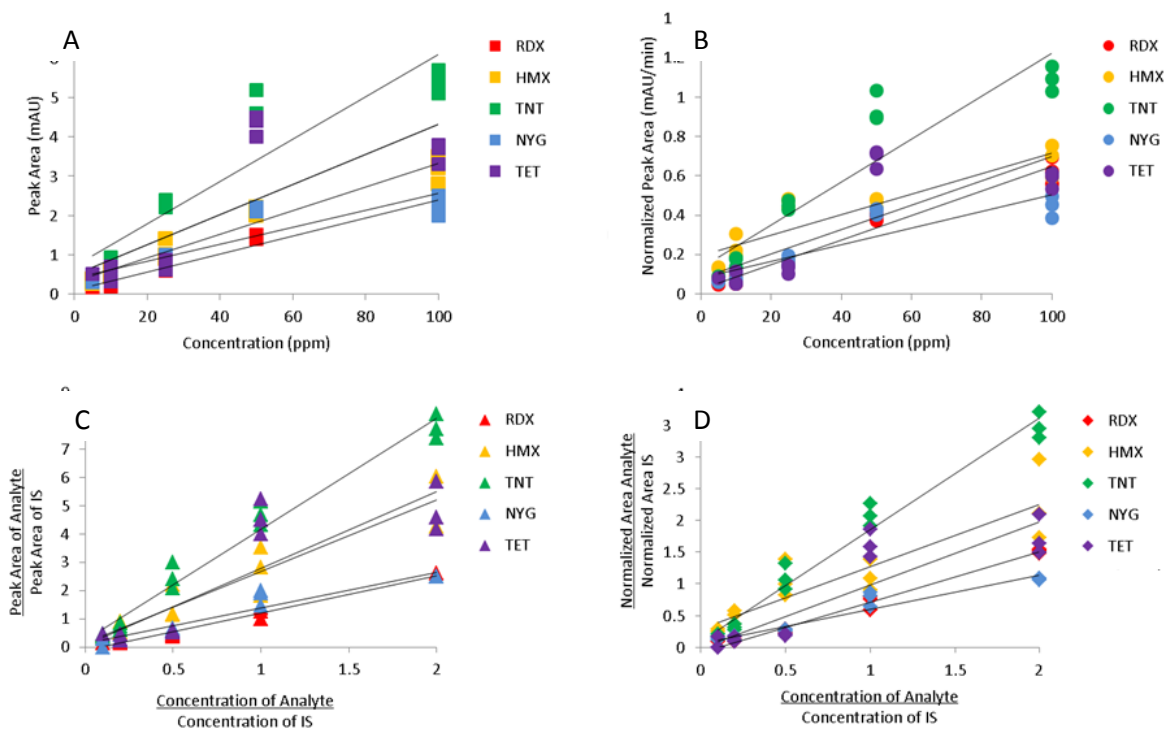


Figure 5-13: Calibration curves for the five high explosives RDX, HMX, TNT, Nitroglycerin, and Tetryl using A) external standard calibration, B) normalized external standard calibration, C) internal standard calibration, or D) normalized internal calibration.

Table 5-7: Comparison of R^2 from Calibration Curves for Explosives Compounds

Explosive	External Standard	Normalized External Standard	Internal Standard	Normalized Internal Standard
RDX	0.9653	0.9636	0.986	0.9869
HMX	0.9485	0.8068	0.8998	0.8248
TNT	0.8484	0.8628	0.9727	0.9756
NYG	0.7957	0.7991	0.9295	0.9299
TET	0.6099	0.616	0.7464	0.7824

These results suggest that normalization results in a slight improvement in the linearity of the calibration, but using an internal standard makes a bigger difference for these compounds. In the case of Tetryl, the linearity appears to plateau at the higher concentration.

The limits of detection and limits of quantitation were determined by using the calibration curve to determine the concentration of the three 10 ppm standards, since they were the lowest concentration that reliably produced a peak distinguishable from the noise for all compounds. The standard deviation of the three concentrations was determined, then multiplied by 3 to find the LOD and multiplied by 10 to find the LOQ. These values and the calibration curve data are presented in Table 5-8.

Table 5-8: LOD, LOQ, and R² values from calibration curves

Analyte	Slope	Intercept	R ²	SD	LOD	LOQ
1,3,5-Trinitrobenzene	0.65	0.03	0.9725	1.7	5.1	17
1,3-Dinitrobenzene	2.75	-0.30	0.9661	0.29	0.88	2.9
2,4-Dinitrotoluene	0.89	0.31	0.9872	3.6	11	36
2,6-Dinitrotoluene	1.02	0.05	0.9889	2.5	7.6	25
2-Amino-4,6- DNT	0.29	0.08	0.9403	7.0	21	70
2-Nitrotoluene	1.29	-0.01	0.9527	0.63	1.9	6.3
3,5-Dinitroaniline	1.34	0.18	0.9516	4.0	12	40
3-Nitrotoluene	1.20	-0.19	0.9459	0.85	2.6	8.5
4-Amino-2,6-DNT	0.54	-0.04	0.9516	1.7	5.2	17
4-Nitrotoluene	1.33	-0.01	0.9909	0.38	1.1	3.8
HMX	0.55	1.10	0.1649	0.82	2.5	8.2
Nitrobenzene	0.02	0.46	0.1477	87	262	876
Nitroglycerin	3.65	-0.20	0.9636	0.46	1.4	4.7
RDX	0.47	0.04	0.9811	4.0	12	40
Tetryl	1.26	0.08	0.9874	2.3	6.9	23
TNT	0.81	-0.07	0.9842	2.8	8.3	28

5.4 Conclusions

This chapter has described the application of cationic latex nanoparticles to the separation of explosives. Both nitroaromatic compounds and anions can be separated using EKC. Three different core chemistries had different selectivities for nitro compounds, and the nanoparticles were significantly different from the surfactants SDS and CTAB. Analytes with increasing number of nitro groups were

more retained, and analytes with methyl or aniline functional groups were retained even more. Most anions showed minimal interactions with the PSPs, except for the hydrophobic anions thiocyanate and perchlorate. These showed retention by PSPs with all three core chemistries and resulted in severe band broadening. In order to carry out the simultaneous separation of nitro compounds and anions, acetonitrile must be added to the BGE to mitigate band broadening of thiocyanate and perchlorate. 20% acetonitrile can be added without disrupting nanoparticle structure.

The best looking electropherograms were obtained with KB3A BAAPTMAC and KB3F MAAPTAC nanoparticles. It is unclear why these nanoparticles in particular produced the best peak shapes, as they were not the highest or lowest for any parameter studied in Chapter 4. The KB4 series of nanoparticles were among the smallest as measured by diffusion NMR and had the worst performance in this application. More work was done with nanoparticles with AETMAC shells than with APTAC shells, and future work on this project should explore APTAC further.

I would have liked to do many more experiments with the optimized BGE with 20% acetonitrile to generate more analytical figures of merit and study the repeatability and inter-capillary reproducibility of this system. Unfortunately, a combination of instrumental failures and family emergencies prevented me from finishing the experiments I had planned. There is still room for optimization in this separation, and I hope someone will pick up this project and see it through to completion.

Chapter 6: Conclusions and Future Directions

6.1 Conclusions

The research presented in this dissertation has explored the synthesis, characterization, and application of cationic latex nanoparticles in electrokinetic chromatography. Much has been learned, but there are still many questions and much room for further research.

Chapter 2 discussed the synthesis and polymerization of cationic latex nanoparticles. RAFT polymerization was found to be an effective way to synthesize cationic latex nanoparticles that are suitable for use as PSPs for EKC. The CTA 2-[[[butylsulfanyl]carbonothioyl]sulfanyl]propanoic acid described by Ferguson is an appropriate choice to polymerize both AETMAC and APTAC cationic monomers into macroCTA, and both AETMAC and APTAC macroCTAs retain their living character and can be chain extended using MA, EA, or BA into diblock copolymers. These copolymers then self-assemble into the latex nanoparticle structures. NMR and non-aqueous CE suggest that the nanoparticle solutions contain additional elements, such as hydrophobic homopolymer, unreacted macroCTA, or short polymer chains not incorporated into the supramolecular nanoparticle structure. The latex nanoparticles range in size from 21 to 55 nm in diameter, according to diffusion NMR measurements.

RAFT polymerization with the 2-[[[butylsulfanyl]carbonothioyl]sulfanyl]propanoic acid CTA can also be used to synthesize larger PAETMAC cationic polymers suitable for use as a cationic capillary coating, as discussed in Chapter 3. PAETMAC coated capillaries prevent the cationic latex nanoparticles from adsorbing to the bare silica surface of the capillary wall, which had been shown to cause excessive band broadening of hydrophobic compounds. A given PAETMAC coated capillary showed good repeatability over a series of 100 injections of the neutral EOF marker acetone. Multiple batches of

PAETMAC were synthesized but had different properties, suggesting there is room for improvement in the synthesis.

In Chapter 4 cationic latex nanoparticles with AETMAC and APTAC shells and MA, EA, and BA core chemistries were evaluated as PSPs through the LSER model. The cationic group chemistry did not appear to play a role in selectivity, but differences were seen between the three different core chemistries. The methylene selectivity increased as the hydrophobicity of the core increased from methyl to ethyl to butyl. Increased nanoparticle size was correlated with higher methylene selectivity for butyl and ethyl acrylate nanoparticles. LSER showed a significant difference between MA nanoparticles and EA or BA nanoparticles. Cationic latex nanoparticles have more similarities with anionic latex nanoparticles with the same core chemistries than they do with cationic surfactants, suggesting that the cationic shell of the nanoparticles is a different environment than the cationic head groups of a surfactant micelle.

These cationic latex nanoparticles were used to separate analytes found in explosives and explosives residues in Chapter 5. Nitroaromatic and nitramine compounds were retained by all three core chemistries, and some resulted in better separations than others. KB3A BAAPTAC and KB3F MAAPTAC PSPs led to the best peak shapes. Under optimized conditions all compounds reach the detector in less than 10 minutes. Anionic analytes can be separated using these conditions, although both perchlorate and thiocyanate appear to interact with the nanoparticles through hydrophobic interactions. Adding 20% acetonitrile to the BGE reduces the interactions, and the decreased retention of the hydrophobic analytes allows a longer capillary to be used without sacrificing analysis time.

This research has shown that cationic latex nanoparticles are an effective PSP for EKC, and have been shown to be useful for the simultaneous separation of anions and nitroaromatic compounds.

6.2 Future Directions

One of the most challenging aspects of this research was the characterization of the polymer chains and polymeric nanoparticles. The MALDI-TOF MS method now provides better information about the macroCTAs, but the diblock copolymers are still poorly understood. It would be useful to know the number average molecular weight, weight average molecular weight, and dispersity of the diblock copolymer chains. It would also be useful to better understand how many diblock copolymer chains are present in a given nanoparticle structure, the way the aggregation number can be found for a surfactant micelle. The DLS and diffusion NMR assume the nanoparticles are spheres, but this may not be the case. The TEM image showed particles that were of a spherical nature, but the shape after drying may not represent the shape of a particle in solution. The new Materials Science program may be able to offer opportunities for collaboration in the future.

The most hydrophobic monomer successfully incorporated into a cationic latex nanoparticle was butyl acrylate, which only has a four carbon-chain. It would be useful to increase the carbon chain or structure of the hydrophobic pendent group, but alternatives to aqueous synthesis may need to be explored. Organic solvents such as dioxane, THF, or DMF may be useful, and Derek Shultz has been using DMF to synthesize amino acid based nanoparticles with promising results.

The original goal of the proposal that provided funding for this project was to develop a detection system that used fluorescence quenching. A system was built in collaboration with Vincent Schnee consisting of a box with mirrors and fiber optic cables that would irradiate a capillary and collect emitted light at a 90° angle. An LED provided the excitation wavelength, and a spectrometer collected the emitted light. A photograph of the system is shown in Figure 6-1. Vince provided CdSe quantum dots to use as a fluorophores, but they were difficult to incorporate into the EKC system and required extensive capillary flushing with harsh HCl and NaOH solutions in addition to generating cadmium waste.

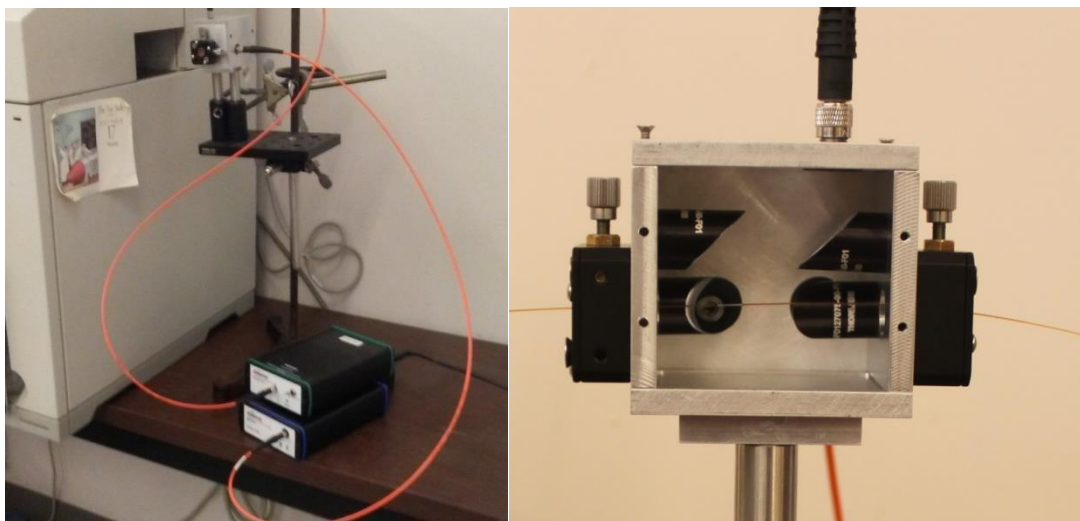


Figure 6-1: The fluorescence quenching detection system designed and built by Vincent Schnee

Organic fluorophores are an alternative to inorganic quantum dots. A fluorescent nanoparticle that could be quenched when a nitroaromatic analyte partitioned into it would be way to incorporate the ideas of fluorescence quenching into an EKC system without the hassles of external fluorophores. Kim Brown assisted with the creation of a Stern-Volmar plot that showed that TNT can quench the fluorescence of fluorescein. She also assisted with the synthesis of a triblock latex nanoparticle with APTAC, BA, and a fluorescein vinyl monomer. This nanoparticle did appear to have fluorescent properties and could separate compounds, as shown in Figure 6-2. I would have loved to pursue this further, but did not have the time. The synthesis of fluorescent nanoparticles and development of a fluorescence quenching detection method could be the subject of a future dissertation.

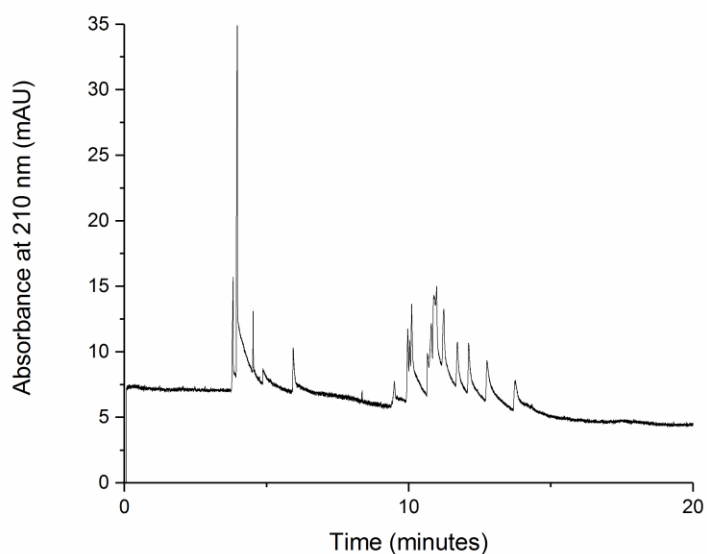


Figure 6-2: The separation of anions and nitroaromatic compounds by JRM27 BAAPTAC-Fluorescein. Compounds were not definitively identified.

Capillary electrophoresis is relatively simple instrumentation, and building a portable device to use with this method would be an excellent next step. The Palmer research group is currently designing and building a portable device, with Tristan McGettrick taking the lead in electronics, hardware, and software development. This portable device could be taken out into the field and used to test suspicious materials. Eventually the portable instrument and fluorescence quenching detector could be combined into a portable instrument capable of trace level explosives detection.

References

- (1) Cressy, D. *Saltpeter: The Mother of Gunpowder*, 1st ed.; Oxford University Press: Oxford, 2013.
- (2) Kelly, J. *Gunpowder: Alchemy, Bombards, & Pyrotechnics: The History of the Explosive that Changed the World*, 1st ed.; Basic Books: New York, 2004.
- (3) VanGelder, A. P.; Schlatter, H. *History of the Explosives Industry in America*, Reprint of.; Arno Press: New York, 1972.
- (4) *Military Explosives: Department of the Army Technical Manual TM 9-1300-214*; 1984.
- (5) Akhavan, J. *The Chemistry of Explosives*; The Royal Society of Chemistry: Cambridge, UK, 1998.
- (6) Zapata, F.; de la Ossa, M. Á. F.; Gilchrist, E.; Barron, L.; García-Ruiz, C. *Talanta* **2016**, *161*, 219–227.
- (7) Yinon, J. *Forensic and Environmental Detection of Explosives*; John Wiley & Sons, Ltd.: West Sussex, England, 1999.
- (8) Kubota, N. *Propellants and Explosives*, 2nd ed.; WILEY-VCH Verlag GmbH: Weinheim, Germany.
- (9) Ettre, L. S.; Sakodynskii, K. I. *Chromatographia* **1993**, *35* (3–4), 223–231.
- (10) Ettre, L. S.; Sakodynskii, K. I. *Chromatographia* **1993**, *35* (5–6), 329–338.
- (11) Martin, A. J. P.; Synge, R. L. M. *Biochem. J.* **1941**, *35* (12), 1358–1368.
- (12) Ettre, L. S. In *A Century of Separation Science*; Issaq, H. J., Ed.; Marcel Dekker, Inc.: New York, 2002; pp 1–17.
- (13) James, A. T.; Martin, A. J. P. *Biochem. J.* **1951**, *50* (5), 679–690.
- (14) Roeraade, J. In *A Century of Separation Science*; Issaq, H. J., Ed.; Marcel Dekker, Inc.: New York, 2002; pp 27–48.
- (15) Scott, R. P. W. In *A Century of Separation Science*; Issaq, H. J., Ed.; Marcel Dekker, Inc.: New York, 2002; pp 87–100.
- (16) Ettre, L. S. In *A Century of Separation Science*; Issaq, H. J., Ed.; Marcel Dekker, Inc.: New York, 2002; pp 115–143.
- (17) *A Century of Separation Science*; Issaq, H. J., Ed.; Marcel Dekker, Inc.: New York, 2002.
- (18) Desty, D. H.; Haresnape, J. N.; Whyman, B. H. F. *Anal. Chem.* **1960**, *32* (2), 302–304.
- (19) Dandeneau, R. D.; Zerenner, E. H. *J. High Resolut. Chromatogr.* **1979**, *2* (6), 351–356.
- (20) Ettre, L. S. *LC GC* **2005**, *23* (5), 486–495.
- (21) Neue, U. D. In *A Century of Separation Science*; Issaq, H. J., Ed.; Marcel Dekker, Inc.: New York, 2002; pp 197–210.

- (22) Majors, R. E. *LC GC* **2015**, 33 (11), 818–840.
- (23) John E. MacNair; Kenneth C. Lewis, and; Jorgenson, J. W. **1997**.
- (24) Jacoby, M. *Chemical and Engineering News*. April 2008, pp 17–23.
- (25) Issaq, H. J. In *A Century of Separation Science*; Issaq, H. J., Ed.; Marcel Dekker, Inc.: New York, 2002; pp 453–482.
- (26) Jorgenson, J. W.; Lukacs, K. D. *Anal. Chem.* **1981**, 53 (8), 1298–1302.
- (27) Dovichi, N. J.; Zhang, J. *Angew. Chem. Int. Ed* **2000**, 39 (24).
- (28) Terabe, S.; Otsuka, K.; Ichikawa, K.; Tsuchiya, a; Ando, T. *Anal. Chem.* **1984**, 56, 111–113.
- (29) Yang, H.; Ding, Y.; Cao, J.; Li, P. *Electrophoresis* **2013**, 34 (9–10), 1273–1294.
- (30) Terabe, S.; Miyashita, Y.; Shibata, O.; Barnhart, E. R.; Alexander, L. R.; Patterson, D. G.; Karger, B. L.; Hosoya, K.; Tanaka, N. *J. Chromatogr. A* **1990**, 516 (1), 23–31.
- (31) Moliner-Martínez, Y.; Barrios, M.; Cárdenas, S.; Valcárcel, M. *J. Chromatogr. A* **2008**, 1194 (1), 128–133.
- (32) Palmer, C. P.; Khaled, M. Y.; McNair, H. M. *J. High Resolut. Chromatogr.* **1992**, 15 (11), 756–762.
- (33) Palmer, C. P.; McNair, H. M. *J. Microcolumn Sep.* **1992**, 4 (6), 509–514.
- (34) Göttlicher, B.; Bächmann, K. *J. Chromatogr. A* **1997**, 780 (1–2), 63–73.
- (35) Nilsson, C.; Nilsson, S. *Electrophoresis* **2006**, 27 (1), 76–83.
- (36) Nilsson, C.; Viberg, P.; Spégel, P.; Jörntén-Karlsson, M.; Petersson, P.; Nilsson, S. *Anal. Chem.* **2006**, 78 (17), 6088–6095.
- (37) Palmer, C. P.; Hilder, E. F.; Quirino, J. P.; Haddad, P. R. *Anal Chem* **2010**, 82 (10), 4046–4054.
- (38) Palmer, C. P.; Keeffer, A.; Hilder, E. F.; Haddad, P. R. *Electrophoresis* **2011**, 32 (5), 588–594.
- (39) Hyslop, J. S.; Hall, L. M. G.; Umansky, A. A.; Palmer, C. P. *Electrophoresis* **2014**, 35 (5), 728–735.
- (40) Ettre, L. S. *Pure Appl. Chem.* **1993**, 65 (4), 819–872.
- (41) Poole, C. F. *The Essence of Chromatography*; Elsevier Science B.V.: Amsterdam, 2003.
- (42) Snyder, L. R. *J. Chromatogr. A* **1974**, 92 (2), 223–230.
- (43) Rohrschneider, L. *Anal. Chem.* **1973**, 45 (7), 1241–1247.
- (44) Vitha, M.; Carr, P. W. *J. Chromatogr. A* **2006**, 1126 (1), 143–194.
- (45) Abraham, M. H.; Ibrahim, A.; Zissimos, A. M. *J. Chromatogr. A* **2004**, 1037, 29–47.
- (46) Wang, J.; Wang, C.; Guo, Z.; Dong, X.; Xiao, Y.; Xue, X.; Zhang, X.; Liang, X. *J. Chromatogr. A* **2014**, 1361, 153–161.

- (47) Terabe, S.; Otsuka, K.; Ando, T. *Anal. Chem.* **1985**, *57* (4), 834–841.
- (48) Silva, M. *Electrophoresis* **2007**, *28* (1–2), 174–192.
- (49) Northrop, D. M.; Martire, D. E.; Maccrehan, W. A. **1991**, No. 6, 1038–1042.
- (50) Wallenborg, S. R.; Bailey, C. G. *Anal. Chem.* **2000**, *72* (8), 1872–1878.
- (51) Giordano, B. C.; Copper, C. L.; Collins, G. E. *Electrophoresis* **2006**, *27* (4), 778–786.
- (52) Yang, Y. Y.; Liu, J. T.; Lin, C. H. *Electrophoresis* **2009**, *30* (6), 1084–1087.
- (53) Johns, C.; Hutchinson, J. P.; Guijt, R. M.; Hilder, E. F.; Haddad, P. R.; Macka, M.; Nesterenko, P. N.; Gaudry, A. J.; Dicoski, G. W.; Breadmore, M. C. *Anal. Chim. Acta* **2015**, *876*, 91–97.
- (54) Copper, C.; Brensinger, K.; Rollman, C.; Clark, A.; Perez, M.; Genzman, A.; Rine, J.; Moini, M. *Electrophoresis* **2016**, *37* (19), 2554–2557.
- (55) Hutchinson, J. P.; Evenhuis, C. J.; Johns, C.; Kazarian, A. A.; Breadmore, M. C.; Macka, M.; Hilder, E. F.; Guijt, R. M.; Dicoski, G. W.; Haddad, P. R. *Anal. Chem.* **2007**, *79* (18), 7005–7013.
- (56) Hutchinson, J. P.; Johns, C.; Breadmore, M. C.; Hilder, E. F.; Guijt, R. M.; Lennard, C.; Dicoski, G.; Haddad, P. R. *Electrophoresis* **2008**, *29* (22), 4593–4602.
- (57) Blanco, G. A.; Nai, Y. H.; Hilder, E. F.; Shellie, R. A.; Dicoski, G. W.; Haddad, P. R.; Breadmore, M. C. *Anal. Chem.* **2011**, *83* (23), 9068–9075.
- (58) Martín-Alberca, C.; Sáiz, J.; Ferrando, J. L.; García-Ruiz, C.; Prada-Rodríguez, D.; Fernández-Fernández, E.; Breadmore, M. C.; Gareil, P.; Dicoski, G. W.; Haddad, P. R. *Anal. Methods* **2012**, *4* (9), 2680.
- (59) Sarazin, C.; Delaunay, N.; Varenne, A.; Costanza, C.; Eudes, V.; Gareil, P. *Sep. Purif. Rev.* **2010**, *39* (1–2), 63–94.
- (60) Sarazin, C.; Delaunay, N.; Varenne, A.; Costanza, C.; Eudes, V.; Gareil, P. *J. Sep. Sci.* **2010**, *33* (20), 3177–3183.
- (61) Kobrin, E.-G.; Lees, H.; Fomitšenko, M.; Kubáň, P.; Kaljurand, M. *Electrophoresis* **2014**, *35* (8), 1165–1172.
- (62) Chiefari, J.; Chong, Y. K. B.; Ercole, F.; Krstina, J.; Jeffery, J.; Le, T. P. T.; Mayadunne, R. T. A.; Meijs, G. F.; Moad, C. L.; Moad, G.; Rizzardo, E.; Thang, S. H.; South, C. *Macromolecules* **1998**, *31* (16), 5559–5562.
- (63) Chong, B. Y. K.; Krstina, J.; Le, T. P. T.; Moad, G.; Postma, A.; Rizzardo, E.; Thang, S. H. *Macromolecules* **2003**, *36* (7), 2256–2272.
- (64) Chiefari, J.; Mayadunne, R. T. A.; Moad, C. L.; Moad, G.; Rizzardo, E.; Postma, A.; Skidmore, M. A.; Thang, S. H. *Macromolecules* **2003**, *36* (7), 2273–2283.
- (65) Mayadunne, R. T. A.; Rizzardo, E.; Chiefari, J.; Krstina, J.; Moad, G.; Postma, A.; Thang, S. H. *Macromolecules* **2000**, *33* (2), 243–245.

- (66) Moad, G.; Rizzardo, E.; Thang, S. H. *Polymer (Guildf)*. **2008**, *49* (5), 1079–1131.
- (67) Ferguson, C. J.; Hughes, R. J.; Nguyen, D.; Pham, B. T. T.; Gilbert, R. G.; Serelis, a K.; Such, C. H.; Hawckett, B. S. *Macromolecules* **2005**, *38* (6), 2191–2204.
- (68) Locock, K. E. S.; Meagher, L.; Haeussler, M. *Anal. Chem.* **2014**, *86* (4), 2131–2137.
- (69) Izunobi, J. U.; Higginbotham, C. L. *J. Chem. Educ.* **2011**, *88* (8), 1098–1104.
- (70) Zhu, H.; Yalcin, T.; Li, L. *J. Am. Soc. Mass Spectrom.* **1998**, *9* (4), 275–281.
- (71) Lou, X.; Fransen, M.; Stals, P. J. M.; Mes, T.; Bovee, R.; Van Dongen, J. J. L.; Meijer, E. W. *J. Am. Soc. Mass Spectrom.* **2013**, *24* (9), 1405–1412.
- (72) Charles, L. *Mass Spectrom. Rev.* **2014**, *33* (6), 523–543.
- (73) Schriemer, D. C.; Li, L. *Anal. Chem.* **1997**, *69* (20), 4169–4175.
- (74) Byrd, H. C. M.; McEwen, C. N. *Anal. Chem.* **2000**, *72* (19), 4568–4576.
- (75) Bushey, M. M.; Jorgenson, J. W. *Anal. Chem.* **1989**, *61* (5), 491–493.
- (76) Righetti, P. G.; Gelfi, C.; Verzola, B.; Castelletti, L. *Electrophoresis* **2001**, *22* (4), 603–611.
- (77) Pei, L.; Lucy, C. A. *J. Chromatogr. A* **2014**, *1365*, 226–233.
- (78) Pappas, T. J.; Gayton-Ely, M.; Holland, L. A. *Electrophoresis* **2005**, *26* (4–5), 719–734.
- (79) Pascoe, R. J.; Foley, J. P. *Electrophoresis* **2003**, *24* (24), 4227–4240.
- (80) Wiedmer, S. K.; Holopainen, J. M.; Mustakangas, P.; Kinnunen, P. K.; Riekkola, M. L. *Electrophoresis* **2000**, *21* (15), 3191–3198.
- (81) Ryan, R.; Altria, K.; McEvoy, E.; Donegan, S.; Power, J. *Electrophoresis* **2013**, *34* (1), 159–177.
- (82) Palmer, C. P. *Electrophoresis* **2007**, *28* (1), 164–173.
- (83) Yang, S.; Khaledi, M. G. *Anal. Chem.* **1995**, *67* (3), 499–510.
- (84) Muijselaar, P. G.; Claessens, H. a.; Cramers, C. a. *Chromatographia* **1997**, *45* (1), 433–434.
- (85) Khaledi, M. G.; Bumgarner, J. G.; Hadjmohammadi, M. *Sect. Title Surf. Chem. Colloids* **1998**, *802*, 35–47.
- (86) Fujimoto, C. *Electrophoresis* **2001**, *22* (7), 1322–1329.
- (87) Schnee, V. P.; Palmer, C. P. *Electrophoresis* **2008**, *29* (4), 767–776.
- (88) Fuguet, E.; Rafols, C.; Bosch, E.; Abraham, M. H.; Roses, M. *Electrophoresis* **2006**, *27* (10), 1900–1914.
- (89) Poole, C. F.; Poole, S. K.; Abraham, M. H. *J. Chromatogr. A* **1998**, *798* (1–2), 207–222.
- (90) Lu, J.; Ni, X.; Cao, Y.; Ma, X.; Cao, G. *Electrophoresis* **2015**, *36* (2), 312–318.

- (91) Vitha, M.; Carr, P. W. *J. Chromatogr. A* **2006**, *1126* (1), 143–194.
- (92) Schnee, V. P.; Palmer, C. P. *Electrophoresis* **2008**, *29* (4), 777–782.
- (93) Penny, W. M.; Steele, H. B.; Ross, J. B. A.; Palmer, C. P. *Electrophoresis* **2017**, *38* (5), 738–746.
- (94) Akbay, C.; Hoyos, Y.; Hooper, E.; Arslan, H.; Rizvi, S. A. A. *J. Chromatogr. A* **2010**, *1217* (32), 5279–5287.
- (95) Damodaran, K. V.; Merz, K. M. *Biophys. J.* **1994**, *66*, 1076–1087.
- (96) Damodaran, K. V.; Merz, K. M. *Langmuir* **1993**, *9*, 1179–1183.
- (97) Slater, S. J.; Ho, C.; Taddeo, F. J.; Kelly, M. B.; Stubbs, C. D. *Biochemistry* **1993**, *32*, 3714–3721.
- (98) Gaurav, D.; Malik, A. K.; Rai, P. K. *Crit. Rev. Anal. Chem.* **2007**, *37* (4), 227–268.
- (99) Germain, M. E.; Knapp, M. J. *Chem. Soc. Rev.* **2009**, *38* (9), 2543–2555.
- (100) Caygill, J. S.; Davis, F.; Higson, S. P. J. *Talanta* **2012**, *88*, 14–29.
- (101) Akhgari, F.; Fattahi, H.; Oskoei, Y. M. *Sensors Actuators, B Chem.* **2015**, *221*, 867–878.
- (102) Grate, J. W.; Ewing, R. G.; Atkinson, D. A. *TrAC Trends Anal. Chem.* **2012**, *41*, 1–14.
- (103) Ewing, R. *Talanta* **2001**, *54* (3), 515–529.
- (104) Crawford, C. L.; Hill, H. H. *Anal. Chim. Acta* **2013**, *795*, 36–43.
- (105) Kapoor, J. C.; Kannan, G. K. *Def. Sci. J.* **2007**, *57* (6), 797–810.
- (106) Sarazin, C.; Delaunay, N.; Varenne, A.; Vial, J.; Costanza, C.; Eudes, V.; Minet, J. J.; Gareil, P. *J. Chromatogr. A* **2010**, *1217* (44), 6971–6978.
- (107) Martín-Alberca, C.; Sáiz, J.; Ferrando, J. L.; García-Ruiz, C.; Prada-Rodríguez, D.; Fernández-Fernández, E.; Breadmore, M. C.; Gareil, P.; Dicinoski, G. W.; Haddad, P. R. *Anal. Methods* **2012**, *4* (9), 2680.
- (108) Martín-Alberca, C.; de la Ossa, M. Á. F.; Sáiz, J.; Ferrando, J. L.; García-Ruiz, C. *Electrophoresis* **2014**, *35* (21–22), 3272–3280.
- (109) Guijt, R. M.; Evenhuis, C. J.; Macka, M.; Haddad, P. R. *Electrophoresis* **2004**, *25* (23–24), 4032–4057.
- (110) Kubáň, P.; Hauser, P. C. *Electrophoresis* **2009**, *30* (1), 176–188.
- (111) Šolínová, V.; Kašička, V. *J. Sep. Sci.* **2006**, *29* (12), 1743–1762.
- (112) Mussenbrock, E.; Kleiböhmer, W. *J. Microcolumn Sep.* **1995**, *7* (2), 107–116.
- (113) Oehrle, S. A. *Electrophoresis* **1997**, *18* (2), 300–302.
- (114) Bailey, C. G.; Yan, C. *Anal. Chem.*, **1998**, *70*, 3275–3279.

- (115) Yeung, E. S. *Acc. Chem. Res.* **1989**, *22* (4), 125–130.
- (116) Hilmi, A.; Luong, J. H. T.; Nguyen, A. L. *Anal. Chem.* **1999**, *71* (4), 873–878.
- (117) Kennedy, S.; Caddy, B.; Doweb, J. M. F. **1996**, *9673* (95) 211-222.
- (118) Goodpaster, J. V.; McGuffin, V. L. *Anal. Chem.* **2001**, *73* (9), 2004–2011.
- (119) Lahoda, K. G.; Collin, O. L.; Mathis, J. A.; LeClair, H. E.; Wise, S. H.; McCord, B. R. *J. Forensic Sci.* **2008**, *53* (4), 802–806.
- (120) Boone, C. M.; Manetto, G.; Tagliaro, F.; Waterval, J. C. M.; Underberg, W. J. M.; Franke, J.-P.; DeZeeuw, R. A.; Ensing, K. *Electrophoresis* **2002**, *23*, 67–73.
- (121) Jones, W. R.; Jandik, P. *J. Chromatogr. A* **1991**, *546*, 445–458.
- (122) Altria, K. D. *Chromatographia* **1993**, *35* (3–4), 177–182.
- (123) Altria, K. D.; Fabre, H. *Chromatographia* **1995**, *40* (5–6), 313–320.